LUT
Lappeenranta
University of Technology

中国科学院大学
University of Chinese Academy of Sciences

Lappeenrannan teknillinen yliopisto
Lappeenranta University of Technology

Kiinan tiedeakatemian yliopisto
University of Chinese Academy of Science

Chao Fang

STUDY ON SYSTEM DESIGN AND KEY TECHNOLOGIES OF CASE CLOSURE WELDING FOR ITER CORRECTION COIL

Thesis for the degree of Doctor of Science (Technology) to be presented with due permission for public examination and criticism in the Auditorium of Technopolis at Lappeenranta University of Technology, Lappeenranta, Finland on the 7th of October, 2016, at noon.

The Thesis was written under a double doctoral degree agreement between Lappeenranta University of Technology, Finland and Institute of Plasma Physics Chinese Academy of Science, China and jointly supervised by supervisors from both University and Institute.

Acta Universitatis
Lappeenrantaensis 714

Supervisors Professor Heikki Handroos
LUT School of Energy Systems
Lappeenranta University of Technology
Finland

Professor Antti Salminen
LUT School of Energy Systems
Lappeenranta University of Technology
Finland

Professor Yuntao Song
Insititute of Plasma Physics
Chinese Academy of Sciences
China

Reviewers Professor Lin Li
School of Mechanical, Aerospace and Civil Engineering
University of Manchester
UK

D.Sc. (Tech.) Tommi Jokinen
Wärtsilä Finland Oy
Finland

Opponents Professor Lin Li
School of Mechanical, Aerospace and Civil Engineering
University of Manchester
UK

D.Sc. (Tech.) Tommi Jokinen
Wärtsilä Finland Oy
Finland

ISBN 978-952-265-997-2
ISBN 978-952-265-998-9 (PDF)
ISSN-L 1456-4491
ISSN 1456-4491

Lappeenrannan teknillinen yliopisto
Yliopisto 2016

Abstract

Chao Fang
Study on system design and key technologies of case closure welding for ITER Correction Coil
Lappeenranta 2016
130 pages
Acta Universitatis Lappeenrantaaensis 714
Diss.Lappeenranta University of Technology
ISBN 978-952-265-997-2, ISBN 978-952-265-998-9 (PDF), ISSN-L 1456-4491,
ISSN 1456-4491.

International Thermonuclear Experimental Reactor (ITER) Correction Coil (CC) case, made of ultra-low carbon austenitic stainless steel 316LN with 20 mm thickness, was designed in the outmost layer of the CC, and was used to protect the internal superconducting coil, resist the deformation effect caused by the powerful electromagnetic force and thermal stress during the operation process. These cases have characteristics of small cross-section, large dimension, and complex structure. They were divided into two parts for the convenience of the internal superconducting coil being inserted into the case, and they will be closure welded together after insertion. Thus, weld seam is located the whole perimeter of the case, which will decide the large quantity weld with the specific distribution caused by the geometric profile of the case. The distribution requires a specific welding system, aim at the CC case closure welding characteristic, should be developed to realize the field welding. The strict deformation requirement, temperature control of internal coil and full penetration with high welding quality brings the technology challenges to this closure welding. The welding system must be constructed and these key technologies must be solved using this welding tooling before the offcial production of CC.

A fibre laser robotic welding system was developed for the case closure welding based on the research, scheme design and analysis in this thesis. The specific qualification experiments were carried out on this laser welding system according to technology challenges on the welding quality, temperature control and deformation. Firstly, according to the distribution of weld seam, the preliminary scheme designs of welding systems based on several different welding methods were carried out. It was found that the laser welding is identified as the most suitable welding method. Based on above, reasonable arrangement of robots and external rail, and simulation of robotic welding motion process were carried out in order to further optimize design and analysis. The simulation results show that there exist the dead zone where the robot arm can not doing the effective welding and the robotic welding workspace should be

increased. A slip plate module for the welding robot was added to assist travel, after that, the robot was successful in covering all weld seams in all cases.

Secondly, to complete this welding system, the welding fixture should be developed to support the welding platform, adjust the assembly tolerance and provide the rigid constrain to control the welding deformation, and electric control should be developed to integrate the welding system and increase its security and stability. A number of ground supports match with the C-type clamps were designed and special distributed aim at the geometric profile of case. The rotatable ground supports, which can provide two types of welding platform, were developed to meet the two different welding positions with arched and concave shape of SCC case. In order to provide the turn over function for SCC case, a welding tilter with tilter framework, single central axis, load-bearing jig was designed base on the good finite element analysis (FEA) result. In addition, the design requirements of the control system of the CC case laser welding were analyzed and the integrated control system was developed based on SIEMENS PLC system S7-300.

Thirdly, narrow gap multi-pass laser welding with hot wire was developed as the welding process for the case closure welding. The welded jointed with defects-free and good mechanical properties was achieved based on good optical system, reasonable groove structure and optimized welding procedure. In order to protect the internal superconducting coil, which is inside of the case, the backing strip was designed and welded by laser welding behind the case in the actual welding structure of the CC case. The temperature distribution of the welding process was simulated by FEA and measured by the thermocouples on a short sample. The FEA temperature distribution shows good agreement with the experimental measurement, the highest temperature of the inner face of case was 255℃, and the highest temperature record of surface of the internal coil was 59℃. The result shows the laser welding process will not harm the superconducting coil, and the welding process, based on the laser welding system, can meet the temperature control requirement. To study the welding deformation, a SCC model case was designed, fabricated and welded by the laser welding system. The principle of positioning welding before continuous welding, as well as segmented, skip, symmetry and repeated turn over, was developed to keep uniform heating of the model case. According to the detected results of welding deformation of the model case, the overall welding deformation was controlled below ±2mm. Satisfactory results of the welding deformation of the model case certify the reasonability of the welding structure, system and process of the CC case closure welding, and also provide technical support for the full scale CC case.

In conclusion, this thesis study to develop a special robotic laser welding system to solve the CC case closure welding, and some key technologies were studied aim at the

related engineering challenges.

Key words: ITER, Correction Coil, fixture, laser welding system, narrow gap, welding deformation

Acknowledgements

Firstly I would like to express my gratitude to Lappeenranta University of Technology and Institute of Plasma Physics, Chinese Academy of Sciences for provide me this study and working journey. I would also like to express my gratitude to ITER International Fusion Energy Organization and China International Nuclear Fusion Energy Program Execution Center for enabling this work. These organizations have funding this project and thus they deserve special thanks for it.

I would like to express my gratitude to my supervisors Professor Heikki Handroos, Professor Antti Salminen, Professor Yuntao Song and to Associated Professor Dr. Huapeng Wu for making this thesis possible. I will always thankful for their reading of early draft of my proposal, their insightful technical and editorial advice, their suggestions and continuous encouragement, and their patient assistance.

I would also like to express my gratitude to Professor Weiyue Wu and Senior Engineer Jing Wei from Institute of Plasma Physics, Chinese Academy of Sciences. I am grateful for this opportunity I was given to working in research group and to participate in this most interesting engineering project, for their tireless efforts to provide me with a great working environment.

I would also like to express my gratitude to the preliminary examiners of the dissertation, Professor Lin Li from the University of Manchester, UK and D.Sc. (Tech.) Tommi Jokinen, Wärtsilä Finland Oy, Finland. Their valuable comments helped to improve the quality of thesis. I would also like to express my gratitude to study secretary Johanna Jauhiainen and study programme coordinator Sari Damsten for their kindly help in my dissertation process.

To all my colleagues and friends at the university and institute, I offer my deepest gratitude for the pleasant work and colorful leisure time.

Finally, I would like to express my special gratitude for my parents and my family who have supported and encouraged me on my studies. Without their help I would not be to finish this project.

Chao Fang
October 2016
Lappeenranta, Finland

Contents

Abstract

Acknowledgements

Contents

Nomenclature **11**

1 Introduction **13**
1.1 Introduction 13
1.2 The International Thermonuclear Experimental Reactor (ITER) 16
1.3 The welding technology in the fusion engineering 18
1.4 The ITER Correction Coil 19
1.5 Objectives of the study 21
1.6 Outline of the thesis 22
1.7 Scientific contributions and publications 23

2 Manufacture and closure welding scheme design of CC case **25**
2.1 Structural characteristics and material properties 25
2.1.1 Structure characteristics of the SCC 25
2.1.2 Structure characteristics of the BTCC 26
2.1.3 ITER CC case material property 27
2.2 The manufacturing process of the CC case 29
2.2.1 Manufacturing process of BTCC case 29
2.2.2 Manufacturing process of SCC case 30
2.3 Design of case closure welding scheme 32
2.3.1 Requirements of case closure welding 32
2.3.2 NG-TIG welding scheme 33
2.3.3 EBW scheme 35
2.3.4 LBW scheme 38
2.3.5 Comparison of the three welding schemes 39
2.4 Analysis of the laser welding scheme 40

3 The welding fixture and electrical control **47**
3.1 Design of the laser welding fixture 47
3.1.1 The design requirement 47
3.1.2 Welding fixture for BTCC case 49

3.1.3 Welding fixture for SCC case 50
3.1.4 Welding tilter for SCC case 51
3.2 Electrical control 57
3.2.1 Main devices 57
3.2.2 Control system 59

4 Laser welding process and temperature control 71
4.1 Narrow gap laser welding with hot wire 71
4.1.1 Narrow gap laser welding 71
4.1.2 Narrow gap design 72
4.1.3 The laser welding with hot wire 78
4.2 Welding experiment on the standard plate 80
4.2.1 Experimental 80
4.2.2 Laser welding parameters 82
4.2.3 Inspection and analysis of weld 83
4.3 Thermal analysis and experiment 88
4.3.1 Welding structure of CC case 88
4.3.2 Thermal analysis of laser welding 92

5 Laser welding on the model case 101
5.1 Structural characteristic and material property 101
5.2 Model case closure welding 102
5.2.1 Deforamtion analysis and control 102
5.2.2 The welding procedure 103
5.2.3 The welding procedure 105
5.2.4 Welding deformation analysis 110

6 Conclusions and recommendations 117
6.1 Key results of the work 117
6.2 Suggestion for the future work 119

References 121

Nomenclature

Abbreviation	Explanation
ITER	International Thermonuclear Experimental Reactor
CC	Correction Coils
VV	Vacuum Vessel
SMAW	Shielded Metal Arc Welding
GTAW	Gas Tungsten Arc Welding
NG-TIG	Narrow Gap Tungsten Insert Gas Welding
IWR	Intersector Welding Robot
TF	Toroidal Field
CS	Central Solenoid
TCC	Top Correction Coils
SCC	Side Correction Coils
BCC	Bottom Correction Coils
CICC	Cable In Conduit Conductor
BTCC	Bottom and Top Correction Coils
VPI	Vacuum Pressure Impregnation
AVC	Automatic Voltage Control
EBW	Electron Beam Welding
LBW	Laser Beam Welding
FEA	Finite Element Analysis
IPC	Industrial Personal Computer
SCM	Single Chip Microcomputer
PLC	Programmable Logic Control
D/A	Digital to Analog
A/D	Analog to Digital
DOF	Degree of Freedom
SEM	Scanning Electron Microscope
EDX	Energy Dispersive X-ray Spectroscopy
HAZ	Heat Affected Zone
HIF	Heat Input Fitting

1 Introduction

1.1 Introduction

With the rapid increase of the world population and the progress of human civilization, energy consumption has increased sharply. Human society cannot develop without energy, therefore energy has become the hottest and most urgent issue in the world. At present, natural fossil fuels for human use, such as coal, oil, and natural gas, all belong to non-renewable energy, and according to expert estimations, the world coal reserves can only be mined for 162 years, 40 years for petroleum, and 65 years for natural gas. Humanity will be in an energy crisis with restricted sources and increasing consumption. Since the beginning of the last century, humans have paid much attention to exploring renewable energy sources, such as hydro, wind, solar, geothermal, ocean and certain results have been achieved. While all these renewable energy sources have limitations (Ma, 2005), a new kind of energy source should be found to meet energy demands and to thoroughly solve the energy problems for the sustainable development of human beings.

Nuclear energy，a new member of the energy source family, includes two main forms: fission and fusion. Fission energy is released from proton fission of heavy metal elements, which have been used for commerce. Due to the rarity of uranium or other heavy metal elements and radioactive nuclear waste of a fission reactor, development of nuclear fission was restricted. Fusion energy, whose fuel is the hydrogen isotopes deuterium and tritium, is another nuclear energy form not yet commercialized. Sea water contains reserves endless deuterium and tritium, which will be available for human use for billions of years. According to projections, the energy released from tritium in a liter of sea water during complete fusion is equivalent to the energy of 300 liters of burning gas oil (Chinese Academy of Science, 2002). Additionally, the waste (helium) from the fusion reaction is clean and safe and has a wide range of uses in the military, scientific research, petrochemicals, refrigeration and manufacturing. Fusion energy, an unlimited, clean, secure new energy source (Li, et al., 2008), has become the main source of future sustainable energy and can totally solve the energy crisis of human society.

In the mid-20th century, mankind had achieved nuclear fusion reaction, namely the hydrogen bomb. The hydrogen bomb is a nuclear fusion process and ignited by the explosion of the atomic bomb. A huge amount of energy is instantaneously released and cannot be controlled. If the released, enormous fusion, energy could be commercialized

for human survival, it would have to be controlled. However, controlling nuclear fusion is very demanding. For example, the sun brings light and heat to the solar system by nuclear fusion reactions where the temperature at the center reaches 15 million degrees Celsius, and great pressure makes the fusion reaction constant. On earth there is no way to obtain such high pressure, it could only be achieved by increasing the temperature to compensate and to reach 100 million degrees.

According to current research, the realization of controlled thermonuclear fusion reaction mainly includes inertial confinement fusion and magnetic confinement fusion (Wessen, 1987; Shi, 1999; Wang, 2008). The inertial confinement fusion reaction is triggered by using laser shock waves to ignite the fuel and which usually includes deuterium and tritium to reach a high temperature and pressure. As the largest inertial confinement fusion device in the world, America's National Ignition Facility (NIF) succeeded in 2013, with the annular device, to achieve a nuclear fusion reaction and realized a fuel ball released with more energy than the laser applied. In addition, there is a similar large-scale device, namely the Million Joule laser (LMJ) in France. The magnetic confinement nuclear fusion is realized by the magnetic field and high thermal plasma to trigger a nuclear fusion reaction. First the fuel is heated, which shapes the plasma, then the charged particle in the hot plasma is put into helical motion by the magnetic field, further heating the plasma till the nuclear fusion reaction is reached. The nuclear fusion reaction device, Tokamak, a feasibly controlled nuclear fusion reactor, is one kind of toroidal vessel to achieve controlled magnetic confinement nuclear fusion. It is named after toroidal, kamera, magnetic and kotushka, and was proposed initially by Aki Mowe Zi at the Kurchatov Institute of the Soviet Union in the 1950s. Fig. 1.1 shows a schematic diagram of a Tokamak.

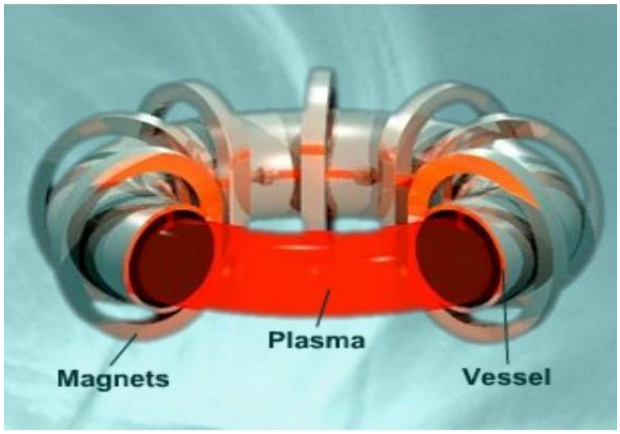

Figure 1.1 A schematic diagram of a Tokamak (ITER)

Compared with other magnetic confinement controlled nuclear fusion devices, the

dominant status of Tokamak was gained from the experimental results of the former Soviet Union T-3 Tokamak. An announcement was made at the third session of the Plasma Physics and Controlled Nuclear Fusion Research International Conference, in August 1968 in Novosibirsk, Soviet Union, by Aki Mowe Zi that the Soviet T-3 Tokamak had realized the electronic temperature 1keV, proton temperature 0.5kev, $n\tau = 10^{18} m^{-3} \cdot s$.This was a major break through in controlled nuclear fusion research and set off an upsurge for tokamak in the world. Many countries have established a number of large Tokamak devices, including the JT-60 in Japan, the TFTR in the United States of America, and the JET and T-15 in Europe. Since the end of the last century, controlled nuclear fusion research has made great progress in these Tokamak devices. In November 1991, the EC JET device successfully implemented the first deuterium and tritium experiment in the history of nuclear fusion. In the mixed fuel with a deuterium tritium ratio of 6 to 1 respectively, the plasma temperature reached three billion degrees Celsius, and the nuclear fusion reaction lasted for 2 seconds. The fusion power was 1.7MW and the energy gain factor Q value reached from 0.11 to 0.12. In December 1993 at the TFTR device in the United States, the fuel mixture with half deuterium and half tritium, reached a temperature of 3 billion to 4 billion degrees Celsius, and 10.7MW fusion output power and energy gain factor Q value up to 0.28. In December 1997, the Japanese JT-60 device succeeded with the deuterium tritium reaction experiment, converting the deuterium tritium reaction, so that the Q value could reach 1.0 and later more than 1.25 (Qiu, 2008; Start, et al., 1998; Gibson, JET team, 1998; Strachan, et al., 1994). This means the generating fusion energy was more than the energy of the input. These breakthroughs, represented by Tokamak, have been confirmed in the scientific theory of magnetic confinement fusion. With further study and experiment of the Tokamak device, research emphasis has shifted from the conventional Tokamak device to the superconducting Tokamak. At the beginning of the 21st century, the Chinese Academy of Sciences, Institute of Plasma Physics, established the EAST Tokamak which was the first full superconducting and noncircular cross section superconducting Tokamak device designed locally. Then South Korea built the KSTAR superconducting Tokamak device. Table 1.1 shows the engineering physical parameters of the main superconducting Tokamak experimental apparatuses in the world.

Table 1.1 Parameters of the main superconducting Tokamak experimental apparatuses in the world (Wen, 2013)

Parameters	Triam-1M Japan	Tore-Supra France	EAST China	KSTAR South korea	T-15 Russian	SST-1 India
Large plasma radius（m）	0.8	2.4	1.7	1.8	2.4	1.1
Small plasma radius（m）	0.12/0.18	0.8	0.4/0.8	0.5/1.0	0.7	0.2/0.4
Extension rate	1.5	1.0	1.6-2.0	2.0	1.0	1.7-2
Intensity of toroidal field（T）	8	4.2	3.5	3.5	4.0	3.0
Plasma current（MA）	0.5	2.0	1.0	2.0	2.0	0.22
Auxiliary heating power(MW)	-	22	20	16-41	-	5

1.2 The International Thermonuclear Experimental Reactor (ITER)

Tokamak research (IAEA, 2001; Wan, 2011) and events leading to the end of the Cold War, mainly Gorbachev's policies of *glasnost* (openness) and *perestroika* (restructuring), saw new developments in nuclear reaction research. The Geneva summit (1985) between the United States and the Soviet Union resulted in the launch of the International Thermonuclear Experimental Reactor (ITER) program, which included Europe and Japan as well—an iconic end of the Cold War.

In 1987, ITER's concept design began and was completed in 1990 by the United States, the Soviet Union, Europe and Japan. In 1998, the four countries jointly completed the engineering design and some technical research of ITER. According to this engineering design, the ITER device investment is expected to be up to $100 billion. In order to reduce the construction costs, the four ITER members began to modify the ITER engineering design. In 1999, the United States withdrew from ITER due to political and domestic disputes. The EU, Japan and Russia continued to carry out the improvement plan for the ITER device and completed it in 2002. The new design, called ITER-FEAT (Fusion Energy Advanced Tokamak), was based on maintaining the original main physical and engineering goals and reduced the investment budget to $46 billion. The expected construction period is 10 years; the projected operation of the experimental period is 20 years. Table 1.2 (Zhao, 2004) shows the main typical parameters of the ITER device.

Table 1.2 Main typical parameters of ITER device（another set of operating parameters for the bracket）

Total fusion power/MW	500(700)
Q(fusion power/heating power)	＞10
14MeV average neutron wall loading/(MW/m^2)	0.57(0.8)
Repeat continued burning time/s	＞500
Large plasma radius /m	6.2
Small plasma radius /m	2.0
Plasma current/MA	15
Extension rate of small cross-section	1.7
Central magnetic field intensity of plasma/T	5.3
Plasma volume/m^3	837
Superficial area of plasma/m^2	678
Power of heating and driving current/MW	73

In 2002 after the redesign, ITER sought the participation of the whole human race, clearly expressing the hope for China and the United States to join, as well as South Korea and India. After several years of negotiations, in 2006 the seven members in the ITER project (the European Union, the United States, China, Japan, South Korea, Russia and India) initiated a cooperation agreement marking the official start of the ITER project. Among them, the EU bears 50% of the cost, and each of the remaining six assumes 10%; the extra 10% will be used to pay for cost overruns during the process of building, due to price fluctuations and other factors. In November of the same year, seven representatives of ITER formally signed the joint experimental agreement and related documents in the French Presidential Palace.

The signing of the ITER project means it is the second most expensive international scientific cooperation project in history, following the International Space Station. According to the agreement, ITER is expected to be completed and put into operation in 2020 with the designed output fusion power of 500-700MW and plasma discharge pulse at 500-1000s. The program is divided into three stages: first, the reactor construction phase from 2007 to 2020; second, the thermonuclear fusion reaction experiment period lasting for 20 years (during this stage, the performance of the fusion fuel and the heap of all the materials developed will be verified for large-scale commercial development); third, the final stage is the experimental stage for reactor disassembly which will last 5 years (Zhang, 2013). Figure 1.2 shows the schematic diagram for ITER.

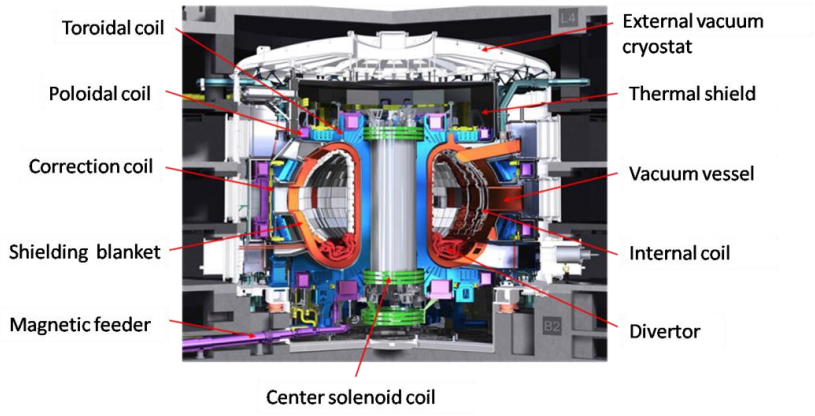

Figure 1.2 Schematic diagram for ITER (ITER)

1.3 The welding technology in the fusion engineering

Welding is the most common work in the fusion engineering since a mass of weldment, vacuum sealing and pressure part in the fusion device. Large size, complex structure, huge amount of welding, high requirement were widespread in the fusion engineering component brings the special difficulty to welding. These difficulties include not only the welding technology, also the design of welding system to realize the field work. Aim to the different component in the fusion engineering, various welding methods were studied, experimented and determined depends on the welding material, welding depth, related requirements (weld quality, deformation, temperature control, etc). And these welding system based on these welding methods should be considered and designed to verify their feasibility in the actual engineering situation includes the dimension, configuration and welding field. Normally, the automatic welding tooling was applied and cooperated with the designed external travelling axis to realize all welding position of the component in fusion engineering.

As a core component in fusion device, vacuum vessel (VV) is the most typical welding components in the fusion engineering. The ITER VV is designed to be a water-cooled, large double-wall structure made of 316L(N)-IG (ITER grade) stainless steel with a D-shaped cross-section over 10 m in height. And it is divided toroidally into 9 sectors, which are manufactured respectively, that joined by field welding on assembly site of ITER. On the whole, the welding work on the VV includes the welding in the manufacturing process of each sector and also the final field welding of sector-to-sector weld. The fabrication tolerances for the whole vessel including field assembly are specified to be less than ± 20 mm for the total height and total width, and ± 5 mm for

the sector wall thickness (Onozuka et al., 2000). The challenges in this welding work were known as the welding process to penetrate the thick welding depth, control the welding quality and strict welding deformation requirement, and also the welding tooling to realize the welding process since the large dimension and specific structure of weldment especially the field welding of sector-to-sector weld. A variety of welding processes include SMAW, GTAW, NG-TIG welding, laser beam welding and electron beam welding were studied aim at the VV welding (Dans et al., 2014; Jones et al., 2012; Nightingale et al., 2002; Martin et al., 2009; Coste et al., 2002; Tommi et al., 2003). Huapeng Wu and his colleagues propose and design several welding toolings to realize the sector-to-sector welding, such as a parallel robot called IWR travel on the track rail or industry robot on the support frame anchored to the equatorial ports (Wu et al., 2011). Similar to the VV, the challenges of CC case closure welding is to develop the feasible welding system because of its specific geometric profile and weld distribution, also the key technologies of welding process to control its related welding requirements.

1.4 The ITER Correction Coil

The ITER magnet system is made up of four main sub-systems: 18 Toroidal Field Coils(TF); the Central Solenoid(CS); 6 Poloidal Field Coils(PF); and 18 Error Field Correction Coils(CC) (Foussat et al., 2010; Mitchell et al., 2008). The 18 CC are used to compensate field errors, arising from coil misalignment, and winding deviations from the nominal shape, resulting from fabrication tolerances, joints, leads, bus bars and assembly tolerances (Huguet et al., 2001; Mitchell et al., 2009). Since any processing and assembly, such as superconducting, needs reasonable tolerance requirements, joint and current leads will inevitably bring deviation between the reality and the design. The errors caused by these tolerances and deviations will impact on the experiment and operation of the device. In order to create better conditions for experimenting, operating and enhancing the stability of the device, it is necessary to correct, eliminate, or reduce the influence of these errors as far as possible.

The 18 correction coils are composed of top correction coils (TCC), side correction coils (SCC) and bottom correction coils (BCC), 6 for each, 18 in total. Each of the BCC and TCC arrangement is at the 60 degree sector and across three toroidal field coils, each SCC arrangement is at the 40 degree radial station across two vertical field coils. Fig. 1.3 shows the schematic diagram of the distribution of the ITER correction coils.

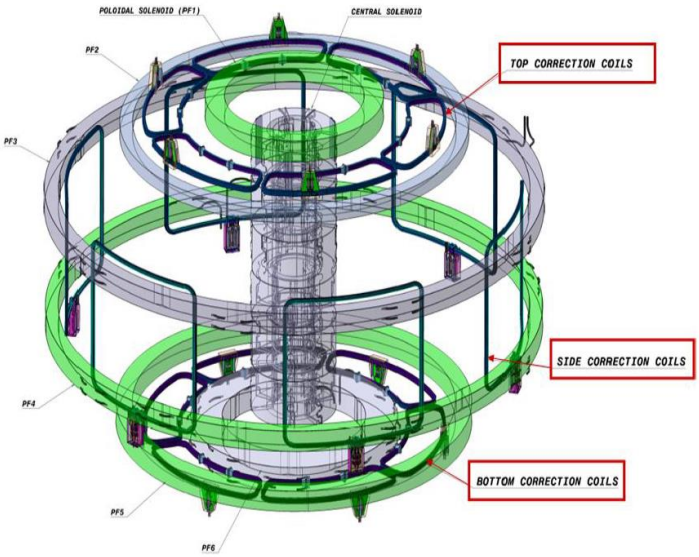

Fig1.3 Schematic diagram of the distribution of the ITER correction coils (ITER)

Each coil is composed of several turns of superconducting coils, the maximum turn current for all coils is 10kA, the highest magnetic field is about 5T. All the coils are protected by a 20mm thick stainless steel case and supported by a splint and relying on the toroidal field magnet. The superconducting conductors are CICC (Cable In Conduit Conductor) made of NbTi, the section size of conductor is 19.2mm* 19.2mm. BTCC has 32 turns with a dimension of 2.5m * 7m, and each coil weight, including the coil case, is about 3 tons. SCC has 20 turns with a dimension of 7.2m * 7.6m, and the entire coil weight, including the coil case, is about 3.65 tons (Wen, 2013).

In consideration of the process of inserting the internal superconducting coil into the case and the two geometry shapes, the BTCC case is designed to a U-shaped body with a cover plate, and the SCC case is designed to two L-shaped cases (Fang et al., 2014; Zhou et al., 2012). Figures 1.4 and 1.5 show the structure of the two types of cases. After inserting the superconducting coil into the case, the case needs to be closure welded to carry out the second VPI (vacuum pressure impregnation) process. Due to its specific geometric profile, weld distribution and the welding technology requirements of the correction coil case, the engineering challenges are raised: how to do the case closure welding and meet the welding quality requirements. Therefore, it is necessary to do feasibility research for the ITER CC case closure welding system design and solve some key technologies.

Figure 1.4 SCC case structure

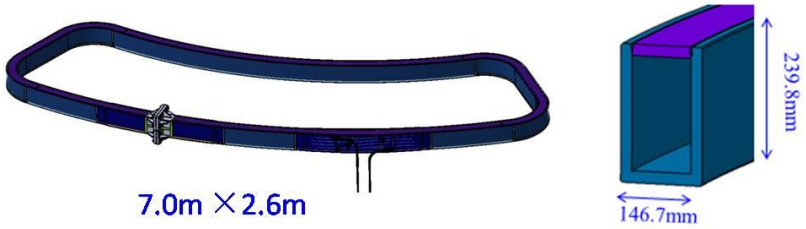

Figure 1.5 BTCC case structure

1.5 Objectives of the study

Due to solve engineering technology challenges, the purpose of this study is to develop a schematic design and analyze a suitable welding system for the actual situation and related requirements of the ITER CC case closure welding. The feasibility of the welding system should be verified by a special test, which could meet the requirements of case closure welding and provide strong technical support for the ITER CC process.

The main objective of the study is divided into three goals. The first goal is study the basic weld distribution and welding requirements of the CC case, and to do several conceptual design scheme based on some potential feasible welding methods, analysis these welding schemes, optimize and determine the finally welding scheme. Considering the strict welding deformation requirement, the traditional arc welding was not taken and some welding methods with low heat input include automatic NG-TIG welding, laser beam welding and electronic beam welding were serious considered. The NG-TIG welding system was designed to the welding tractor travel on the flexibility rail which is fixed on the case by vacuum chuck. The laser beam welding system was designed to the industrial welding robot travel on the ground rail. The electron beam welding was designed to workpiece put on the large movable workbench, and electron gun assembled on the portal frame. The laser beam welding was determined as the best

alternative to be applied to the CC case closure welding based on the comparison of three welding schemes. In order to optimize the laser welding system and make the welding robot covering all weld seams in the case, the reasonable arrangement of robots and simulation of robotic welding motion process were carried out.

The second goal is to design the welding fixture and build the electric control module to complete this welding station in the commissioning state. According to the actual engineering requirement, the welding fixture should be developed to provide the welding platform for the case, adjust the assembly tolerance, and provide the rigid constraint to control the welding deformation. The welding fixture consists of the ground support and the C-type clamp which are aim to the specific geometric profile of two types of case. Moreover, the welding tilter, which used to realize the rotating process of the SCC case during its welding, was designed and optimized by FEA. Finally, the integrated electric control module of this laser welding system was developed based on the SIEMENS PLC system S7-300.

The third goal, some key technologies should be experimented and developed based on the suitable welding process. These key technologies include the basic welding procedure, the back temperature control, and the welding deformation. They are carried out on the standard plate, a short sample and a small scale mock up respectively. A narrow gap multi-pass laser welding process with hot wire was developed as the basic welding procedure for the CC case closure welding. And the welded jointed and mechanical properties based on optimized welding parameters were presented. A short sample was fabricated and used to study the temperature distribution during the case welding process. The results of the temperature distribution, which were simulated by thermal analysis and measured by the thermocouple, were presented. Finally, a small scale mock up of SCC case was designed, fabricated and used to qualify the welding deformation of the case welding. The welding process was analyzed and developed to control the welding deformation. According to this welding process, the overall welding deformation result was presented after the welding.

1.6 Outline of the thesis

The following sections present the work carried out in this study.

Section2

According to the basic shape and size of the coil case and the weld distribution characteristics, several different welding methods were carried out, compared and analyzed. Ultimately, laser welding was determined as best for the ITER CC case

closure welding. Through simulation analysis, the optimum design of the laser welding scheme was further optimized and determined finally.

Section3

This section describes the designs and analysis for the closure welding fixtures of two types of case, including the special rotatable function for SCC. It also simulates the turn over process of SCC and establishes the electrical integrated control system for the ITER CC case laser welding workstation.

Section 4

According to the quality requirements of coil case closure welding, narrow gap multi-pass laser welding with hot wire technology was developed. Based on the analysis of laser beam propagation in the narrow gap and the groove design principle of the foundation, the shape of the narrow gap groove was designed and laser welding of the butt joint was tested. Tests showed good results which meet weld quality requirements. Based on the actual coil case welding structure, the experiment and numerical simulation were carried out to study the safety of the superconducting coil inside the case during the laser welding process.

Section5

An SCC model case was designed and welded based on the case closure welding system and test parameters. The welded case was used to analyze welding quality and welding deformation to provide powerful technical reference for the case closure welding.

Section 6

The conclusion and recommendations for the further research are provided.

1.7 Scientific contributions and publications

The main scientific contributions of this thesis follow:

- The laser welding system was successfully applied to the ITER CC case closure welding which is greatly significant for laser welding and for the engineering application of large size and complex structural weldment.
- A typical design of a laser robotic system is presented. The system uses two robots and their external rails to cover all the weld seams of the ITER CC case, a large size

of 7.2m×7.6m, by optimizing the layout of the weldment and welding tooling.

- The entire welding fixture was designed to provide the welding platform, adjust the assembly tolerance, control the weld deformation, and satisfy the special requirements for the SCC case.

- A suitable laser welding procedure was developed to verify that the welding system is feasible for the ITER CC case closure welding.

Referred scientific publications

- Chao Fang, Yuntao Song, Weiyue Wu, Jing Wei, Shuquan Zhang, Hongwei Li, N. Dolgetta, P. Libeyre, C. Cormany, S. Sgobba. The laser welding with hot wire of 316LN thick plate applied on ITER correction coil case. *Journal of Fusion Energy*, Vol.33,No.6, 2014, pp. 752-758.

- C. Fang, Y.T Song,J. Wei,J.J Xin,H.P. Wu, A. Salminen,H. Handroos,Design and analysis of the laser robotic welding system for ITER Correction Coil case, *Journal of Fusion Energy*, Vol.34, No.5,2015,pp.1060-1066.

- Chao Fang, W.Y. Wu, J. Wei, J. J.Xin, H.P. Wu, A. Salminen, Thermal analysis of laser welding for ITER correction coil case, *Fusion Engineering and Design*, Vol.100,2015,pp.357-363.

- S.Q Zhang, J.F Wu, C. Fang, W.Y Wu, J. Wei, Research on the focused spot diameter and butt joint gap margin in laser welding with hot wire filler，*Chinese Journal of Lasers*，Vol.41,No.10，2014, pp. 1003006.

International conferences publications with review process

- C. Fang, S. Zhang, Z. Zhou, W. Wu, J. Wei, C. Li, W. Dai, P. Libeyre, N. Dolgetta, C. Cormany, M. Gandel. Study on laser welding of case closure welding for ITER Correction Coil.*Proceedings of 23rd International Conference on Magnet Technology*, 14-19 July 2013, Boston, USA.

- Chao Fang, Yuntao Song,Jing Wei,Jijun Xin, Huapeng Wu, Hekki Handroos, Antti Salminen, Hongwei Li, Paul Libeyre, Nello Dolgetta. Microstructural characteristics of the laser welded joint of ITER Correction Coil Sub Case. *Proceedings of 24th Symposium on Fusion Technology*, September 29th–October 3rd2014.San Sebastian, Spain.

2 Manufacture and closure welding scheme design of CC case

2.1 Structural characteristics and material properties

2.1.1 Structure characteristics of the SCC

The SCC case presents in the shape of a three-dimension tile consisting of two large arc segments (radius 11287 mm and central angle 36.2°), two linear segments (length 6794 mm) and four small arc segments (radius 500 mm).A superconducting coil inside the SCC case has four layers, five turns in each layer, i.e. 20 turns totally. The superconducting coil is bent continuously by a length of 545 m superconducting cable. The thickness of the turn insulation, located between each turn, is 1 mm. The thickness of the layer insulation, located between each layer, is also 1 mm. The thickness of the ground insulation, located between the case and superconducting coil, is 8 mm. The turn and ground insulation are composites made of fiberglass and epoxy glue, and the layer insulation is made of fiberglass. Figures 2.1 and 2.2 show the engineering drawing and cross section of SCC. According to the figure, the weld seam of the SCC case is located diagonally of the case in the contact with the two L-shaped half-cases.

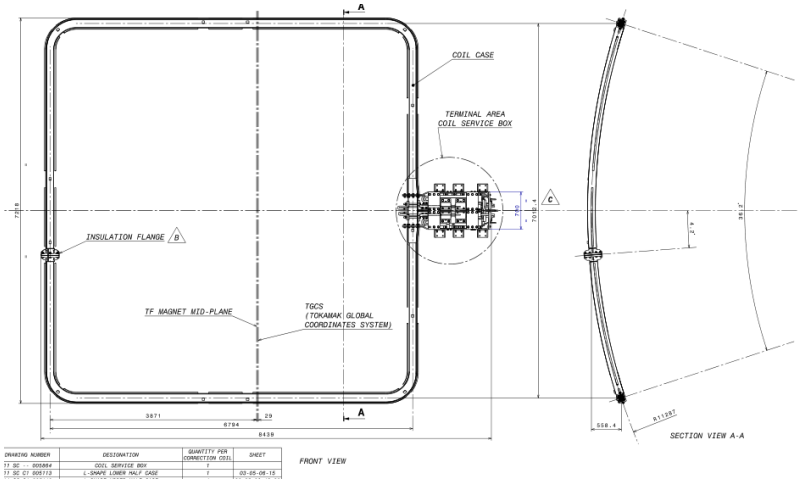

Figure 2.1 Engineering drawing of SCC (ITER)

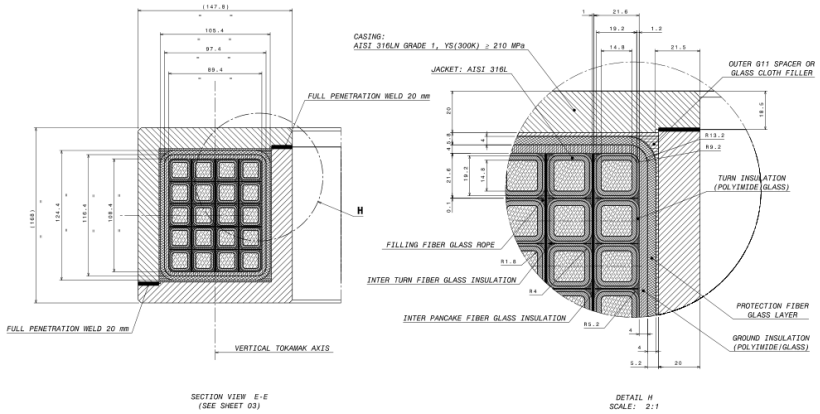

Figure 2.2 Cross-section of SCC (ITER)

2.1.2 Structure characteristics of the BTCC

Compared to the SCC case, the B/TCC case presents as a two dimensional shape, consisting of two large arc segments (radiuses of 7453.5 mm and 5666.5 mm), two linear segments (length 781 mm) and four small arc segments (radius of 500 mm each). The superconducting coil inside the SCC case has eight layers, four turns in each layer and 32 turns totally. The superconducting coil is bent continuously by a length of 505 m superconducting cable. The insulation is the same as SCC: 1 mm thickness of turn insulation, 1 mm thickness of layer insulation and 8 mm thickness of ground insulation. Figures 2.3 and 2.4 show the engineering drawing and cross section of B/TCC. According to the figure, the weld seam of the B/TCC case is located at one side in contact with the flat cover plate and the U-shaped case.

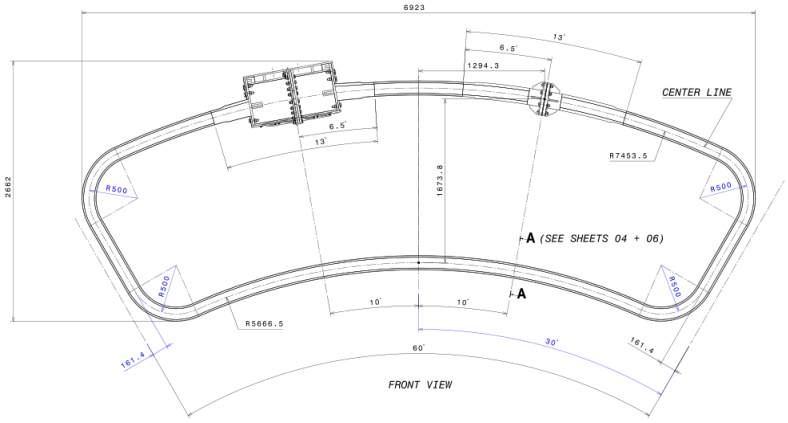

Figure 2.3 Engineering drawing of B/TCC (ITER)

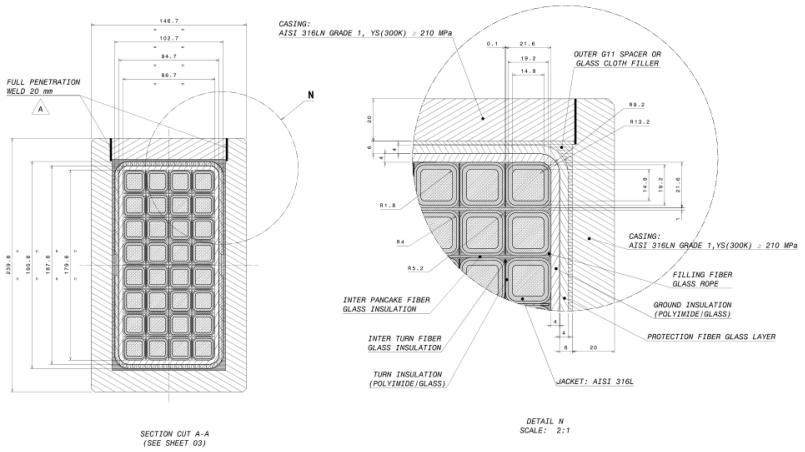

Figure 2.4 Cross-section of B/TCC (ITER)

2.1.3 ITER CC case material property

The structural design criteria have been developed to cover some special features of the ITER magnets and structures that are not adequately covered by a single existing design code (the ASME pressure vessel code being a well-known example) (ITER_D_22HV5L v2.2).

1. Yield criterion: In the case of static load, Tresca stress checking was used for the yield criterion of the metal component of ITER CC. The evaluation criteria for the base material and weld with different thickness are shown in Table 2.1.

Table 2.1 Evaluation criteria of static stress for metal components of CC (ITER)

Base material and weld with thickness＜20mm and no heat treatment after welding		
membrance stress（Pm）	membrance stress+bending stress（Pm+Pb）	primary stress+secondary stress（Pm+Pb+Q）
Sm	1.5*Sm	2.0*Sm
Base material and weld with 20mm＜thickness＜150mm and no heat treatment after welding		
membrance stress（Pm）	membrance stress +bending stress（Pm+Pb）	primary strss+secondary stress（Pm+Pb+Q）
0.9*Sm	1.35*Sm	1.8*Sm

Where Sm=2*Sy/3,Sm represents the allowable stress intensity at a certain temperature, and Sy represents 0.2% yield stress at the temperature of the metal component material. Because austenitic stainless steel 316LN was used for the material of the ITER CC case,

Sy＞700MPa at 4.2K must be ensured.

2. Fracture criterion: A fast fracture assessment was performed. The design stress intensity factor, Km, should compare with the fracture toughness KIC at the design temperature. Km is calculated using the expression (in normal operation) (ITER_D_2FMHHS v2.0):

$$K_m = Y * \sigma(\pi * a)^{\frac{1}{2}} < K_{IC}/1.5, \quad (2\text{-}1)$$

Where, σ is the maximum principal tensile stress, Y is a stress intensity factor, a is the crack size calculated including growth due to fatigue effects. The factor of 1.5 is a safety factor. Safety factors are also applied to the initial crack size and the rate of crack growth.

3. Fatigue criterion: The S-N fatigue life curves method is used as the fatigue assessment of CC; the safety factor of cyclic stress increase is 2, and the safety factor of the cyclic number increase is 20. The allowable cyclic number of the CC is 60000 based on designment.

During the operation process of CC, the main force consists of two parts. One is the powerful electromagnetic force from the interaction of the working current of the conductor inside the coil and the TF (toroidal field) and PF (poloidal field) magnet field. The other is the thermal stress generated from the different thermal expansion coefficient of the inside of the superconducting coil. In order to ensure the strength of CC so it can resist the deformation effect of a powerful electromagnetic force and thermal stress, the case was designed with coils to resist these forces. Moreover, because the high Young's modulus of the case material should have high enough strength at a low temperature (Liu, 2010), 316LN was selected as the case material. The mechanical properties of 316LN at room temperature and low temperature are shown in Table 2.2 (Foussat, 2010).

Table 2.2 Mechanical properties of 316LN at room temperature and low temperature

Temperature（K）	Young modulus （MPa）	Yield strenth （MPa）	Ultimate strength （MPa）	Elongation (%)	Fracture toughness （MPa*$m^{1/2}$）
300	＞190	＞250	＞480	＞35	N/A
＜7	＞205	＞800	＞1100	＞35	＞180

2.2 The manufacturing process of the CC case

ITER CC includes B/TCC and SCC; a different manufacturing process was developed based on the different shapes and structures of the components. According to the previous finite element analysis, the thickness of the coil case is 20 mm. The following will present the manufacturing process of the two types of CC coil cases.

2.2.1 Manufacturing process of BTCC case

TCC and BCC are located at the top and bottom of the ITER device, and present two-dimension structures. Their shape and structure are identical. According to the assembly process of the superconducting coil and BTCC case, the case was divided into a flat cover plate and a U-shaped case. The two parts were manufactured separately, and the final closure welding will be done after the superconducting coil was inserted into the case. The cross-section structure of BTCC case is shown in Figure 2.4. From the Figure, it can be seen that the cross section dimension of 239.8×146.7 mm is very small compared to its overall dimension of 7.0×2.6mm. The machining precision accepts an overall deformation of ±2mm, a verticality of 0.4mm and a flatness of 2mm (ITER_D_2N6NUK v1.13), which increases the manufacturing process difficultly. The key point of the BTCC case manufacture achieving its requirements is to control the overall deformation based on the reasonable machining and welding process.

According to the traditional machining process, the structure of a U-shaped case is usually welded together by three plates. For the BTCC case, this manufacturing method would have the characteristics of along weld seam and excessive heat input which would result in difficult control of the welding deformation. On that basis, rectangular steel, used for the BTCC case, was developed to decrease the weld quantity, control welding deformation, and increase machining productivity. The 35mm thick rectangular steel beam was extruded and applied to the BTCC mock-up case successfully.

Figure 2.5 Extruded rectangular steel beam

The segmented machining method was used for the U-shaped case manufacture because of its large dimension and the complex structure of the large and small arc segments.

Figure 2.6 shows a detailed segment; each U-shaped sub-segment was processed by extruded rectangular steel and the assembly welded together into a complete U-shaped case and finishing.

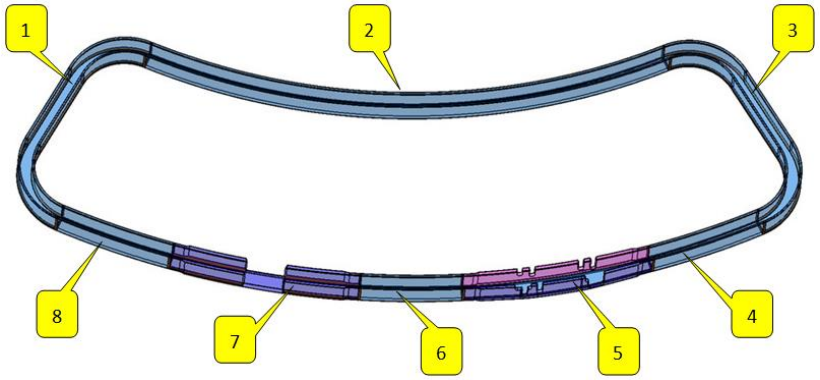

Figure 2.6 Overview of detailed segment machining of a U-shaped case

The flat cover plate is a simple but long, narrow thin structure. According to the design requirements, the flatness of the cover should be less than 1mm. Thus, the difficult point of the cover plate manufacture is also controlling deformation. The segmented machining and welding method is also applied to the cover plate (the detailed segment was shown in Figure 2.7).

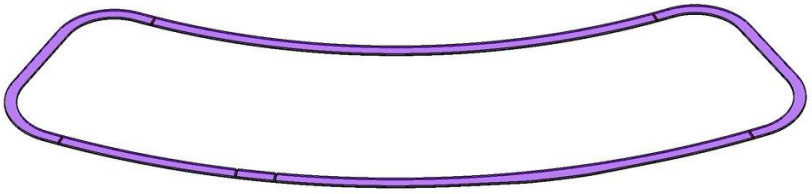

Figure 2.7 Overview of detailed segment machining of cover plate

2.2.2 Manufacturing process of SCC case

SCC is located at the side of the ITER device and presents a three-dimensional structure which is more complex than the two-dimension BTCC structure. The cross section structure of the SCC case is shown in Figure 2.2. From the Figure, it can be seen that the dimension of 147.8×168mm of the cross section is very small compared to its overall dimension of 7.2×7.6m. The strict machining requires a height of 168 mm (+0.5/0), a width of 147.8 mm (0/-0.5), a verticality of 0.4mm, an outer surface profile tolerance of 2mm and a profile of 4mm at the center line (ITER_D_2N6NUK v1.13), increasing its processing difficultly.

According to the assembly process of the superconducting coil and the SCC case (a more complex structure), the case was divided into two L-shaped cases. The two parts were manufactured separately with the final closure welding to be done after the superconducting coil is inserted into the case. Each L-shaped case was welded together by several sub-L-shaped cases done by the segmented machining method. The whole L-shaped case was segmented into 11 sub-parts (the detailed segment is shown in Figure 2.8). The large arc segment and the linear segment is processed by extruded L-shaped steel. The extruded L-shaped steel, after straightening, is shown in Figure 2.9. The most complex structure of the small arc segment was machined and welded by bottom and vertical plates. Figure 2.10 shows the machining of a small arc segment.

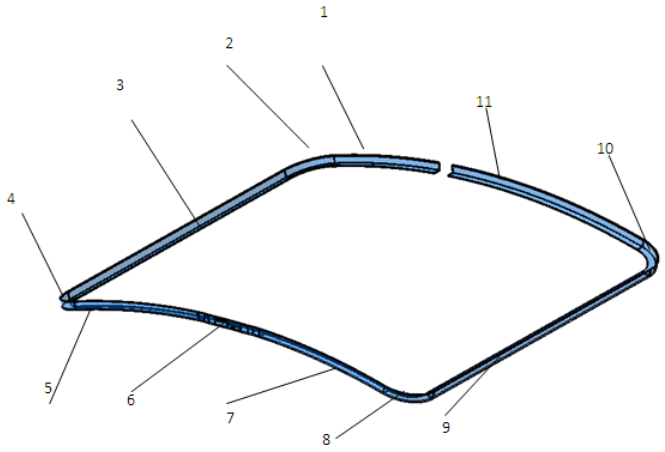

Figure 2.8 Overview of detailed segment machining of L-shaped case

Figure 2.9 Extruded L-shaped steel（before and after straightening）

Figure 2.10 Overview of manufacturing the small arc segment

Due to the marginal consideration of welding deformation and machining, the blank material thickness of the case is 35 mm. After the parts are finished, they are milled to a thickness of 20mm together with machining the groove for the closure weld.

2.3 Design of case closure welding scheme

2.3.1 Requirements of case closure welding

Case closure welding is the next work phase after the superconducting coil is inserted into the case. In order to satisfy the welding structure of the case closure welding and its special requirements, the demands of the devices and weld of case closure welding system are as follows (Wei, et al., 2010; Wei, et al., 2014; Fang, et al., 2011; Fang, et al., 2014):

1. The welding system must cover the entire weld seam of the case closure welding. The weld lengths of the BTCC case and the SCC case are 19 m and 28 m, respectively. Special attention must be paid to the 18° vaulted space weld seam of the SCC case and the SCC case double sides weld machining.

2. The weld quality should achieve level B of the ISO 5817 or ISO 13919-1 for the austenitic stainless steel 316LN of the CC case with 20mm weld penetration.

3. The most difficult point of CC case closure welding is the requirement concerning welding deformation. The center line deviation after case closure welding for the cases should meet the tolerance requirement of ±4mm for the SCC case and ±2mm for the BCC case.

4. In order to protect the superconducting property of CC, the surface temperature of

the superconducting coil must remain below 250°during case closure welding.

According to the above requirements, the preliminary design of welding method for case closure welding was done. Welding methods with a characteristic low heat input were considered initially: NG-TIG welding (narrow gap-Tungsten Inert Gas arc welding), LBW (laser beam welding) and EBW (electron beam welding). All three were studied, designed and contrasted.

2.3.2 NG-TIG welding scheme

NG-TIG welding retains the advantages of good welding quality, controllable parameters, widely applicable material and all position welding of traditional TIG welding. It is commonly used in some important alloy component welding, such as pressure vessels, primary circuit piping of nuclear power, and super-critical boiler piping. The aim of NG-TIG applied to a thick plate of welding is a depth of less than 30mm. A traditional welding torch with a 6-8mm U-shaped or V-shaped groove is usually used including increased tungsten extension length and shielded gas flow to the weld. However, for a thicker plate, the special NG-TIG welding torch will be used to insert into the deeper groove for welding. In order to ensure the heat input and avoid uncompleted fusion of the sidewall, pulse welding with a magnetron arc swing or tungsten (torch) mechanical swing was used (Zhang, 2011; Yang and Tang, 2010). Commonly, hot wire technology was used in conjunction with NG-TIG. A deposition rate and productivity was developed and higher than cold wire based on the advance heating wire.

NG-TIG welding has been used on large-size weldment with the requirements of high quality and low deformation in the fusion project. An example is the manufacturing of the ITER full-size vacuum vessel sector (Koizumi, 2001); NG-TIG welding was used on the final closure welding for the two sectors. Figure 2.11 shows the closure welding for the two sections of the ITER full-size vacuum vessel.

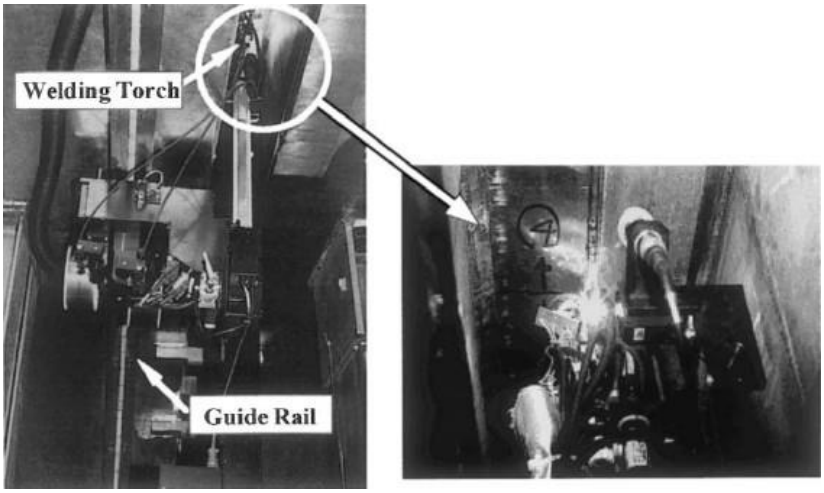

Figure 2.11 Closure welding for the two sections of the ITER full-size vacuum vessel (Koizumi, 2001)

The advantage of NG-TIG welding applied to the ITER CC case closure welding makes it easy to ensure high welding quality, also to ensure low deformation, contrasted with tradition TIG welding. The NG-TIG welding scheme for the BTCC case closure welding, showing the characteristics of the dimensions and structure of the CC case, is shown in Figure 2.11.

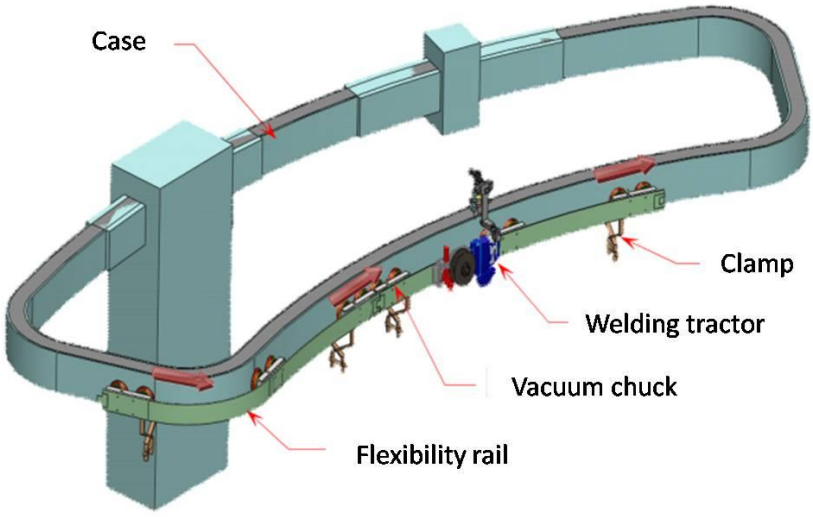

Figure 2.12 NG-TIG welding scheme for the BTCC case closure welding

As shown in Figure 2.12, the NG-TIG welding system includes a welding tractor, a flexibility rail, a vacuum chuck, a welding torch, a seam tracker with position adjusting, an automatic voltage control (AVC) module, a swing module, an angle adjusting

module and a wire feeder module. Welding preparation includes: a) connecting the vaccum chuck and flexibility rail; b) placing them on the outside of the case and start the vacuum chuck; c) fixing the vacuum rail to the case with the clamp; d) assembling the welding tractor; and finally e) using the AVC module, swing module, seam tracker and angle adjusting module to adjust the position of the welding distance and angle.

The welded case alternates removal and connection via two flexibility rails (rail A and rail B respectively) according to the travel direction of the welding tractor. The two flexibility rails use the dedicated interface to connect. Assume the welding direction is from rail A to rail B, rail A will be removed when the welding tractor is located on rail B. Rail A will be connected with rail B on the next segment. This will continue until the entire seam is completed.

2.3.3 EBW scheme

EBW is a welding method where a concentrated electron flow with high speed is used to bombard the workpiece seam and produce heat to the weld. As an advanced high-energy beam welding, EBW has the favorable characteristics of high energy density, strong penetrating ability, high welding speed, a narrow heat-affected zone, low welding deformation, a high depth to width ratio (up to 50:1), and good welding quality. Obviously, EBW is a potential welding method to apply to the ITER CC case closure welding. EBW is a mature welding technology for welding austenitic stainless steel; the most important point is designing the EBW system to successfully adapt to the structural characteristics of the ITER CC case. The medium-pressure electron gun, rectangular vacuum vessel and indoor movable gun are considered in this system.

1. Medium-pressure electron gun

Because a high-pressure electron gun is more expensive than a medium-pressure electron gun and needs lead shielding, it will cause problems for the design and manufacturing of the vacuum vessel and, additionally, for the manufacturing and processing cost. For the ITER CC case closure welding, a medium-pressure electron gun is more appropriate since it can also meet the required penetration depth of the of CC case weld.

2. Rectangular vacuum vessel

Commonly, the vacuum vessel of the EBW system utilizes a rectangular structure. Specially, a large-size vacuum vessel with a rectangular structure will decrease manufacturing risk and cost for the large size weldment needed for the ITER CC case. A circular vacuum vessel would need a top door, and the required form of the top lift

would be inconvenient when placing and removing the weldment. In contrast with a circular vacuum vessel, the rectangular vacuum vessel with a mobile sliding door has the advantage of being easily removed from the workbench. In addition, the rectangular vacuum vessel can be manufactured with a segmented seal and therefore have an easy mechanical connection.

3. Indoor movable gun

The indoor movable gun technology with a medium-pressure electron gun is mature, and its stationary workpiece is more applicable for the ITER CC case because of the large-sized structure. It will decrease the size of the vacuum vessel and movement demand of the workbench and will increase movable accuracy.

In conclusion, the EBW system for the ITER CC case is designed with a medium-pressure electron gun, a rectangular vacuum vessel and an indoor movable gun base in accordance with the characteristics and requirements of the workpiece and the welding capacity, accuracy and manufacturing cost of the system. The EBW system for the ITER CC case closure welding is shown in Figure 2.13. According to the dimensional demands of weldment and workbench, the dimension of the vacuum vessel is designed at 12000mm×9000mm×3500mm. The electron gun is assembled on the fixed mount which is 8000mm distance from the mobile sliding door. As shown in Figure 2.13, the travel distances of Y and Z directions are 7200mm and 800mm. The electron gun also has a ±20° swing capability to adapt to the SCC case shape of the three-dimension tile. The workbench can move out of the vacuum vessel along the rail of the X axis and also has a 4000mm travel distance inside the vacuum chamber.

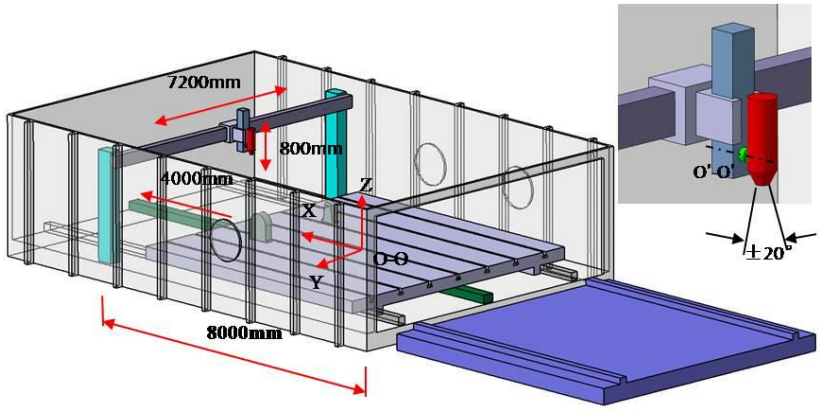

Figure 2.13 Overview of vacuum EBW designed for CC case closure welding

For BTCC case closure welding, the BTCC case will be assembled and positioning welded by a TIG weld outside of the vacuum chamber. Then the BTCC case will be put

into the vacuum chamber and reinforced by an EBW positioning weld. As shown in Figure 2.14, all the weld seams of the BTCC case can be covered based on the 7200mm travel distance of the Y direction of the electron gun and the 2500mm travel distance of the X direction of the workbench.

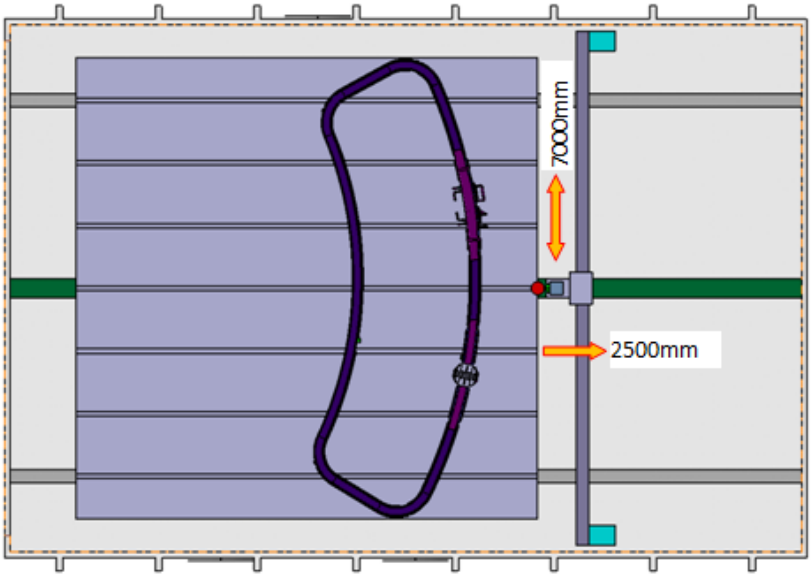

Figure 2.14 Overview of the BTCC case EBW closure welding

For the SCC case closure welding, the SCC case will also be assembled and positioning welded by a TIG weld outside of the vacuum chamber. Then, the SCC case will be put into the vacuum chamber and reinforced by an EBW positioning weld. The weld seams of the SCC case are located on two sides. The case will be moved out of the vacuum chamber, rotate, and move into the vacuum chamber in order to start the BEW positioning weld of the other side. Based on the 7000mm travel distance of the Y direction of the electron gun and the 4000mm travel distance of the X direction of the workbench, the electron gun can cover half the perimeter of the weld seam. Thus, the case rotating process will be finished when the welds of both perimeter seams are completed. Many movements of the case and vacuumize process will have happened during the EBW closure welding.

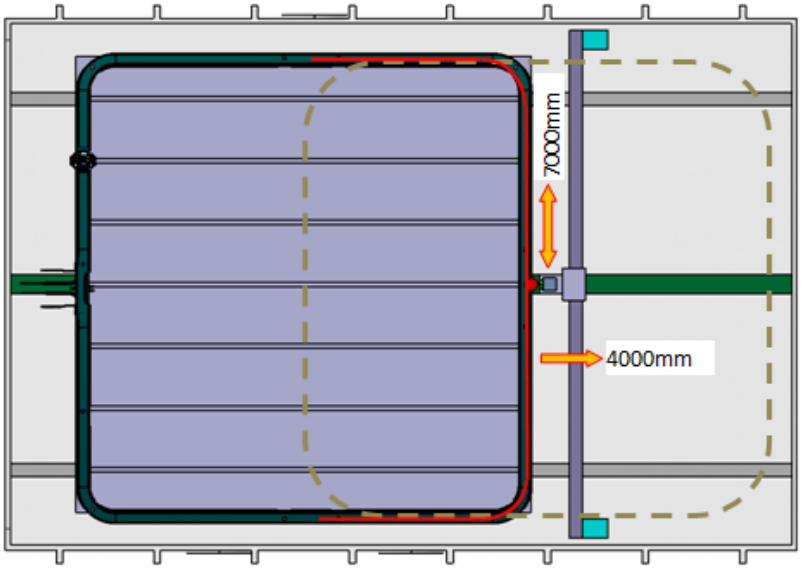

Figure 2.15 Overview of SCC case EBW closure welding

2.3.4 LBW scheme

LBW is the welding method of use when a focused laser beam is needed to bombard the workpiece seam and produce heat to the weld. As an advanced high-energy welding technology, LBW has the important characteristics of high energy density, high welding speed, a narrow heat-affected zone, low welding deformation, a high depth to width ratio, high accuracy and high welding strength. For the CC case closure welding, the low heat input combined with reasonable welding structure and technology will easily control the surface temperature of the superconducting coil inside the case and also decrease welding deformation.

Figure 2.16 shows the overview of laser welding of ITER CC case closure welding. The BTCC case laser welding workshop is separate from the SCC case laser welding workshop. In order to complete the ITER CC case closure welding, four industrial robots, with their respective linear rails, were designed for this laser welding system. Because of the size and shape of the CC cases, robots with their linear BTCC rails were designed for the outside of the case and, likewise, robots with their linear SCC rails were designed for inside the case. Based on a reasonable arrangement of the robots and linear rails, the whole weld seam of the ITER CC cases were covered via the operating range of the robots and the linear rails. The rotating process of the SCC case will be achieved by the external rotating tooling.

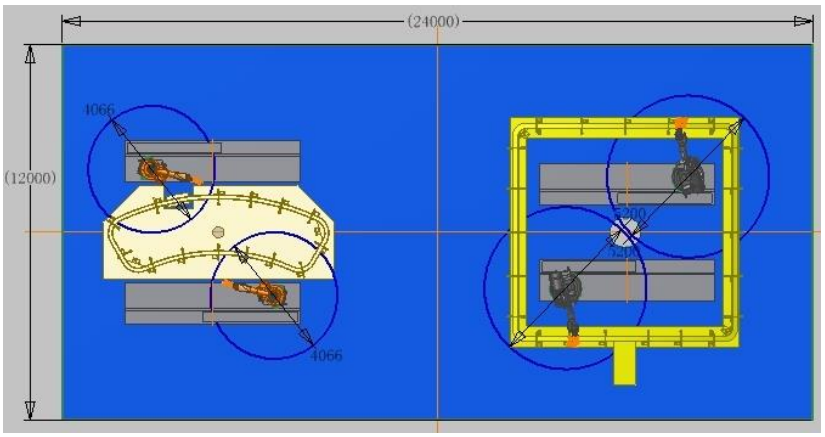

Figure 2.16 CC overview of laser welding of ITER CC case closure welding

2.3.5 Comparison of the three welding schemes

Contrasted with traditional welding methods, the three welding processes all have the advantages of low heat input and low welding deformation. Theoretically, each of the three welding processes has the feasibility for the ITER CC case closure welding and can achieve the welding requirements.

The three welding processes all belong to the type of precision welding which will meet the high requirements of the precision manufacturing and assembly of the case. Based on a 20mm welding depth, the CC case can be welded in one pass by EBW but in multi-pass by NG-TIG welding and LBW. Multi-pass filler wire welding technology will further decrease the welding heat input and control the welding deformation by low power welding. On the other hand, the filler wire will decrease the precision of the manufacture and assembly of the CC case, which is particularly important for the larger size and complex structure of the CC case.

The EBW was worked in a vacuum environment and a large vacuum chamber needed to be built for the large size of the CC case. Moreover, the SCC case needed to pass in and out of vacuum chamber many times which brought the vacuum process of the vacuum chamber. An autogenous welding process of EBW welding for the CC case was considered, which would have brought the requirements to a nearly non-assembly gap of the case. A non-assembly gap would require an extremely strict manufacturing precision, difficult to achieve for such a large and complex structure. For this reason, plus the expensive hardware cost and electron radiation, EBW applied in the CC case closure welding was restricted.

In contrast with EBW and LBW, NG-TIG welding technology was the most advanced and stable for welding austenitic stainless steel. However, NG-TIG will take maximum time for the case closure welding based on the welding structure and the amount of welding. Moreover, NG-TIG welding will bring more heat input and welding deformation than high energy beam welding. According to the NG-TIG welding scheme for the CC case, the two flexible rails were designed to support the welding carriage. It is complicated to alternate remove and install rails and fixtures to work continuously. Because the NG-TIG welding devices were fixed on the case, they would certainly have affected the welding process and increased preparation before welding.

In contrast with EBW, LEW can work in a non-vacuum environment, and its welding process will decrease the requirements of manufacturing and assembly precision. Contrasting with NG-TIG welding, LBW belongs to a high energy beam welding process which would bring lower welding heat input and lower welding deformation. Moreover, laser welding belongs to the non-contact welding process; the laser welding process will not affect the case rotating process. Based on a series of investigations, discussion and preliminary pre-research experiments, the laser welding process was determined as the best alternative to be applied to the ITER CC case closure welding.

2.4 Analysis of the laser welding scheme

As an automatic welding, laser welding has two welding processes. One has a movable workpiece and stationary laser beam, the other has a movable laser beam and stationary workpiece (Wang, 1992). Considering the large size and complex structure of the CC case, the welding process of a stationary workpiece and movable laser scanning was used on this scheme.

Usually, a laser processing head as the laser welding tooling is realized by a portal frame and an industrial robot. The portal frame has the characteristic of a large welding space and the industrial robot with more freedom has the characteristic of high precision for especially complex workpieces. For the large size and complex structure of the CC case, the industrial robot is more suitable because of its high precision. The laser welding space limitation of the industry robot can be solved by increasing the number of robots and adding external axis (linear rails).

Because of the large size, complex structure and long weld seam in this case, the basic requirement of the laser welding scheme design is that the robotic arm must arrive at each weld seam accurately. Two laser welding schemes were designed based on this basic requirement.

Scheme 1 uses one robot and rotary table as shown in Figure 2.17. The case is put on the rotary table, and the robot is seated on the external rail and located on one side of the case. The laser beam covers all weld seams via the robotic motion on the external rail and the motion of the rotary table. The robot is moved to the far end to avoid interference with the motion process of the rotary table. The rotary table and external rail are stationary and only the robot travels in order to decrease the manufacturing costs of the rotary table and external rail, and to increase arrival accuracy.

Scheme 2 uses multi-robot and external rails as shown in Figure 2.18. The four robots and their external rails were designed for this scheme. Each robot is located at each side of the case and is responsible for the weld seam of its side. Considering the size of two types of CC cases, one robot is designed to be inside the SCC case and BTCC is inside the SCC case. As with the scheme 1, only the robot arm will travel to increase arrival accuracy during the welding process. After one welding, the robot will travel on the external rail to the next welding position and only the robot arm will be moved during the welding process of the next welding position.

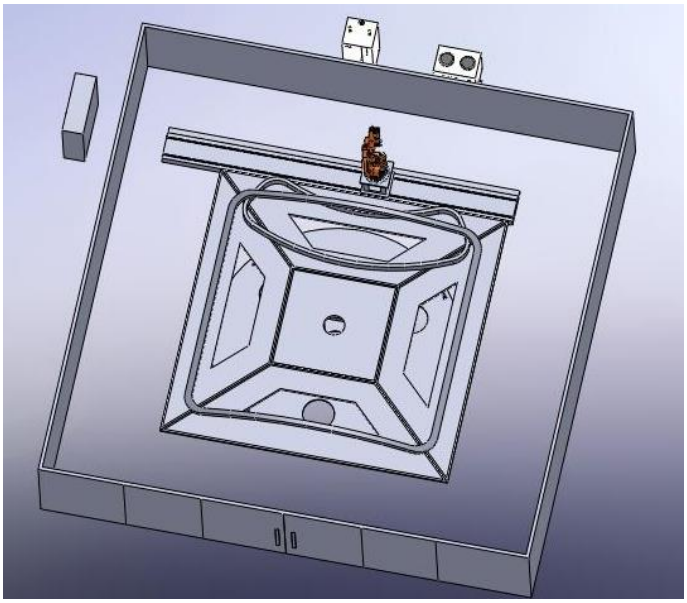

Figure 2.17 Overview of Scheme 1 for case laser welding

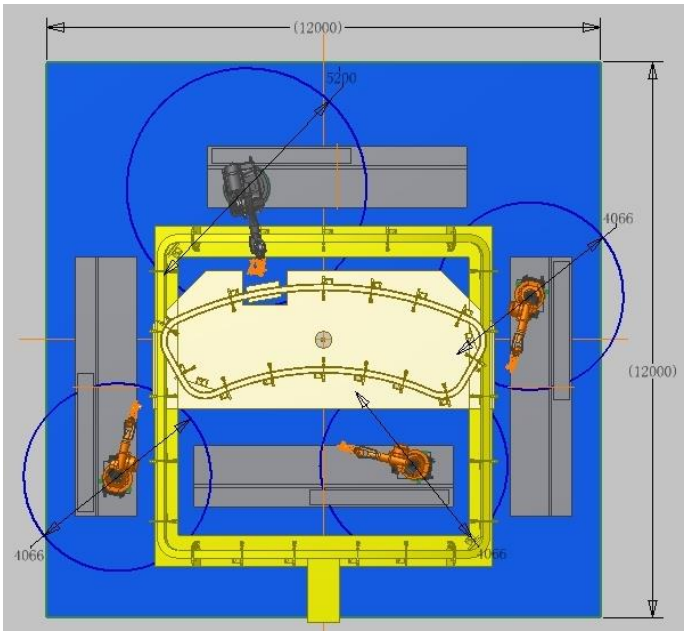

Figure 2.18 Overview of Scheme 2 for CC case laser welding

The robot arm can arrive at all weld seams and weld them in both schemes. Scheme 1 uses a single robot but needs the rotary table to move the case. A reasonable welding sequence to control welding deformation is crucial for the CC case with its large size. Thus, scheme 1 is inconvenient since the rotary table needs to move frequently. Scheme 2 uses four welded robots with their external rails. This scheme is simple and easy to work during the welding process, but its disadvantage is an excess of robots.

Based on an analysis of the two schemes, and keeping in mind the size and shape of two types of CC cases, scheme 2 best optimizes the final laser welding scheme. The number of robot arms is decreased by a reasonable layout of the case, robot and external rail. The final laser welding scheme is shown in Figure 2.19.

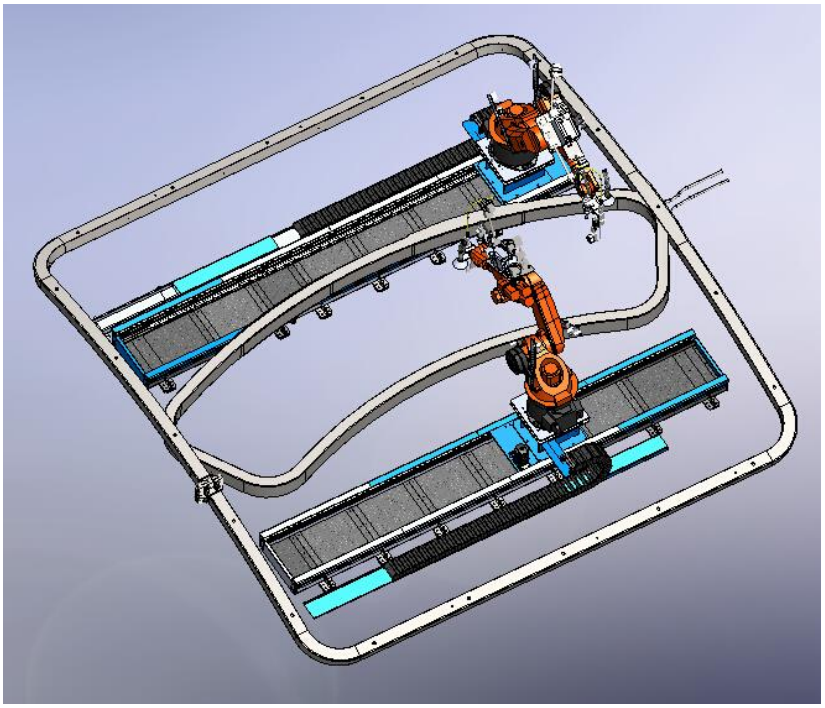

Figure 2.19 Overview of the final laser welding scheme of the ITER CC case

As shown in Figure 2.19, this scheme was achieved by two robots and their external rails. Because the two types of cases are welded separately, no position interference happens. The BTCC case is located inside the SCC case and the robots and their external rails are designed to be located at the middle of the two types of cases. The weld seam of the case will be covered by robot arms based on a reasonable arrangement of the external rails. In order to ensure the feasibility of this scheme, the welding motion simulation of the robots was done based on the operating space of the robots (using the KUKA professional welding robot KR60HA). The simulation process determined the reach ability of the robot arms along all the weld seams of the case.

The simulation results show that the overlapping space of the two robots is small during the welding process. Furthermore, a dead zone exists where the robot arm fails to arrive during the SCC case welding process. As shown in Figure 2.20, the robot arm arrives at the dead zone by adjusting each axis, but the robot has no effective welding at this posture.

According to the simulation result of the robotic motion, the welding space should be increased. Since the operating space is limited by the robot and the installed position of the external rail, an external module was added. A manual slide (shown in Figure 2.21), which has a 120mm sliding distance, was added to the robotic base. During the SCC

case welding process, it will be pushed to close the welding position of the dead zone mentioned in the previous simulation.

Figures 2.22 and 2.23 show the simulation result before and after the manual slide was added. For the SCC case, the overlapping spaces of the two robots, before and after adding the manual slide, were 150 mm and 422 mm, respectively. In the BTCC case, the overlapping space of the two robots, before and after adding the manual slide, were 232 mm and 422 mm, respectively. The robot arm arrives at the dead zone of the SCC case easily and has the enough space to achieve effective welding.

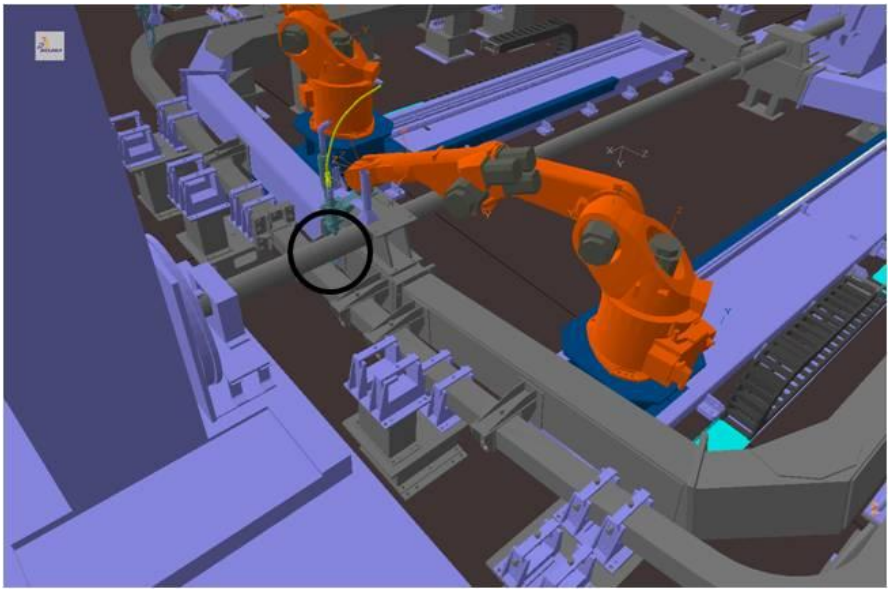

Figure 2.20 Dead zone of the motion simulation of the robot

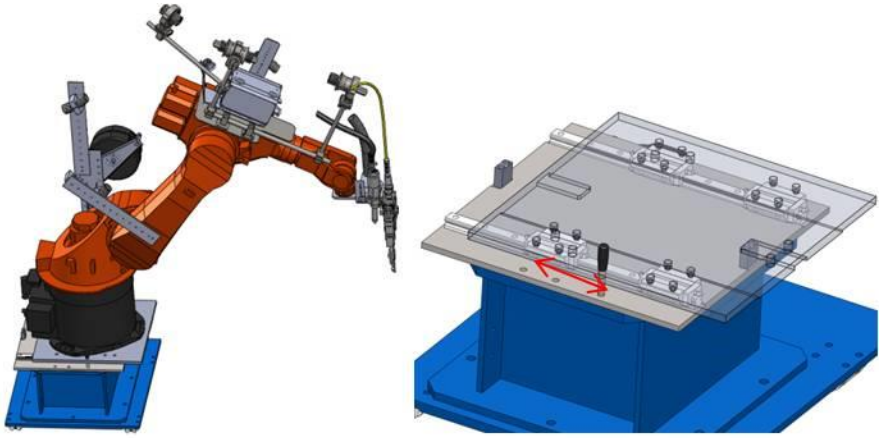

Figure 2.21 Manual slide of the robot

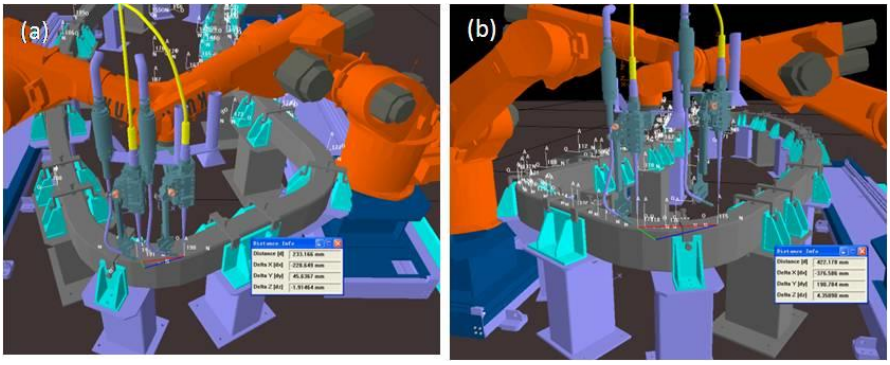

Figure 2.22 Simulation result of the BTCC case before and after the manual slide was added

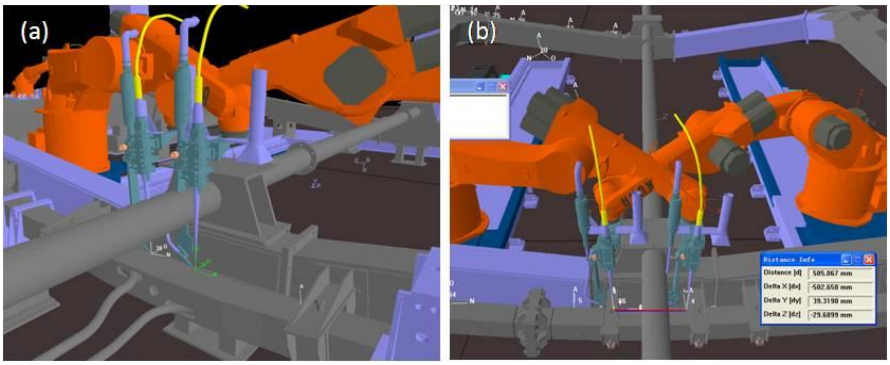

Figure 2.23 Simulation result of the SCC case before and after the manual slide was added

3 The welding fixture and electrical control

The preliminary laser welding system for CC case was designed in last chapter. The layout of welding robot, external rail and cases was determined. The integral system also needs the welding fixture for two cases and the electrical control module for the system.

Firstly, the welding fixture with planar structure for BTCC case and welding fixture with three-dimensional structure for SCC case were designed based on their special geometry. Secondly, according to the distribution characteristic of weld seam of SCC case, a special tilter for SCC case was designed, analyzed and optimized. Finally, the main devices for this laser welding system were introduced, and the electrical control module was designed and analyzed.

3.1 Design of the laser welding fixture

3.1.1 The design requirement

In order to reasonable control welding deformation of the large weldment, reasonable welding technology includes welding process, welding parameter and welding sequence should be chose, and also rigid fixation should be used which means utilize the fixture or temporary support to give the mechanical fixation and remove them after the cooling of weldment. In the traditional welding orientation usually use the positioning principle of 6 points. The principle is shown in Figure 3.1, three points of a_1, a_2, a_3 reflect the main positioning surface to limits the rotating freedom of X and Y direction and movable freedom of Z direction, a_4, a_5 reflect the side surface B to limits the movable freedom of X direction and rotating freedom of Z, a_6 reflect the side surface C to limits the movable freedom of Y direction. 6 degrees of freedom of weldment are all limited and completely fixed by this method. In the actual welding situation and detailed requirements of welding fixation, welding fixture was designed based on the positioning principle of 6 points (Chen, 2004).

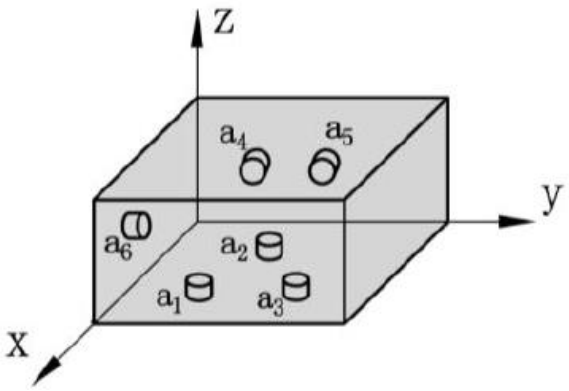

Figure 3.1 Overview of positioning principle of 6 points

Aim at the ITER CC case closure welding, the requirements of welding fixture during the assembly and welding process are following:

1. According to the geometry characteristic, the welding platform should be designed for the welding process. A planar structural platform will be designed for BTCC case. Moreover, a three-dimensional structural platform should be designed for the SCC case, also satisfying the situation of different geometry profile based on the different side.

2. Because of the large size and complex manufacturing process of CC case and the strict requirement of assembly precision of laser welding, the fixture should be designed to make the two parts of case was fixed and provide the clamp force to decrease or relief the assembly gap. Moreover, the fixture also needs to ensure the unfitness of groove during the case assembly process. Figure 3.2 shows the overview of the gap and unfitness during the case assembly process.

3. The fixture will provide the clamp force to restrain the welding deformation in the welding and cooling process.

4. Aim at weld seam are located at upper and lower sides of SCC case, a special tilter and its loading clamp should be designed to provide the rotating function and prevent the drop and shift of case under the influence of gravity during the rotating process, respectively.

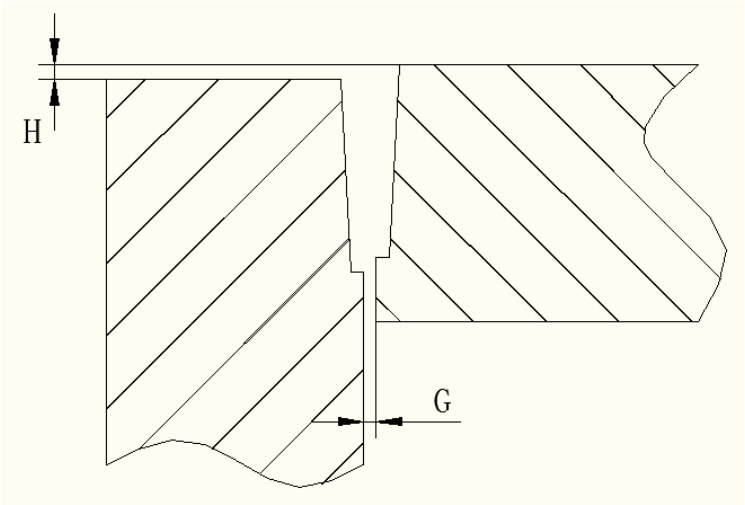

Figure 3.2 Overview of gap and unfitness during the case assembly（H-joint miss match，G-air gap）

Thus, according to the large size, complex geometry profile and special welding structure of CC case, reasonable design of welding fixture to meet the requirements of case assembly, welding and deformation control is extremely important.

3.1.2 Welding fixture for BTCC case

According to the design requirements of laser welding fixture for BTCC case, fixture should be provide the functions of welding platform and adjust the assembly tolerance and rigid constraint. The assembly figure of welding fixture for BTCC case was shown in Figure 3.3. The BTCC case welding fixture includes a number of ground support bases and C-type clamps. The ground support bases provide the welding platform and the C-type clamps will provide the clamping force to adjust the assembly tolerance by the blots together with the ground support bases. The structure of ground support base and C-type clamp was convenient to assembly and separate. The assembly process is level the adjustment plate to install the ground support base by installation of chemical blots, then put on the BTCC case and assemble the C-type clamps to ensure the assembly tolerance. Also the welding fixture will provide the function of rigid fixation to restrains the welding deformation. The specific C-type clamps will be removed if the C-type clamps will limit the continuous movement of laser welding head to ensure the feasibility of laser welding process.

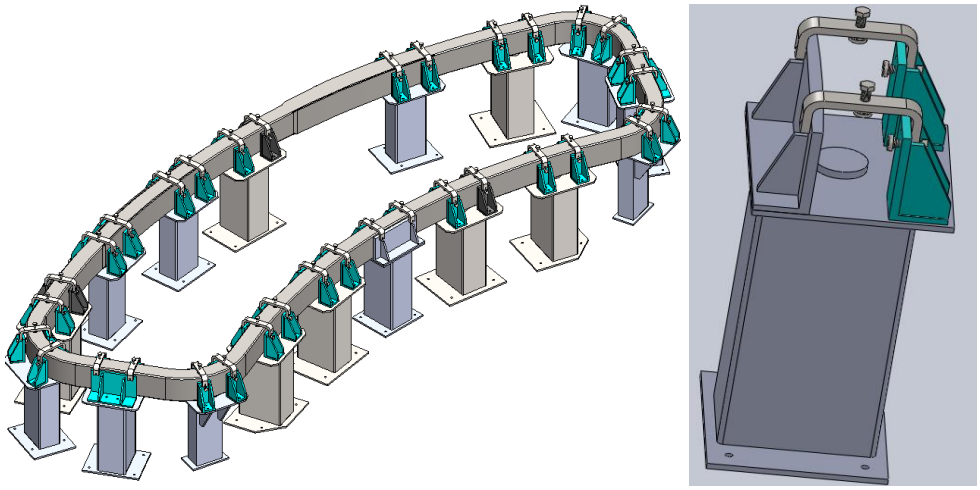

Figure 3.3 Overview of welding fixture for BTCC case

3.1.3 Welding fixture for SCC case

According to the profile geometry, dimension and welding structural characteristic of SCC case, the dimension is larger than BTCC case and the three-dimensional structure which presents shape of tile is complex than BTCC case. Because of the design of L-shape of SCC case, the weld seams of SCC case are located at front and back sides. Thus, the design of platform of SCC case welding must considerate and adapt of the two types of shape in the different side of SCC case. Doubtlessly, the fixture also needs to restrain the assembly tolerance and the welding distortion during the case assembly and welding process.

The assembly figure of welding fixture for SCC case was shown in Figure 3.4. The SCC case welding fixture includes a number of ground support bases and C-type clamps. Each ground support base was designed based on the actual height distribution of each segment of SCC case. The function mode of SCC case welding fixture and the welding assembly process is consistent with BTCC case. Aim at three-dimensional structural characteristic of SCC case, the case will presents arched shape when case is assembled in front (front is defined when the large arc segment is upward, otherwise is back) and the case will presents concave shape when the case is assembled in back. Thus, according to this special situation, ground support base is designed to include two parts to provide welding platform for front and back. As shown in Figure 3.5, the ground support base can be rotated to achieve this supporting process.

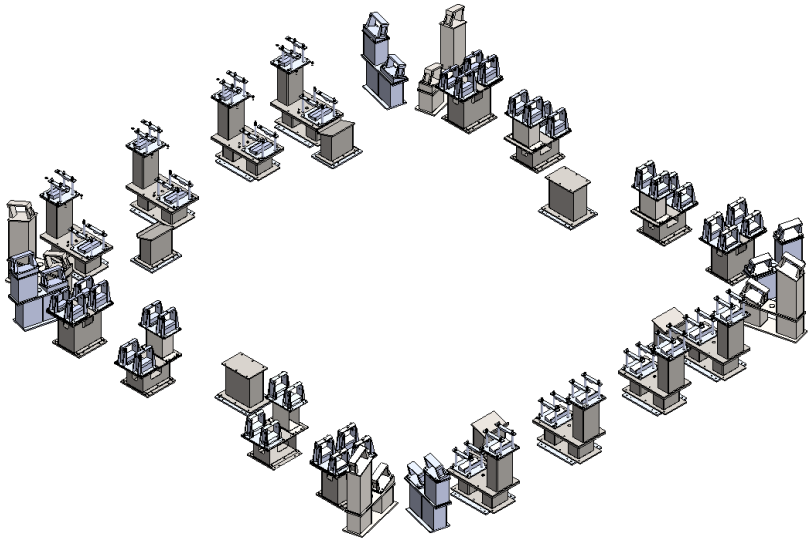

Figure 3.4 Overview of the assembly of welding fixture for SCC case

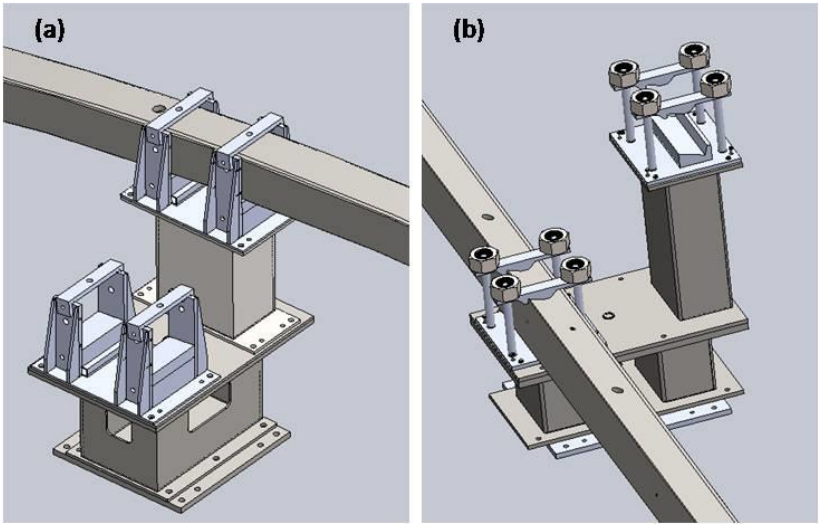

Figure 3.5 SCC case welding fixture (a for large arc segment，b for linear segment)

3.1.4 Welding tilter for SCC case

According to the design requirement of welding fixture for SCC case, a welding tilter must be developed to meet the demand of rotation during the welding process. According to the geometry characteristic of SCC case, the mechanical parts of welding tilter should include tilter framework, rotating axis, load-bearing jig and ground support base. The tilter framework, which used to assemble the case, was designed to be manufactured by several sub-parts welded together and has the same shape with case.

The rotating axis is used to realize the rotating process and the load-bearing jig is used to fixation. On the basis of above analysis, the welding tilter for SCC case was analysed by FEA and optimized.

Figures 3.6-3.8 show the results of equivalent stress and deformation of cruciform structural tilter during the rotating process from FEA. Three figures show the position results of horizontal, 45° and vertical, respectively. Table 3.1 lists the material properties used in this analyzation.

Table 3.1 Materials properties of analysis of welding tilter (Augey, 2008)

		Elasticity modulus E(GPa)			Passion ratio V			Shear modulus G(GPa)		
		E_x	E_y	E_z	V_{xy}	V_{yz}	V_{xz}	G_{xy}	G_{yz}	G_{xz}
Winding pack	Composite	22.4	21.5	67	0.37	0.11	0.33	2.85	11.5	20.4
Ground insulation	Composite	12	20	20	0.33	0.17	0.33	6	6	6
Case	316LN	205			0.3			78.8		
Tilter framework	Q235B	206			0.3			79.2		
Central axis	Q345B									
Load-bearing jig and support base	Q235B									

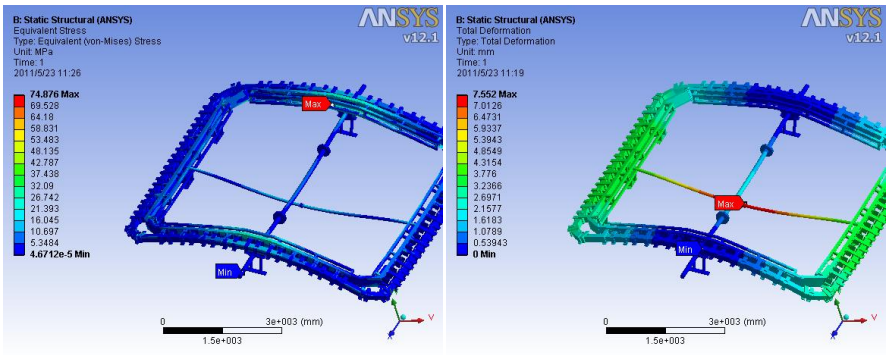

Figure 3.6 Distribution of stress and deformation of cruciform structural tilter (horizontal)

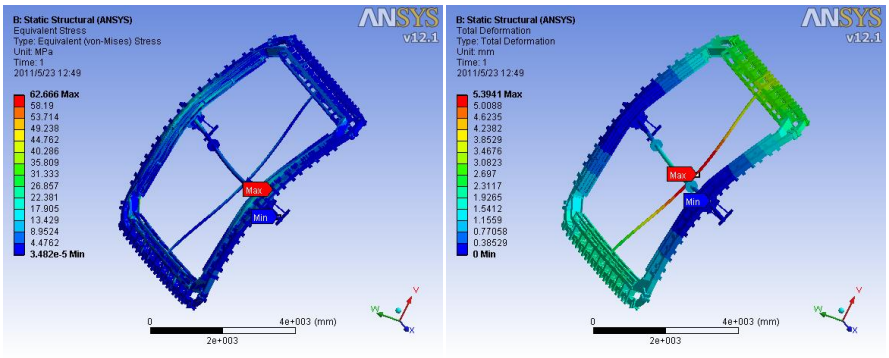

Figure 3.7 Distribution of stress and deformation of cruciform structural tilter (45°)

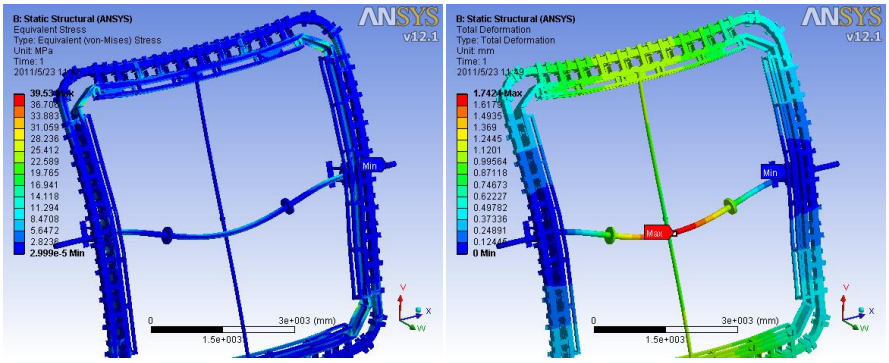

Figure 3.8 Distribution of stress and deformation of cruciform structural tilter (vertical)

According to the results of FEA in rotating process, the highest deformation of horizontal, 45°and vertical positions are 7.6mm、5.4mm、1.7mm respectively and highest stress of horizontal, 45° and vertical positions are 75Mpa、63Mpa、40Mpa respectively. Obviously, the structural strength of welding tilter is enough to realize the rotating process based on the stress analysis. On the basis of the sufficient strength to realize the rotating process, the structure of welding tilter should be as simple as possible. Thus, the welding tilter was optimized based on the cruciform structural tilter. The structure of framework was optimized to the square tube, the number of load-bear jigs was decreased and the type of rotating axis was optimized to single central axis.

Figures 3.9-3.11 show the distribution of stress and deformation during the rotating process after optimization. These Figures show the positions results of horizontal, 45°and vertical, respectively.

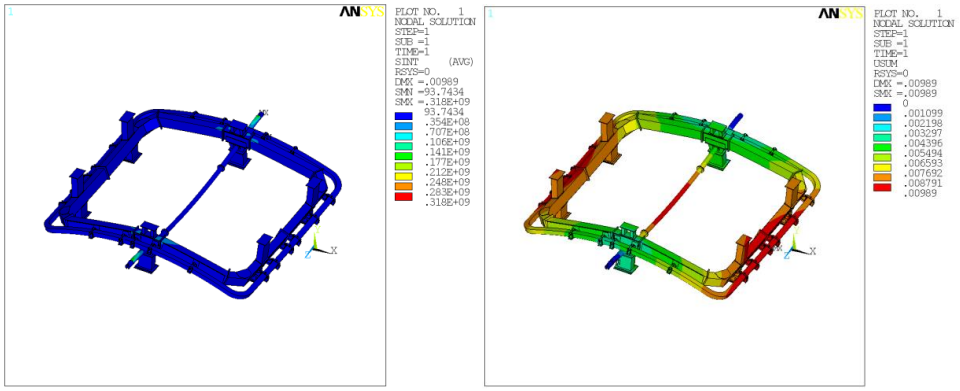

Figure 3.9 Distribution of stress and deformation after optimization (horizontal)

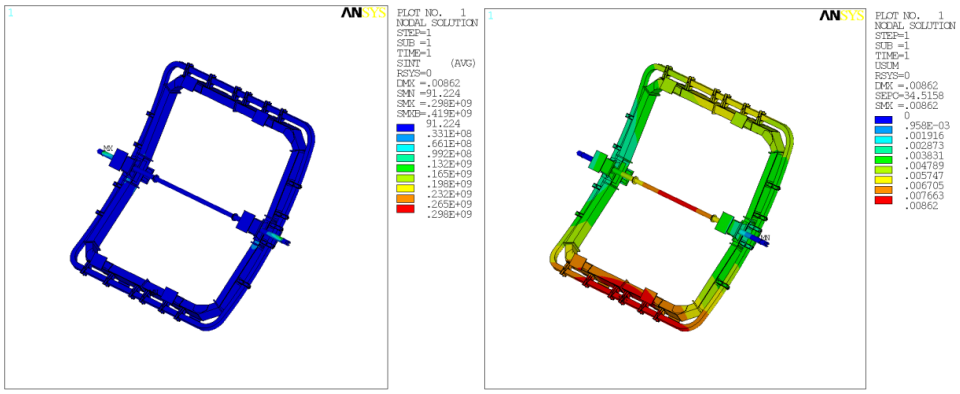

Figure 3.10 Distribution of stress and deformation after optimization (45°)

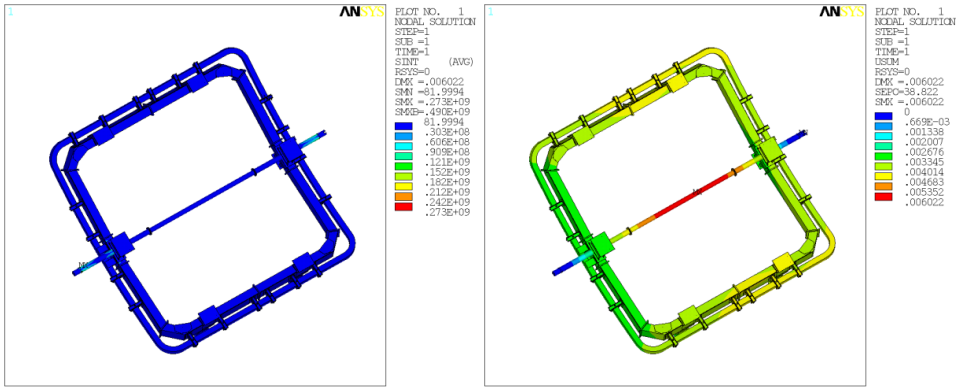

Figure 3.11 Distribution of stress and deformation after optimization (vertical)

According to FEA result of deformation in rorating process, the highest deformation of horizontal, 45°and vertical positions are 9.9mm、8.6mm、6.0mm respectively. According

to FEA result of stress, the highest equivalent stress of horizontal, 45° and vertical positions are 318MPa、298MPa、273Mpa respectively. The highest stress was occurred at the two sides of the rotating axis in the rotating process. The position of highest stress has the structural characteristic of discontinuous. The type of structure usual has the high peak stress, while peak stress was an impact factor for fatigue not for static analysis according to the ASME VIII standard. In the static analysis, a path in the section for the maximum linearization stress for Pm and Pm+Pb was defined. Figure 3.12 shows the stress distribution of horizontal on the path defined on the maximum section.

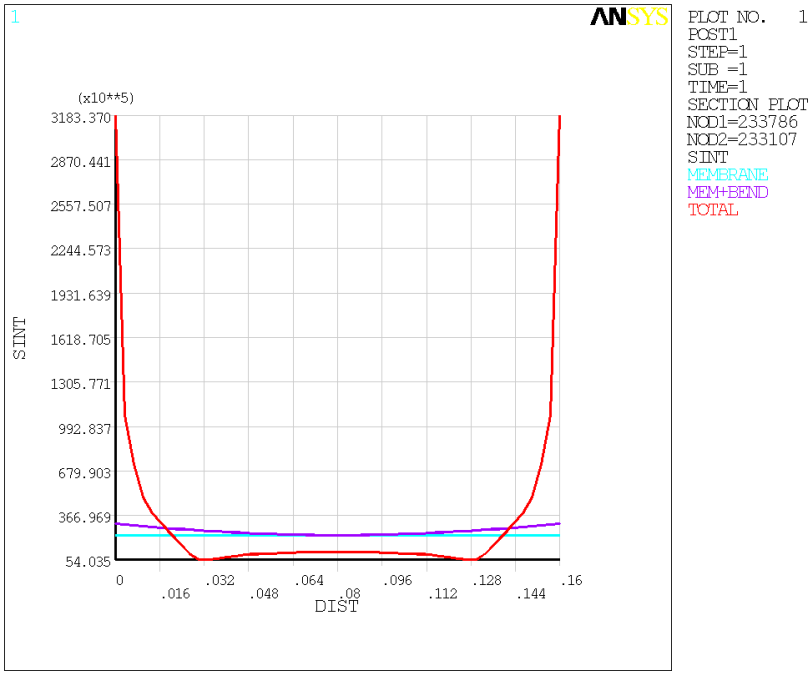

Figure 3.12 The stress distribution of horizontal on the path defined on the maximum section (Pm and Pm+Pb)

The stress distribution of three positions on the path defined and their evaluation criteria was listed in Table 3.2. It is clear to found that the strength of optimized welding tilter meet the requirement of rotating process.

Table 3.2 Stress evaluation for rotating process

position	Pm(MPa)	Allowable stress	Pm +Pb (MPa)	Allowable stress
horizontal	24		30	
45°	22	Sm=230MPa	28	1.5*Sm=345
vertical	21		26	

The final welding tilter includes the tilter framework, rotating axis, 20 load-bear jigs, ground support and modules of driving and controlling. The welding tilter has two linear degrees of freedom and 1 rotating degree of freedom. In the rotating process, the tilter will up to a certain height, move away to keep a distance from welding area, realize the rotating process, move back to the welding area and assembly. The whole moving and rotating process should keep slow and uniform. Figures 3.13-3.14 show the rotating process of SCC case and the actual welding tilter, respectively.

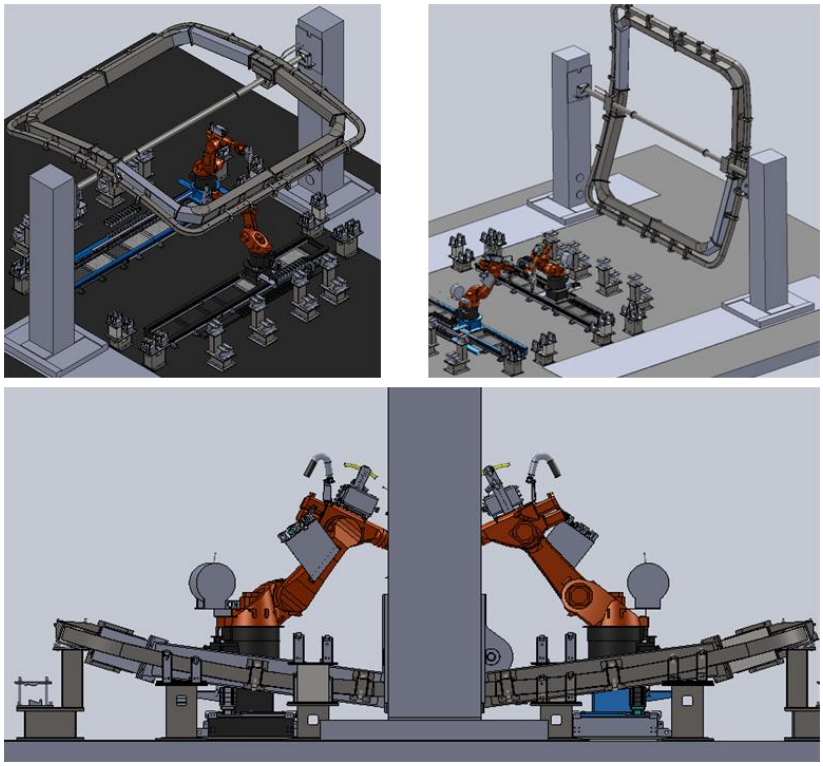

Figure 3.13 Rotating process of SCC case

Figure 3.14 Overview of actual welding tilter

3.2 Electrical control

3.2.1 Main devices

1. Laser

YLS-4000 fiber laser of IPG produced was used on this welding system. The fiber laser uses the optical fiber to transmit laser beam which is easy to integrate with robot. Because of the large size of CC case, fiber transmission is particularly reasonable to realize the wide range activities of robots. Moreover, the fiber laser with the wavelength of 1070-1080 nm has a good laser beam absorption for the steel (Liu. 2003; Yang et al., 2002; Richardson et al., 1997). And YLS-4000 fiber laser has two channels to alternately support two laser welding head with rated power by control the optical gate. The 4kW laser power cannot penetrate the 20mm thick austenitic stainless steel 316LN in one layer. Thus, the technology of multi-pass with filler wire will be applied.

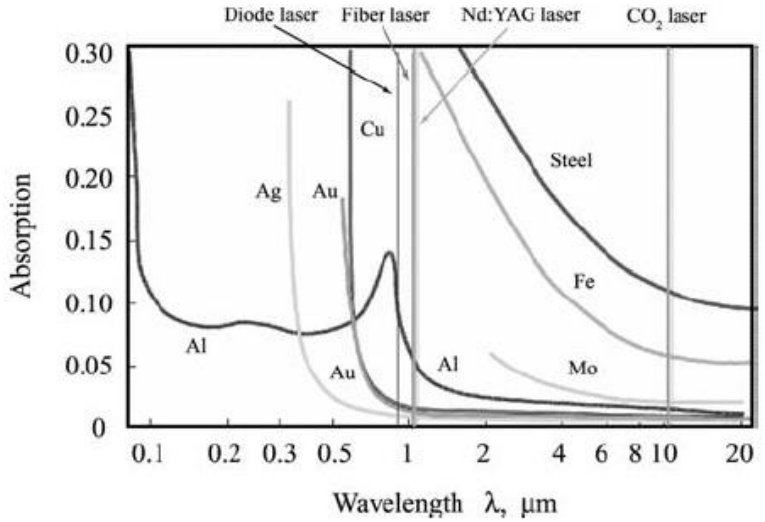

Figure 3.15 Laser absorption curves of different metal material under different wavelength (Zuo, 2002)

2. Welding robot

Contrast with manpower, industry robot has the advantages of high speed, high productivity, good stability and high fatigue resistance. Currently, industrial robots include arc welding robot, spot welding robot and laser welding robot are widely applied on the welding industry. Because of the laser welding belongs to the high accuracy welding process, the robotic movement must has the high repeatability in positioning accuracy and high trajectory accuracy to ensure the required accuracy of tool center point and the weld quality.

The professional laser welding robot KR60HA produced by KUKA company was chose in this welding system. The robot includes the robot arm, control cabinet, handheld teaching box. The KR60HA has 6 degrees of freedom and an external axis in the type of linear rail was added to increase the working range. The high repeat positioning accuracy and trajectory accuracy of KR60HA can be controlled inside ±0.05mm and ±0.16mm, respectively. The KR60HA has the several communication interface module (internet, profibus and devicenet) to connect with peripheral equipment by these standard bus.

3. Wire feeder

Wire feeder includes wire feed machine and hot wire power was using the TS5000 produced by Fronius. The adjusting range of heater current is 0A-270A and the

adjusting range of wire feed speed is 0.2m/min-22m/min. The wire feeding process using the type of push and pull which is more stable than general type of push during the wire feed process. Wire feed nozzle was fixed on the laser weld head and was designed with the function of adjust the wire position and wire angle.

The final laser closure welding workshop was shown in Figure 3.17. The welding robot and welding fixture was inside of protection room and other devices were outside of protection room.

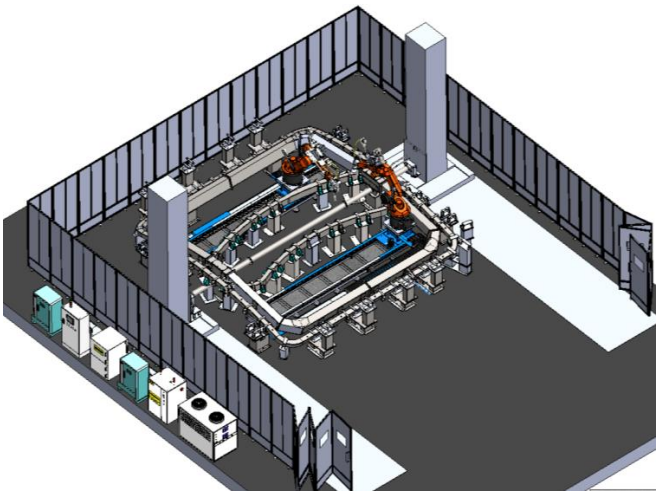

Figure 3. 17 The layout of the final laser closure welding workshop

3.2.2 Control system

3.2.2.1 Design requirement of control system

The basic components of laser welding system for ITER CC case include laser and chiller, robot system, hot wire feeder system and gas circuit (shielding gas and compressed gas). In order to achieve the easy operation and safe operation and increase the flexibility and mobility during the welding process, the four parts should be integrated together by electric control system.

Laser welding as a special process method and ITER CC case welding belong to large quantities of non-standard product processing, the welding system work must be ensured in long-term security and stability. Thus, a control system must be developed to ensure the security of processing system and long-term stability of manufacturing environment.

The functions of electric control system in the laser welding system include:

1.To achieve the integrated control of high-power fibre laser and its chiller and to ensure the security and stability of operation of fiber laser.

2.To achieve the external integrated control of the robot system and configure its external rail. The gear and rack of external rail was driven by motor. And external rail was controlled as an external axis of robot by robot control system.

3.To setup and real-time monitoring of the wire feed speed, welding voltage and welding current to ensure the stability and control of hot wire feed process.

4.To control the solenoid valve to setup and monitor the gas channel to cooperated protect and the security and stability of welding system.

5.To create a user-friendly and simple operation interface to achieve the human-computer interaction and convenient operation for operator.

3.2.2.2 The master controller of control system

The control system of ITER CC case welding is a real-time monitoring of intelligent automatic control system. The core part of the control system is central control unit. In the industrial control computer system, several typical control system includes industrial control computer IPC (Industrial Personal Computer), SCM (Single Chip Microcomputer) control system and PLC (Programmable Logic Controller) control system. Table 3.3 shows the comprehensive comparison includes their characteristics and stability of these control system (Peng, 2009).

Table 3.3 Comparison of control system of IPC, SCM and PLC

Controller	IPC	SCM	PLC
Reliability	High	Low	higher
Working mode	Interrupt mode, satisfaction of program waiting condition		Circular scanning mode
Programming language	Assembler, high-level programming language		Standard programming language
Working environment	High demand	Clear, less interference	Low demand, adapt to industrial field environment
Requirements of user	Need special training	Difficult programming	Simple programming
System software	Strong function, need large storage space	Small storage space	Special function, small storage space
Cost	higher	low	high
Application fields	Family, office, management and scientific computing	Instruments, household appliances and other electronic consumer products	Specialized in industrial process control

In the laser welding system of ITER CC case, this kind of high-power fibre laser was applied on industrial field with complicated environment and the continuous working time is long. Thus, the reliability is the key technology requirement for the development of this electric control system. PLC control system is designed for the industrial field environment. Also, PLC has a good interface performance and can process analog input and output signals via A/D, D/A converter just like IPC and SCM. Moreover, PLC can control the level signal to drive solenoids, relays and solenoid switches directly. And PLC control system applied widely on the large laser welding system. Therefore, PLC control system was used as the core control unit of the laser welding system for ITER CC case.

3.2.2.3 Controlled object

The purpose of the electric control system is to achieve the control requirements of the controlled devices or manufacturing process to increase the productivity and product quality. The first step to build the electric control system for ITER CC laser welding system is also to determining the controlled object. ITER CC case laser welding system

includes several parts: laser and water-cooling machine, robot system, hot wire feeder system, gas circuit system, user interface and security alarm system.

1. Control analysis of laser and chiller

IPG fiber laser has a variety of interface communication abilities (serial interface and parallel interface).The main laser setting parameters will be written in the laser programme before the welding process. The setup signals of these laser setting parameters will send to PLC and PLC will response to realize monitoring and work.

Chiller was used to provide the cooling of laser and laser processing head during the welding. The temperature and flow of cooling water was demanded based on the actual work situation during the laser process. The laser will send the alarm signal and stop working if the temperature and flow of the not achieved the demand. Also PLC will receive these signals and stop all the welding related work. These will be back to normal until the alarm signal is removed.

2. Control analysis of robot

As the most common laser welding tooling, robot has the high repeat positioning accuracy and trajectory accuracy, especially the multi-DOF (degree of freedom) robot. As the complex structure and large-size of ITER CC case, multi-DOF industrial robot was chosen as the laser welding tooling for ITER CC case closure welding.

According to the actual project situation, the welding mode of one fibre laser and two robots were designed. The fibre laser was has two channels to alternately support two laser welding head with rated power by control the optical gate. During the welding, PLC will realize the time-sharing control of two robots. These control signals include the robot corresponding optical gate number, laser program number, welding speed, wire feeder speed, hot wire current and voltage.

3. Control analysis of hot wire feeder system

There are two hot wire feeder machines corresponding to each robot in the ITER CC case laser welding system. The wire feeder machine was connected with robot by devicenet directly. Base on the connection with robot, PLC can setup and monitor the hot wire parameter in the touch screen during the welding.

4. Control analysis of gas circuit

The gas circuit will provide the compressed air for motion of cylinder and the shielding gas for welding. In the control of gas circuit, PLC will control the corresponding solenoid valve to open and close the shield gas and compressed air.

5. Control analysis of safety door

According to the safety knowledge of laser welding and laser welding device, the safe protective measures must be ensured in the laser welding workshop. The safe protective measures include wear protective glass and protective room. All the personnel close the welding area must wear protective glass during the laser is open, and the safety door as a double protective method for personnel. There is a limit switch was installed in the safety door. The laser will be enabled if PLC received the limit switch signal of safety door was closed. Otherwise, the laser was disenabled whatever the safety door is not closed or not closed completely. Before reopen the safety door, the PLC must receive the signal of laser is closed, robot is stop and the welding finished. After these steps, the PLC will send the signal to drive motor of safety door and the safety door can be opened.

3.2.2.4 Total design of control system

Electric control system as the core unit of intelligent laser welding system, PLC control system was used on this laser welding system based on the previous analysis of controlled object and requirements. The PLC uses the medium-sized PLC S7-300 of Siemens. The electric control system composed of human-computer interaction module, PLC control module, digital signal input and output module. PLC is the core of electric control system, operation of system and monitoring of state were done on the touch screen. The real-time data measured from welding site will send to PLC to process and send to the human-computer interaction interface. On the other side, the setting parameter on the touch screen will send to each part via PLC, and realize to integrated control the laser and water-cooling machine, robot and wire feeder machine. If there dangerous or error signals are occurred, the alarm information will be appeared on the touch screen.

The overall structure design diagram of control system was shown in Figure 3.18. The unit design method was used: PLC is the control core, touch screen is display and input to build the real-time communication with laser and robot and control the welding gas circuit and safety door. Based on the network communication and upper computer system, electric control system of overall ITER CC case laser welding system was built.

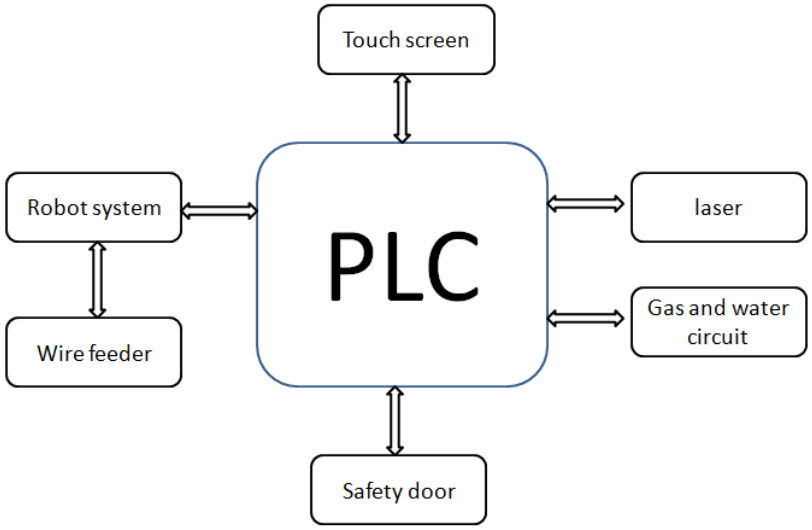

Figure 3.18 Schematic diagram of control system

In this control system, PLC will connect with laser, gas and water circuit, and safety door by signal line and connect with robot by profibus DP, wire feeder will connect with robot directly by devicenet. Building the hardware configuration of master-slave station relations to realize the data communication and monitoring and control all the system by touch screen.

3.2.2.5 Software design

According to the controlled requirements of ITER CC case laser welding system, human-computer interface display was designed combined with hardware system in this project. Human-computer interface composed of main control interface, laser control interface, robot control interface, wire feeder control interface, gas circuit control interface. Figure 3.19-3.20 shows the organization chart of human-computer interface and main control interface, respectively.

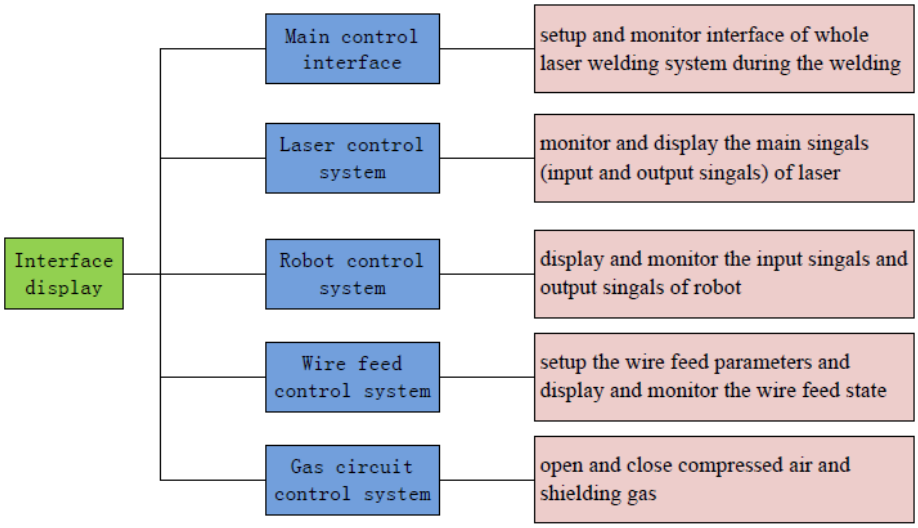

Figure 3.19 Organization chart of human-computer interface

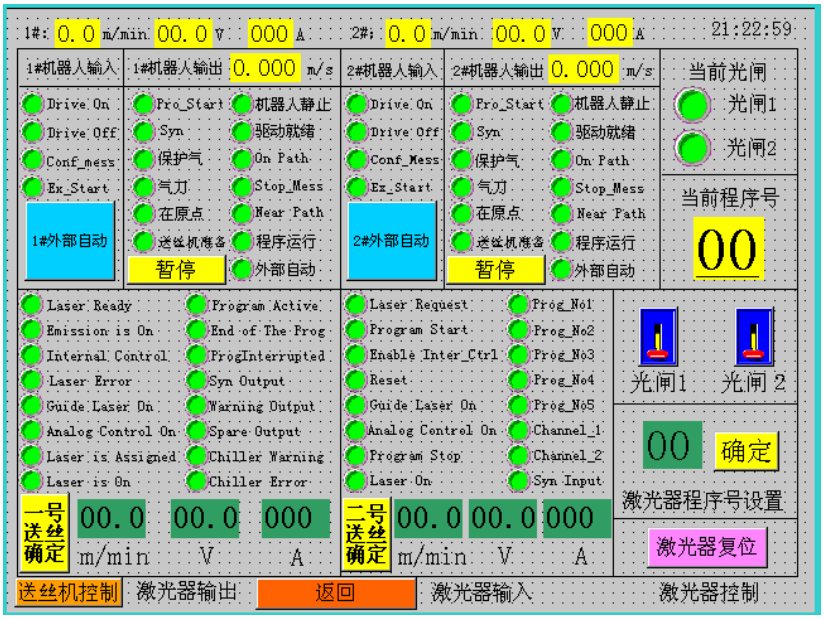

Figure 3.20 Main control interface

1. Main control interface

Main control interface is the setup and monitor interface of whole laser welding system during the welding. After the welding program is written and taught, the robot will

adjust to external automatic mode and enter automatic welding mode. The operating state and related signal of all devices were monitored and displayed on the touch screen.

2. Laser control interface

This interface monitors and displays the main signal (input and output signal) of laser. At the same time, the corresponding optical gate number and the corresponding laser program number with welding program of robot will be chosen in this interface.

3. Robot control interface

The robot control interface is used to display and monitor the input signals and output signals of robot. Input signals include robot drive open, drive close, manual wire feeder, etc. Output signals include laser program execution, air-knife state, light guiding state, optical gate state and program execution state, etc.

4. Wire feeder control interface

Wire feeder control interface is used to setup the wire feed parameters and display and monitor the wire feed state. The main parameters of wire feed include wire speed, hot wire current and voltage can be set on the interface. Also, according to the real-time communication with wire feeder, the actual value of wire parameter will be monitored.

5. Gas circuit control interface

This interface used to open and close compressed air and shielding gas. The gas circuit situation will be monitored before and during welding, and the compressed air will be manual opened to cleaning the weld seam after welding.

The programming software used STEP 7 of S7 series PLC in this PLC control system. STEP 7 is one of the SIMITIC industrial software of Siemens, and used to configure and program of SIMATIC PLC. The standard SETP 7 software package was equipped with three basic programming language of ladder diagram, function block diagram and statement list. The ladder diagram was used in this system because of its advantage of intuitive and easy to understand, also especially suitable for digital logic control.

According to the technology requirements and control requirements, the PLC control and robot control will be separate programmed in this welding system. Ladder diagram will be used on PLC program and KRL language of KUKA robot will be used on the robot program. The key points of the overall control system are the communication of PLC and laser, gas circuit, the communication of PLC and robot, the communication of robot and wire feeder. Thus, it is important to define the communication agreement of

PLC and robot, PLC and laser. According to the above communication agreement, program design was composed of communication control of PLC and laser, communication control of robot and wire feeder, communication control of PLC and robot, control program of welding robot. Figure 3.21 shows the communication control principle diagram of this laser welding system.

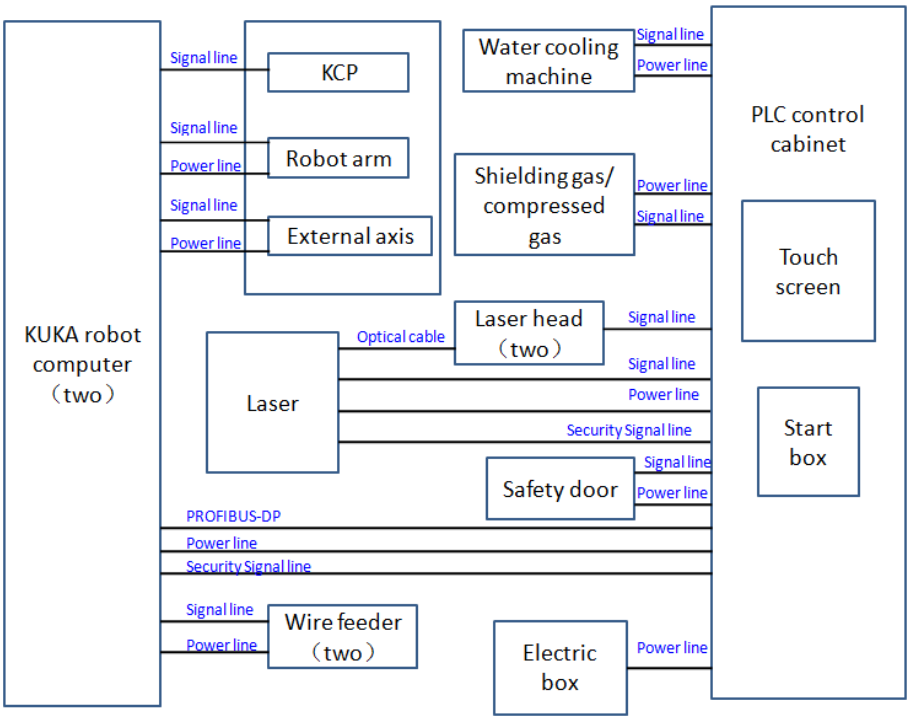

Figure 3.21 Communication control principle diagram

Figure 3.22-3.23 shows the PLC program flow and flow chart of robot welding

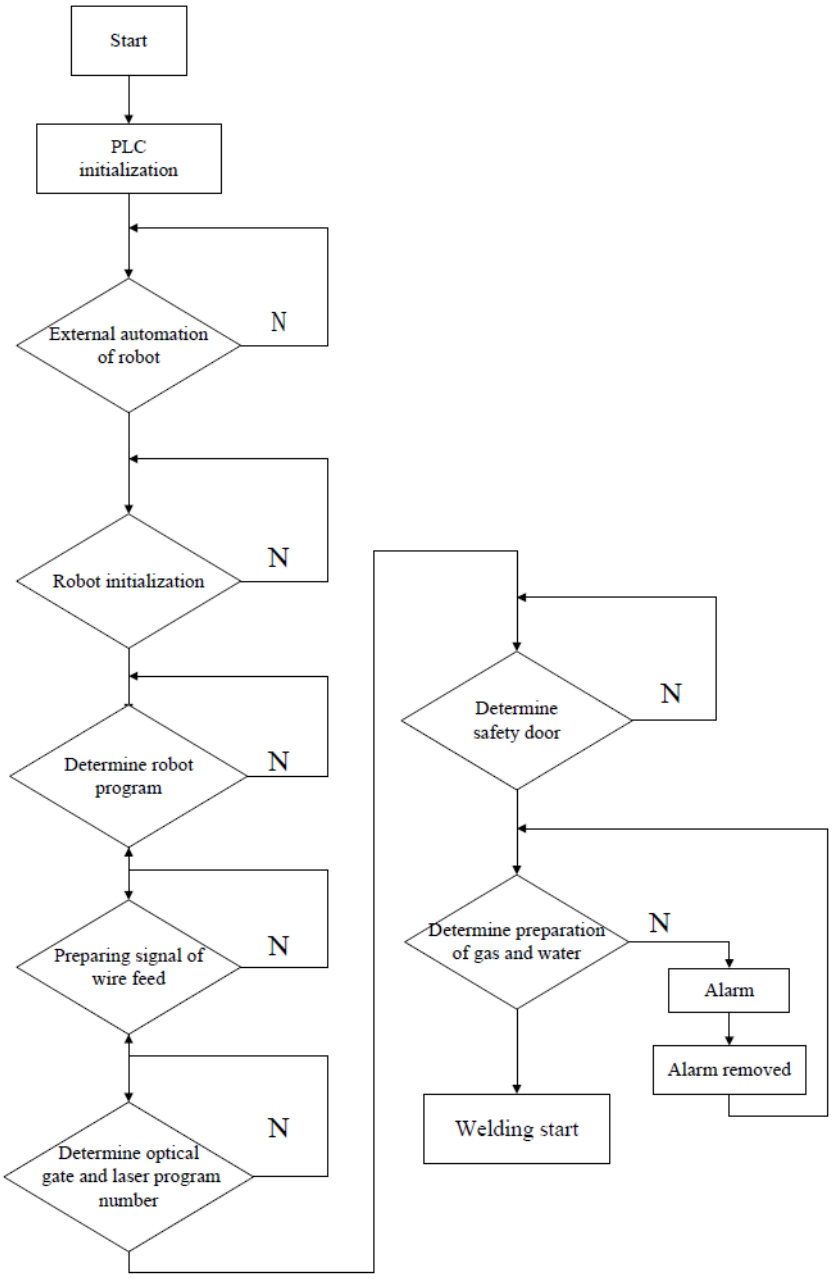

Figure 3.22 PLC program flow

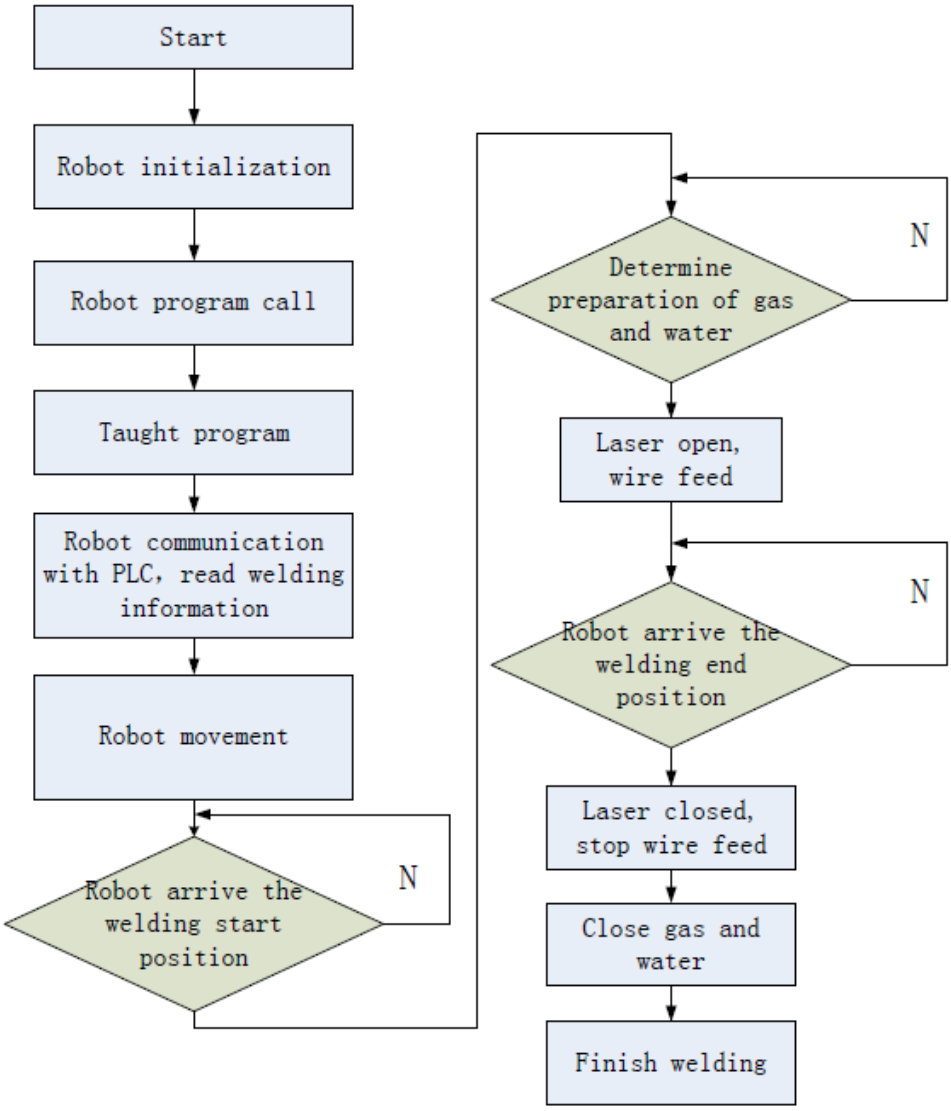

Figure 3.23 Flow chart of robot welding

4 Laser welding process and temperature control

According to the welding requirement of ITER CC case, the welding quality should meeting the level B of ISO 13919-1. Moreover, the heat generated by laser welding must not harm the superconducting coil behind of the case. The verification test was done to verifying these requirements.

4.1 Narrow gap laser welding with hot wire

4.1.1 Narrow gap laser welding

Laser welding of the thick plate has the problems of high requirement of assemble accuracy, difficult to control the welding quality, and rely on the high power laser. For the large size and 20 mm thick ITER CC case laser welding, it should take more attention on the problems of assemble accuracy, control of welding quality and the laser power for full penetration. Thus, the narrow gap laser welding was applied. The narrow gap laser welding has the advantage of decrease the requirement of assemble accuracy, also realize the lower heat input and cost to extremely decrease the welding deformation, improve the welding quality and reflect the advantage of laser welding (Guo, 2009; Xie et al., 2008; Beretta and Previtali, 2009; Kong et al., 2013). Figure 4.1 shows the schematic diagram of narrow gap laser welding process.

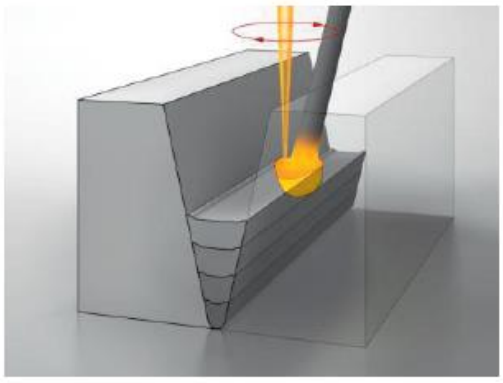

Figure 4.1 The schematic diagram of narrow gap laser welding process

According to the thickness of CC case, the width of laser welding groove should be designed in 2 mm-5 mm. Because of the divergence of laser beam propagation, the adaptation of laser beam propagation in the narrow gap was a challenge of narrow gap laser welding. During the narrow gap laser welding, the fusion problem of welding pool

and side wall should be considered based on the feasible laser beam propagation. If the smaller laser spot was used bring the small scope of laser welding pool, the flowing pool was expected to fusion with side wall together. However, the smaller laser spot generate the small molten pool, depend on the molten pool flow to solve the incomplete fusion of side wall is poor. Domestic and foreign scholars have the research of double beam or multi-beam and beam weaving to solve the incomplete fusion of side wall (Dahmen et al., 2000; Tsukamoto et al., 2011; Phaoniam et al., 2013; Xiao et al., 2006). In this project, the feasible design of narrow gap groove and beam propagation system was studied to decrease the sensibility of incomplete fusion of side wall.

The basic point to get good laser welding quality is to ensure the stability of welding process. The premise to ensure the stability of narrow gap laser welding process is to ensure the stability of wire feed process. Conventional narrow gap laser welding usually uses laser melt wire directly with mode of metal transfer or model of liquid bridge transfer. Because of irregular reflect of laser and wire, volatile molten pool and splash will lead to instability of welding process which easy to generate the defects of incomplete fusion and pore (Yu, 2010; Yu et al., 2010; Arata et al., 1986; Coste et al., 2003). The mode of hot wire was used in this project which means wire will be preheat by resistance heat and to combine with laser to generate molten pool. The hot wire has the advantages of better liquidity and better laser absorptivity, they will increase the stability of wire feed and laser welding process.

4.1.2 Narrow gap design

For the narrow gap laser welding of thick plate, the reasonable design of groove has an essential effect to welding productivity, seam quality and properties of welded joint.

4.1.2.1 Design rules

Contrast with design of traditional welding groove, the design of narrow gap laser welding groove not only related to material and thickness, also related to limited factors of laser beam quality, propagation quality, focus quality, and interactive of laser and wire. The design of narrow gap laser welding groove should aim to particularity of laser welding. The following there principles should be followed:

Firstly, the narrow gap groove should be as narrow as possible. Although laser welding with filler wire was different with laser autogenous welding, their welding nature are rely on the laser radiation to reach the purpose of metal melting. Wider groove needs wider molten pool which will needs increase the higher laser energy to provider the high-energy density of laser beam, this is limited of 4 KW laser in this laser welding

system. Under the reasonable groove, side wall may has the function of limit the wire swing in the groove which will increase the stability of wire feed and beneficial side wall absorb energy from laser and wire, and increase the fusion of side wall and filler wire. Moreover, the wider groove needs more filler wire which will lead to more welding layer, higher energy input and increase the welding deformation. Thus, the groove should be as narrow as possible to decrease the filling volume and deformation is the basic principle of design principle of narrow gap groove.

Secondly, in order to ensure the width of narrow gap groove cannot affect the laser beam, the flexibility of laser beam propagation in the narrow gap should be ensured. Basically, the laser beam can propagation to the bottom of groove based on groove of as narrow as possible. If laser beam is blocked by groove, the bottom of groove cannot absorb enough energy and other zone will be excessive melted which will lead to easy to generate incomplete penetration and fusion.

In addition, based on the previous two principles, the actual welding situation should be considered. Such as wire diameter which means the groove dimension should ensure the moving stability of wire in the space of narrow gap groove.

4.1.2.2 Design principle

According to the welding structure of ITER CC case, the groove will be designed to U-shaped with root or I-shaped with root. Because of the divergent of laser beam propagation, the flexibility analysis of beam propagation should be done before determine the groove dimension. Therefore, the laser beam propagation theory will be analysed. Figure 4.2 shows the laser beam propagation characteristic in narrow gap groove.

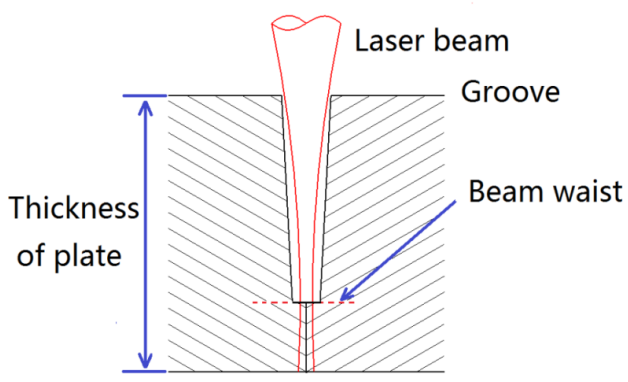

Figure 4.2 The laser beam propagation in narrow gap groove

1. Laser beam propagation characteristic

In order to different from fundamental-mode Gaussian beam, the beam quality was used to describe the propagation and focus of multi-mode laser beam. The Rayleigh length, beam divergence angle and transmission equation of multi-mode laser beam are:

$$Z_R = \frac{\pi {\omega_0}^2}{\lambda M^2} \tag{4-1}$$

$$\theta = \frac{\lambda M}{\pi \omega_0} \tag{4-2}$$

$$\omega(z) = \omega_0 \sqrt{1 + (\frac{z}{z_R})^2} \tag{4-3}$$

where ω_0 is beam waist radius, λ is the wavelength, M^2 is the beam quality factor, Z_R is the Rayleigh length, θ is beam divergence angle, z is the distance from the waist, $\omega(z)$ is beam radius at the distance z from the waist.

Figure 4.3 shows different propagation results of different M^2 value along Z direction. According to the equations, it is found that beam divergence angle was proportional to M and Rayleigh length was inversely proportional to M^2. Therefore, in order to maximize to use the optical system, the M^2 beam should small enough.

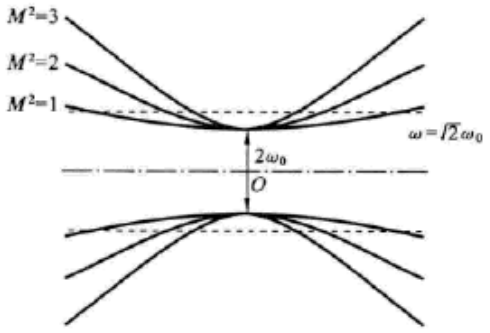

Figure 4.3 Different propagation results of different M^2 value (Liu,2011)

If the laser beam propagation is the type of gaussian beam, the beam is also the gaussian beam after focusing by optical system. Defining the laser beam waist radius is ω_0 and focal length is f, then the focal radius is (Liu,2011):

$$\omega_0{}' = \frac{\lambda f M^2}{\pi \omega_0} \tag{4-4}$$

Based on the same waist radius of laser beam, the focal radius is proportional to M^2. The corresponding relation of laser beam of different $M^2$with focal size is shown in Figure 4.4. Generally, In order to get the density, the focal size is demanded small enough which need the small M^2.

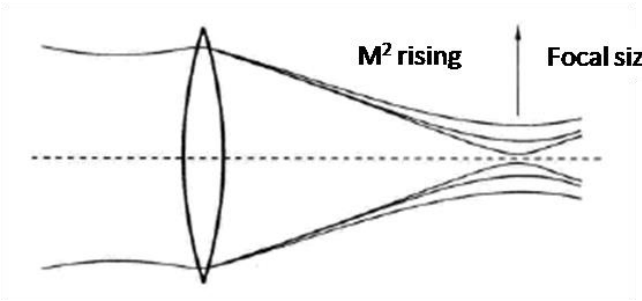

Figure 4.4Relationshipbetween laser beam and focal size based on the differentM^2 value (Liu,2011)

2.Beam propagation characteristic of narrow gap laser welding

Simultaneous equations of 4-1 and 4-3, the distance (*z*) from beam waist can be defined in (Zhang, 2014):

$$Z = \frac{\pi}{\lambda M^2}\sqrt{(\omega(z)^2 \omega_0{}^2 - \omega_0{}^4)} \tag{4-5}$$

From this equation, it is found that the beam propagation distance has the relation with beam quality, wavelength, beam diameter of *Z* and beam waist diameter.

The final beam waist diameter depends on the optical propagation system. Figure 4.5 shows the optical propagation system of fiber laser.

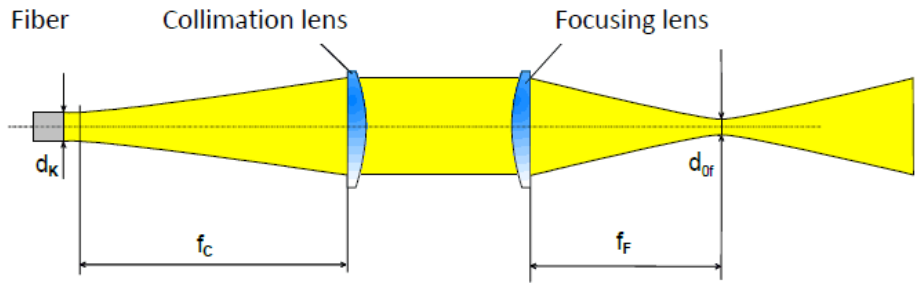

Figure 4.5The optical propagation system of fiber laser

In the fiber laser, the laser beam waist diameter was depends on the focal length of collimating lens, focal length of focusing lens and fibre core diameter.

$$D = \frac{f_F}{f_c} d_K \tag{4-6}$$

Where D is beam waist diameter, d_K is fiber core diameter, f_F and f_c is focal length of collimating lens and focusing lens, respectively.

Aim at the laser welding of CC case which has the definite welding depth, the key point to increase the flexibility of laser beam propagation in narrow gap is to determine reasonable beam waist diameter and beam diameter of *Z*.

4.1.2.3 Design of optical propagation system

The optional experiment apparatus in this optical propagation system includes: 0.2 mm d_K of fiber, two types of collimating lens (focal length f_c is 120 mm and 200 mm), two types of focusing lens (focal length is f_F 200 mm and 250 mm).

According to the laser power and welding thickness of CC case, the welding thickness is designed to 5 mm. In order to ensure the laser beam perfect transfer to the bottom of groove during the root welding, the beam waist diameter and the beam diameter of 15mm distance from bottom of groove will be calculated.

Assemble the two types of collimating lens and focusing lens respectively, the four cases of optical propagation systems were obtained. The fibre core diameter, focal length of collimating lens and focusing lens are known quantity. The Rayleigh length was measured by diagnosis instrument of beam quality UFF100 which is produced in Prometec. The beam waist diameter and the diameter of 15 mm were computed according to equations 4-6 and 4-3. The detailed information was shown in Table 4.1.

Table 4.1Different optical propagation system depend on different lens

Fiber core diameter/mm	focal length of collimating lens/mm	focal length of focus lens/mm	Beam waist diameter/mm	Rayleigh length/mm	Beam diameter of 15 mm/mm
0.2	200	200	0.204	1.378	2.23
0.2	200	250	0.26	2.144	1.84
0.2	120	200	0.33	2.488	2.02
0.2	120	250	0.416	4.278	1.52

The Rayleigh length is an important indicator to evaluate the laser beam quality. In order to obtain a good flexibility of beam propagation in narrow gap groove, the Rayleigh length should be as longer as possible. In addition, according to the Table 4-1, the focused beam waist diameters are all smaller than 0.5 mm. In the laser filler wire welding, too small spot is bad for alignment of spot and wire. Because of the ultra-high energy density characteristic of small laser spot, a slight misalignment of wire and spot will lead the instability of wire fusion. Moreover, the small laser spot has the higher requirement of assemble accuracy of weldment. In addition, smaller beam diameter of 15 mm was more reasonable to ensure the laser beam transfer to the bottom of groove. This point was beneficial to design the narrower groove which is follows the previous design principle of groove to decrease the filling volume and welding deformation.

According to the computed results, the computed data of group 4 which has the most suitable beam waist diameter, longest Rayleigh length and smallest beam diameter of 15 mm is the best optical propagation system. Therefore, the optical propagation system of group 4 was determined.

4.1.2.4 Groove optimization

Based on the optical propagation system, the design, experiment and optimization of narrow gap groove will be done. Since known variable are welding depth and root depth, the root width and groove angle will be the designed variables.

Three different groups of narrow gap groove were designed. They are U-shaped groove with 3 mm root width, V-shaped groove with 2 mm root width and 6° groove angle, V-shaped groove with 2 mm root width and 8° groove angle, respectively. The laser welding experiments under the three types of group were done to evaluating their adaptations. The materials used are same with the case which is 316LN of base material and 316LMn of wire with 1.2 mm diameter. Figure 4.6-4.8 shows the typical results of three types of narrow gap groove.

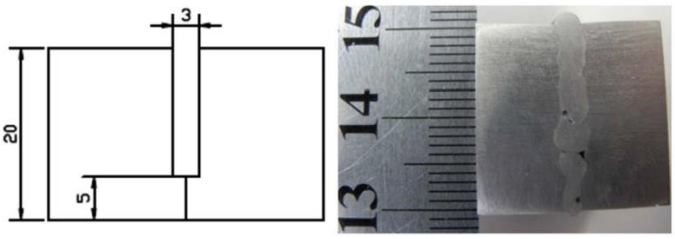

Figure 4.6 The welding result of group 1

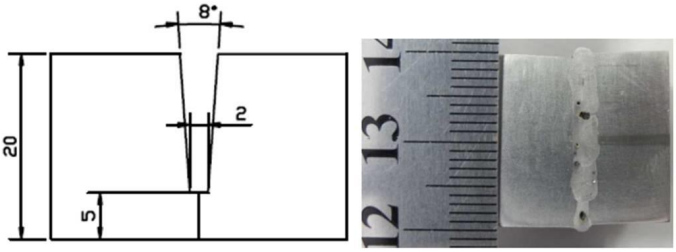

Figure 4.7 The welding result of group 2

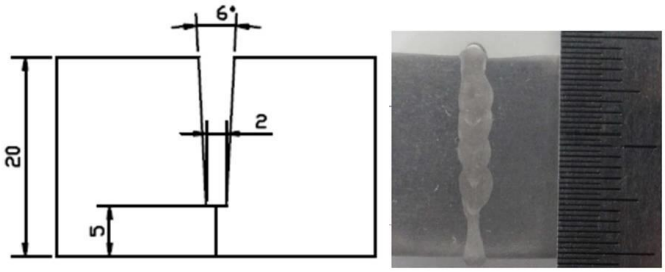

Figure 4.8 The welding result of group 3

From the welding results, it was found that the group 1 and 2 easily appear the defects of pore and incomplete fusion because of its large groove size. The optimized group 3 always presents the defect-free welded joint. Thus, the group 3 with V-shaped groove with 2 mm root width and 6° groove angle was determined as the final groove structure of CC case laser welding.

4.1.3 The laser welding with hot wire

As the previous description, in the laser filler wire welding, too small spot is bad for alignment of spot and wire. Because of the ultra-high energy density characteristic of small laser spot, a slight misalignment of wire and spot will lead the instability of wire fusion. Many researchers focusing on the laser welding using the hot wire, and they founds the hot wire technology is able to increase the process stability, minimize the weld defects, improve weld-metal toughness, hardness, and microstructure (Kitahara, et al., 2011; Dzelnitzki, 2004; Jones, et al., 2004; Phillips, et al., 1992). In order to obtain

the stability of wire feed process and good welding quality, the hot wire technology which means the resistance heat will be preheat the wire close to the melting state was applied. It will decrease the wire melting depending on the laser energy and decrease the accuracy requirement of wire and spot to increase the deposition efficiency and stability of wire feed process.

During the laser welding with filler hot wire, the melting transfer mode of wire has three transfer modes (Dilthey and Schneegans, 1994; Zheng et al., 2014; Wen et al., 2011), they are excessive melting transfer, continuous transfer and inadequate melting transfer, respectively. The excessive melting transfer belongs to the instability transfer type is defined that the resistance heat will heating the wire exceed the melting temperature which means the wire was melted before it inserting into the molten pool. The continuous transfer belongs to the stability transfer type is defined that the resistance heat will heating the wire closed the melting temperature which means the wire will melting immediately when it inserting into the molten pool. The inadequate melting transfer belongs to the instability transfer type is defined that the resistance heat will heating the wire much less than melting temperature which means the wire will inserting into the molten pool in solid state. Therefore, in the laser welding with filler hot wire, the preheating process for the wire is important to the stability of laser welding with filler hot wire.

Assuming the loss energy which is generated by heat convection and heat radiation during the preheating wire process was ignored. Then, the energy absorb from resistance heat is:

$$W=Q \tag{4-7}$$

$$W = I^2 \cdot R \cdot t \tag{4-8}$$

$$Q = C_w \cdot m \cdot \Delta T \tag{4-9}$$

Where W is the output energy of hot wire feeder, Q is the resistance energy which absorbed by wire, I is the preheating current, R is the wire resistance, t is the preheating time, C_w is specific heat of wire, m is the volume of wire feed, ΔT is the temperature rising value of wire, $\Delta T = T - T_P$, T is the wire temperature after preheating, T_P is the initial temperature of wire.

If the extension length of wire is ensured, then, the volume of wire m is:

$$m = \rho_w \cdot \pi \cdot r^2 \cdot l \tag{4-10}$$

Resistance R is:

$$R = \frac{\rho_{rs} \cdot l}{\pi r^2} \tag{4-11}$$

Where ρ_w is the wire density, r is the wire radius, l is the distance from contact tube to end of wire which is the preheating length of wire called extension length, ρ_{rs} is the resistivity of wire.

The preheating time of wire is：

$$t = \frac{l}{V_w} \tag{4-12}$$

Where V_w is the wire feed rate. Inserting the equations (4-8)-(4-12) into equation (4-7),

$$\Delta T = \frac{\rho_{rs} \cdot l \cdot I^2}{\pi^2 \cdot r^4 \cdot C_W \cdot \rho_w \cdot V_w} \tag{4-13}$$

From the equation, it shows that the rising temperature of wire related to the material properties, wire condition, preheat current, extension length and wire feed speed. ΔT is proportional to the extension length, was reverse proportional to the wire feed speed and presents quadratic function relation with current.

4.2 Welding experiment on the standard plate

4.2.1 Experimental

In the experiments, the base materials used for the welding were 316LN austenitic stainless steel plates with 20mm thickness. The welding wire used was 316LMn with a 1.2mm diameter. In addition, to obtain high strength and toughness for welded joints and to decrease welding deformation, 316LMn, which is fully austenitic stainless filler material, was used for the manufacturing development of the CC case. For ITER, the use of high-Mn content (6%-10%) welding filler is required for welding of 316LN. The high-Mn of filler metal is effective at preventing the formation of the ferritic phase at the weld region (Kim et al., 2009). The dimensions of the completed laser welded samples are 300mm×300mm×20mm (thickness). The chemical composition (wt.%) and material properties of base and filler metal are summarized in Table.4.2 and 4.3.

Table 4.2 Chemical composition of 316LN and ER316LMn

316LN (wt.%)									
C	Si	Mn	P	S	Cr	Mo	Ni	N	Cu
0.012	0.5	1.57	0.015	0.001	16.62	2.16	13.40	0.158	0.015
Ti	Nb	Al	V	Fe					
0.009	0.009	0.009	＜0.01	Bal.					
316LMn (wt.%)									
C	Si	Mn	P	S	Cr	Mo	Ni	N	Fe
0.018	0.46	7.01	0.017	0.003	20.59	2.83	15.37	0.156	Bal.

Table 4.3 Material properties of 316LN and ER316LMn

	Tensile strength /Mpa	Yield strength /Mpa	Elongation /%	Density /g·cm^{-3}	Thermal conductivity /W·m^{-1}	Solution treatment /℃
316LN	637	304	53	7.98	15.21	1010-1150
316LMn	734	540	20	7.85	15	

The laser welding was carried out using the ITER CC laser welding system. Aim to the narrow gap laser welding, the welding processing head compose of horizontal gas curtain, wire feed nozzle, shielding gas nozzle and its position, and laser connection was shown in Figure 4.9. In order to protecting focusing lens against the damages cause by the splash and smoke generated in the welding process, a supersonic horizontal gas curtain was set under the focusing lens. This supersonic horizontal gas curtain can jet a thin supersonic flow with certain width to blow away the splash and smoke quickly and effectively, and realizes the protection of optical system components.

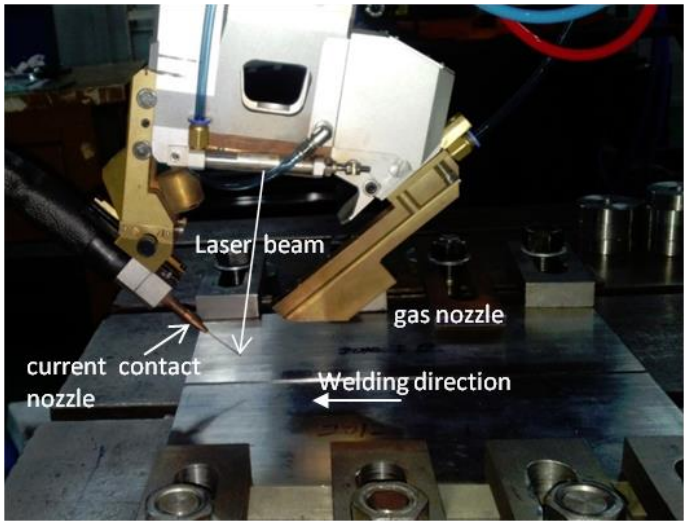

Figure 4.9 System of laser head

4.2.2 Laser welding parameters

According to the theory of narrow gap laser welding, laser welding system and groove structure, the laser welding parameters compose of welding parameter of 5 mm root, 15 mm filling in the groove and cosmetic welding. Therefore, three kinds of parameter were developed and the 20 mm 316LN plate was welded by laser welding with hot wire based on these parameters.

The developed welding parameters were shown in Table 4.4. The root layer has the 6V of heat voltage and 100A of heat current, and the filling and cosmetic layer have the 6V of heat voltage and 250A heat current. The high purity argon was used as the shielding gas. The weld surface appearance was shown in Figure 4.10. From the figure, it is found that the welded seam was present good appearance, well fusion, no surface defects of overlap, undercut and pit.

Table 4.4 Cosmetic parameter and filling parameter

	Laser power(KW)	Wire feed speed (m/min)	Welding speed (m/min)	Defocusing distance (mm)
Root	3.5	1.5	1.0	+5
Filling layer	3.8	4.3	1.5	+25
Cosmetic layer	3.95	3.5	0.6	+45

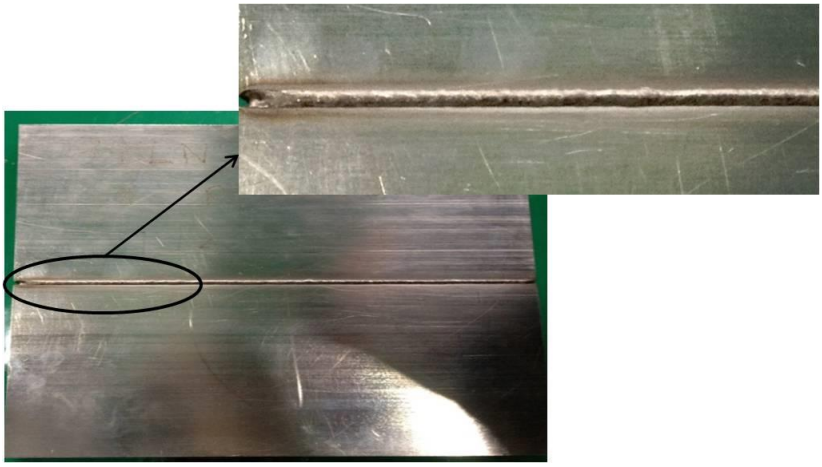

Figure 4.10 The weld surface appearance after the cosmetic welding

4.2.3 Inspection and analysis of weld

Based on the welding parameters of root layer, filling layer and cosmetic layer, the 20 mm 316LN plate was welded. Figures 4.11, 4.12 show the cross-section of welded joint and X ray inspection. From the cross-section of welded joint, it was found there are no typical defects of pore, crack, incomplete fusion of groove and interlayer. The welded joint presents no internal defects under the X-ray inspection.

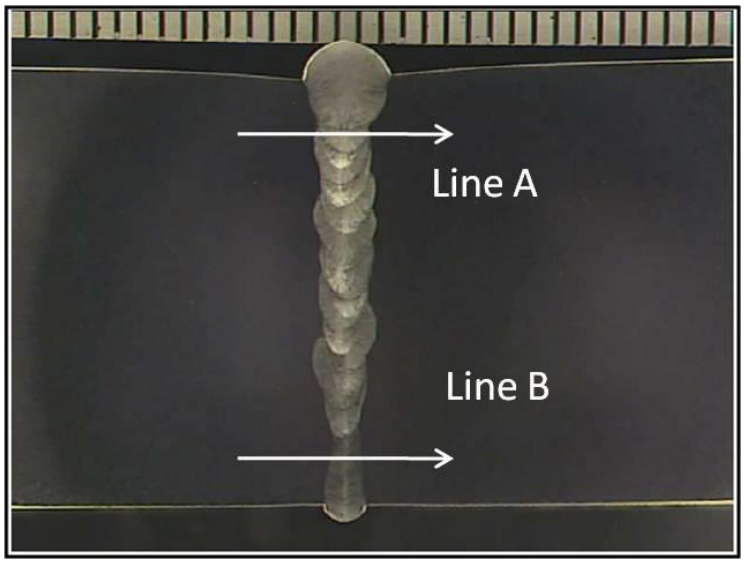

Figure 4.11 Cross-section of welded joint of 20mm 316LN

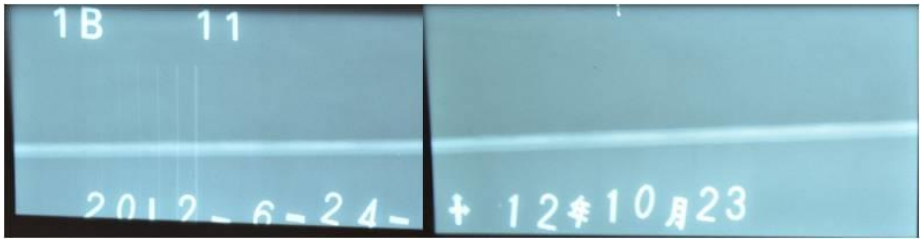

Figure 4.12 Overview of X-ray inspection of 20mm 316LN

1. Microstructure observation and hardness test

The welds were chemically etched for observation of the microstructure using optical microscopy. According to the international standard EN ISO 9015-1, hardness distribution at various positions on the welded joint was measured using a Vickers hardness tester, with a testing load of 10Kg. The microstructure of the base metal, fusion line and the fusion metal are shown in Fig 4.13.

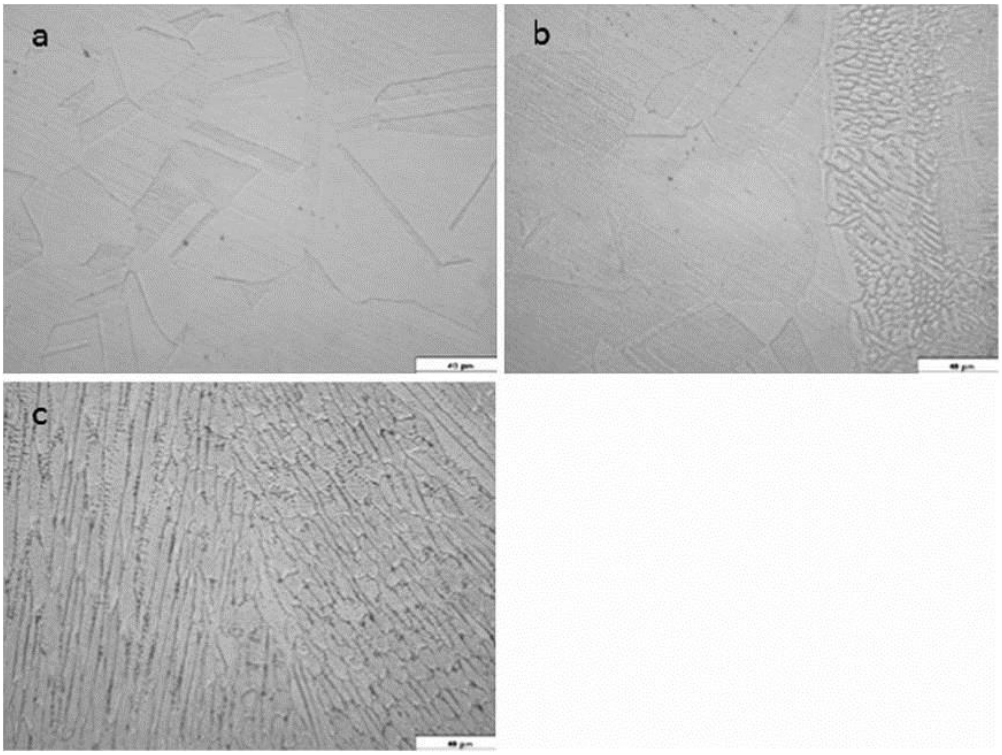

Figure 4.13 Optical microstructures of base metal (a), fusion line (b), and fusion metal (c) in welded joint.

It was observed that the base metal, fusion line and the fusion metal had a fully

austenitic microstructure, and the base metal recrystallized by the solution treatment processing, displayed uniform equiaxed grains of austenite microstructure. By careful examination of the micrographs, it was revealed that mainly cellular and dendrite grains were formed in the fusion metal. The weld metal formed with these grains perpendicular to the fusion line and growth to the weld centre. This is the typical characteristic of the primary austenitic solidification. It is well known that the solidification model depends on the ratio of the Cr and Ni, and the primary austenitic solidification was expected since the ratio of the chromium equivalent and nickel equivalent was less than 1.5 (Brools et al., 2009; Clippold and Kotecki, 1991; Shankar et al., 2003). So, no δ-ferrite was detected in the laser welded steel. The grain size of fusion metal was finer than that of base metal and the grain size of fusion line did not grow obviously as the result of rapid solidification and alloying elements. Laser welding of high cooling rate is conducive to grain refinement (Tjong et al., 1995).Fig 4.14 shows the SEM micrographs of microstructure of the cosmetic layer. There are two points, located on the boundary and inside of grains, are marked in the Figure and their chemical compositions are analysed by the EDX analysis. The result show that the chemical compositions (wt%) of point 1 and point 2 consist of 21.51 Cr, 12.91 Ni, 8.84 Mn, 3.20 Mo, 1.50 Si, balance Fe, and 19.43 Cr, 11.50 Ni, 8.39 Mn, 1.52 Mo, 1.12 Si, balance Fe. The EDX analyses also reveal the Cr and Mo of boundary of the grains significantly higher than inside of the grains. There are a small amount of finer particles are located on the boundary of grains from the Figure. These particles may be the carbides and nitrides of Cr and Mo. And these particles of carbides and nitrides located on the boundary of grains will prevent the grain growth and obtain the finer grains.

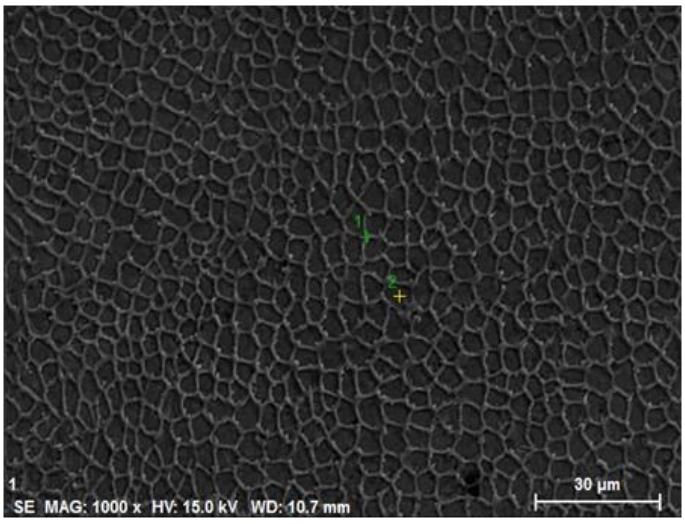

Figure 4.14 SEM of microstructure of the weld centre

The macrograph and Vickers hardness distribution of the welded joints are shown in

Figure 4.11. The trend of the hardness variation is shown in Figure 4.15(a) and (b). The locations for measurements are also depicted in Figure 4.11: line A located at 2mm from the top surface of the welded plate and line B located at 2mm from the bottom surface of the welded plate. It can be seen that the top and bottom weld hardness values were consistent. The maximum hardness was in the HAZ zone, 228 HV (top line) and 217 HV (bottom line). The minimum hardness was located in the base metal, 152 HV (top line) and 150 HV (bottom line). The characteristics of hardness distribution were essentially determined by the microstructure of the various zones, owing to their different welding thermal cycles during welding. Such hardness profiles are considered to be associated with the high cooling rates from the liquid state that lead to the formation of microstructure and fine grains in the fusion metal. Furthermore, The wire of 316LMn was applied to increase the alloy element content of weld zone and existence of residual stress in the weld zone will integrated impact the hardness of weld.

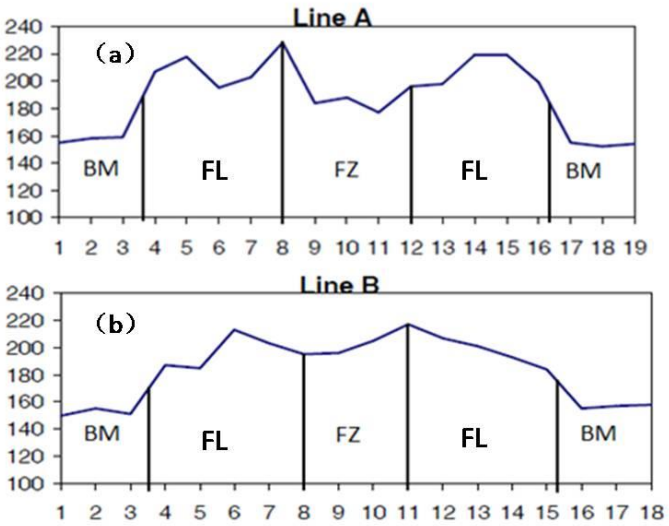

Figure 4.15 Vickers hardness distribution in cross-welded joint

2.Tensile test and Charpy-V impact toughness test

The tensile strength of the two welded joints specimens, which were up to 632MPa and 646MPa, reached the design requirement at room temperature (＞480Mpa) (ITER Design description document, 2009). Figure 4.16 shows the photograph of one broken specimen after tensile testing and the force-deformation curve. It was found that all tensile specimens were fractured in the base metal zone and the welded joint had significant plastic deformation before fracture. This confirmed the fact that the tensile strength of the weld joint was higher than that of the base metal and the welded joint

had good ductility. This result indicates the welding procedure of the experiment is quite reasonable.

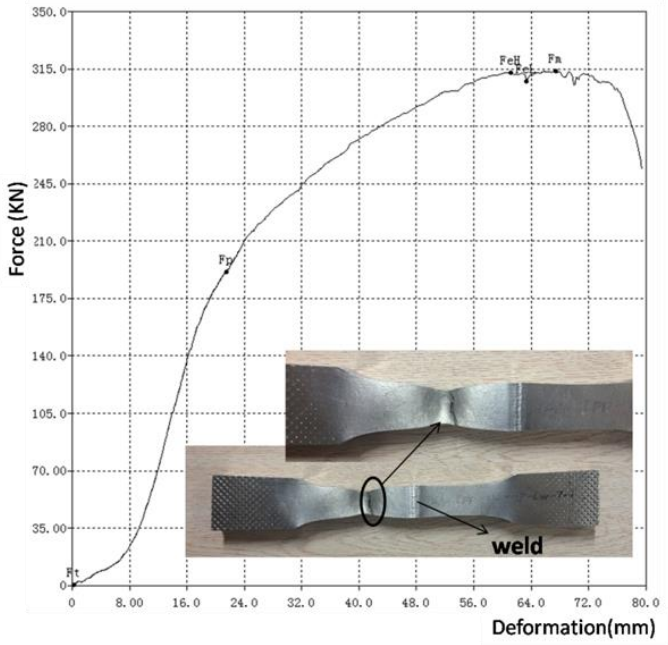

Figure 4.16 Force-deformation curve of tensile test and broken specimen

According to the actual running condition of ITER CC case, the Charpy-V notch-impact tests were done at 4.2K. Figure 4.17 shows the results of notch-impact toughness value of weld metal and fusion line. The results show that the notch-impact toughness value of weld metal was 250 J/cm²， while the notch-impact toughness value of fusion was 69 J/cm^2. The average impact toughness value of weld metal and HAZ were higher than Chinese industrial standards (＞ 37J/cm^2) (Chinese industrial standard NB/T 47014-2011), so the impact strength of the welded joint was qualified. Obviously, the impact toughness of fusion line was far less than that of weld metal. It was mainly caused by the grain size of notch-impact specimens. The notches of the weld metal impact tests specimens were located the weld centre where the grain was finer than that of fusion. Though the grains of fusion line is not coarsened, while the microstructure distribution is uneven and with big gradient. Moreover the second phase precipitates like carbide and nitride may generated in the fusion line which will result in lower toughness and easier brittle fracture. Thus, the impact toughness value of HAZ was decreased, while the hardness was increased.

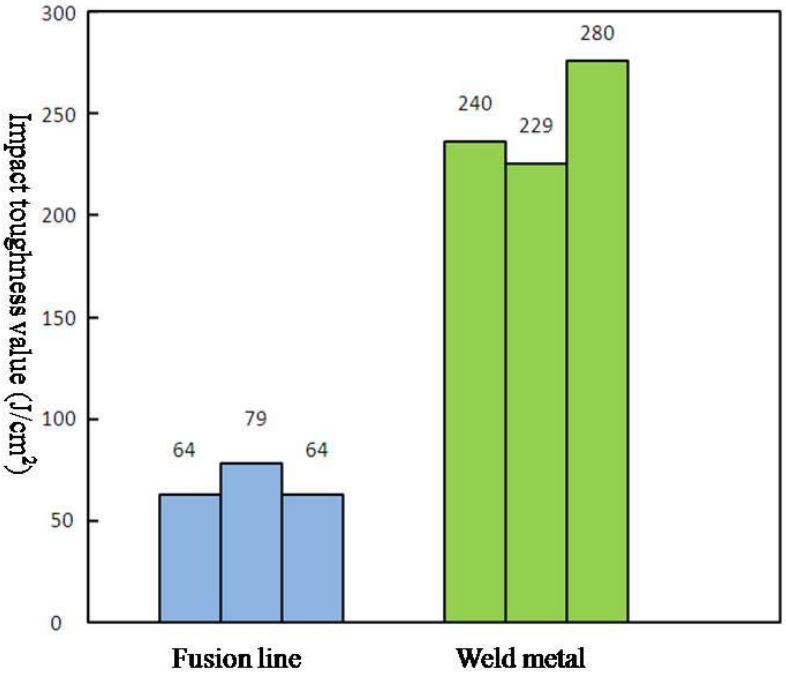

Figure 4.17 Impact results of weld metal and fusion line

4.3 Thermal analysis and experiment

According to the closure welding requirement, the temperature of back of case should be controlled because of the superconducting coil is inside of case during the welding process. The surface temperature of superconducting coil should be less than 250° which means the insulating properties of superconducting coil will be damaged. A backing strip is designed behind the case to prevent the laser beam contact and harm the superconducting coil directly if there is a gap after the case assembly.

4.3.1 Welding structure of CC case

The backing strip is designed to protect the superconducting coil, and also has the function of assembly and position. Figure 4.18 shows the welding structure of ITER CC case. According to the dimension of case and superconducting coil and their assembly, the backing strip was designed to 2 mm width and 3 mm thickness. As shown in Figure 4.18, the backing strip is welded on the L-shaped case ahead of assembly (U-shaped case for BTCC). Because of machining the backing strip and case as a whole brings

high manufacturing difficulty, the backing strip will be machined independently, sectionally, and be welded on the L-shaped or U-shaped case by laser welding.

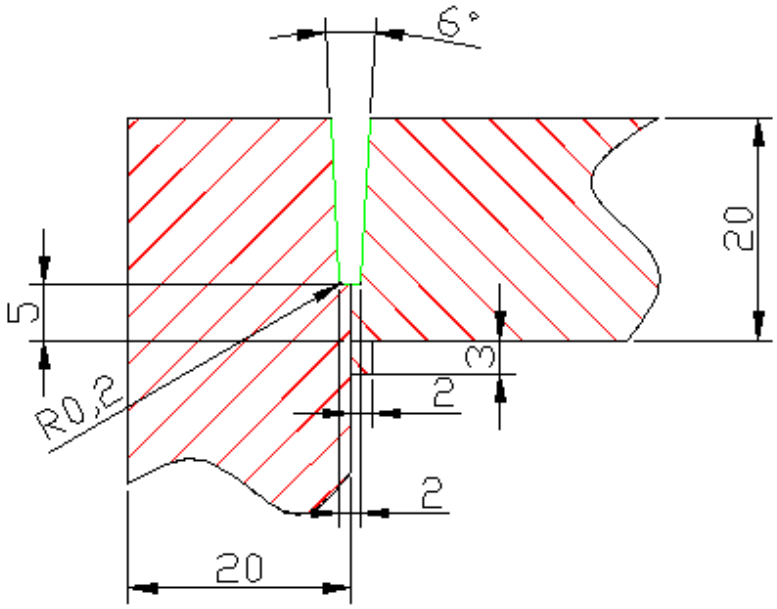

Figure 4.18 Welding structure of ITER CC case

Because of the small size of backing strip, the laser welding was considered to be used on the welding of backing strip. According to the welding processing head and 107.8 mm of opening size of BTCC case, the weld space should be analysed based on the limited space. Figure 4.19(a) shows the schematic diagram of robot weld backing strip on the U-shaped case. As shown in the figure, it is found that the laser processing head need deflect a little angle to ensure the effective welding. Based on the above analysis, two welding schemes were designed: one is welding the backing strip and the case as a type of T joint and another is welding on the side of backing strip. Figure 4.19(b) shows two welding scheme, the arrows show the directions of laser beam.

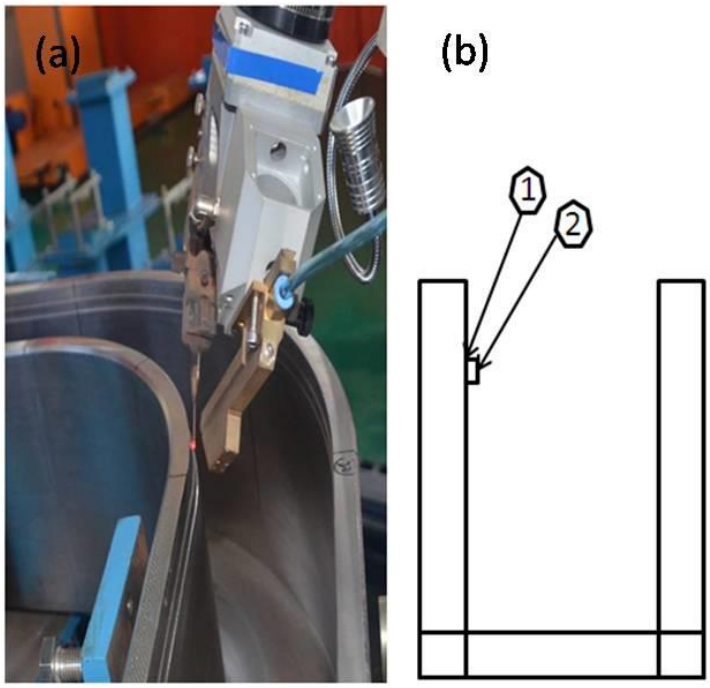

Figure 4.19 (a) The schematic diagram of robot weld backing strip on the U-shaped case (b) two welding scheme

For the scheme 1, the welding position is the upper of backing strip where contact with case. This welding scheme with advantage of littler welding angel, but the reinforcement of welded seam will impact the assemble process which means the reinforcement need to be grinded. Aim at this welding scheme, the welding experiment was done to verifying the feasibility of its welding technology. The case sample and backing strip was designed as shown in Figure 4.19. Before the laser welding, the TIG welding was used to positioning the backing strip.

Due to the small size of backing strip, the laser beam needs to deviate to the case to avoid the excessive fusion and serious deformation of backing strip. The deviated angle cannot too big because of the limited welded space. The deviated angle was control inside of 25°-30° based on the travelling test. The laser autogenous welding and small laser spot was used to ensure the small reinforcement. According to the above analysis, good parameter was obtained and the smooth and flat welded seam was shown in Figure 4.20.

Figure 4.20 Laser welding results of scheme 1 for backing strip

For the scheme 2, the laser beam will welded on the side of backing strip directly to connect them together. The advantage of this scheme is the successful seam will not remain the reinforcement to impact the assemble process. According to the 3 mm width and 2 mm thickness of backing strip, weld width should be ensured less than 2mm, while the weld depth should be ensured greater than 3 mm. The laser welding is easy to generating such weld seam, while the backing strip with the characteristic of small and thin which means the slow cooling and easy to deformation. Furthermore, the laser processing head will a deflection angle because of the welding space. The deflection angle will increase the laser spot which will against the narrow width and deep depth of weld seam.

Based on the above analysis, the welding experiment was done to verify this scheme. The welding results were shown in Figure 4.21. Figure 4.21(a) shows the welded seam according to the scheme 2, it was found that the welding results were not satisfied because of the discontinuous weld seam. The reason was analysed that the deviated angle causes the large laser spot and melt the whole backing strip. In order to smallest laser spot whether can realize the welding of backing strip, the laser beam was designed to welding backing strip in vertical direction. The defocusing distance was designed to 0 mm and the laser spot size is 0.42 mm. The welding result was shown in Figure 4.21(b). As shown in the figure, weld seams of several groups are all not satisfied with wide seam and excessive melt of backing strip. According to the above experiments, the weld seam of backing strip and case cannot generated satisfying and meet the welding requirement even the smallest laser spot was used. The reason was analysed that backing strip with small size is not an integral part with case and their discontinuous structure will cause the slow cooling. Moreover, the laser welding with the high temperature rise rate resulting in the backing strip will instantaneous melted.

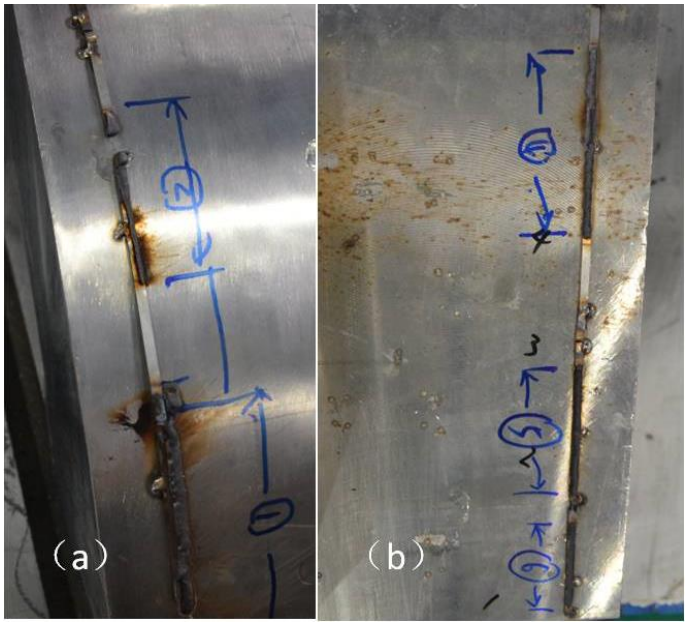

Figure 4.21 Laser welding results of scheme 2 for backing strip

According to the welding experiments of two schemes, the welding scheme 1 was determined as the welding process of backing strip.

4.3.2 Thermal analysis of laser welding

In order to measuring the temperature of the coil case during the welding, a sub coil sample, using wood which was twined with fiberglass to replace the superconducting coil was inserted into the case. The section dimensions were same as the real coil and the length of the sample was 320mm. The welds were carried out using a laser welding process. The back strip used was 316LN with the dimension of 3mm thickness and 2mm width. Thermocouples were used to record the temperatures curve of the inner face of the case and surface of the winding pack. They were inserted into and fixed on the surface of the superconducting coil and inner surface of case in this experiment. In order to obtain the detailed temperature distribution, SYSWELD, a specialized welding simulation software based on the thermo-elastic-plastic FEA method was used to simulating the welding process and to compare them to the temperature distribution results measured by thermocouple.

In order to predict the thermal process on a welding component accurately, the most critical factor is precise the definition of the heat source. An accuracy heat source was depended on the thermal-physical properties of 316LN (shown in Table 4.5) and reasonable heat source model. For the current welding numerical simulation, heat

source model mainly covered 2D Gaussian heat source model (Chakravati, 1986; Fujii, 2000), double ellipsoid heat source model (Karlesson, 1989; Brown, 1992; Josefson, 1993; Canas, 1996; Michaleris, 1997; Sarkani, 2000; Leung, 1990; Teng, 2001), 3D Gaussian heat source model and combined heat source model (Fang, 2001; Frewin, 1999; Reinhart, 1999; Carmignani, 1999; Kang, 2001). Laser welding as the high-energy welding, 3D Gaussian heat source model (conical heat source) was usual considered as its heat source for the simulation (Casalino&Ghorbel, 2008; Lankalapalli et al., 1999; Lampa et al., 1997; Williams et al., 1999). Moreover, in order to ensure the accuracy of simulated heat source, the actual molten pool contrast with simulated heat source as a reference.

Table 4.5 Thermal-physical properties of 316LN

temperature(℃)	20	100	200	300	500	700	1400
Specific heat(J/(KgK))	450	490	522	545	566	600	700
Thermal conductivity(W/mm)	0.014						0.034
density(Kg/mm^3)	7966						7966

For the volume heat source model, its mathematic model is depends of two assumptions. One is the maximum affect zone heat flux is located at upper surface of weldment, the minimum affect zone heat flux is located at the lower surface of weldment. In a series of planes which are vertical to the direction of thickness (z axis), heat flux of each section presents linear attenuation along the thickness direction. Two is the density of heat flux remains unchanged in z axis. The whole volume heat source will be generated by a series of planar Gaussian heat source along the thickness direction of weldment.

In any planes vertical to the z axis, the distribution of heat flux can be represented (Wu, 2008):

$$qv(r,z) = qv_0 \exp(-\frac{3r^2}{{r_0}^2}) \tag{4-14}$$

Where,qv_0 is the maximum value of heat flux, r_0 is the distribution diameter of heat flux and r is radial distance.

According to the conservation of energy, there

$$Q_0 = \int_0^H \int_0^{2\pi} \int_0^{r_0} qv(r,z) r dr d\theta dh = \int_0^H \int_0^{2\pi} \int_0^{r_0} qv_0 \exp\left(-\frac{3r^2}{{r_0}^2}\right) r dr d\theta dh$$

$$= -\frac{\pi q v_0}{3} \int_0^H r_0 \int_0^{r_0} \exp\left(-\frac{3r^2}{{r_0}^2}\right) d\left(-\frac{3r^2}{{r_0}^2}\right) dh$$

$$= -\frac{\pi q v_0 (1-e^{-3})}{3} \int_0^H {r_0}^2 dh \quad (4\text{-}15)$$

Where, Q_0 is the effective heat input, H is the height of weldment. Different volume heat source model responding to different qv_0 and r_0.

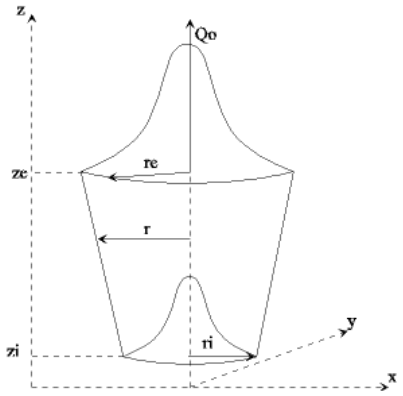

Figure 4.22 Schematic diagram of 3D Gaussian heat source model

3D conical heat source model is shown in Figure 4.22, its distribution diameter of heat flux presents linear attenuation along the thickness direction. Assuming the height of heat source $H=z_e - z_i$, the z coordinate of upper and lower plane of weldment is z_e and z_i, the distribution diameter of upper and lower plane of weldment is r_0 and r_i. There, r_0 was represented as:

$$r_0 = r_e - (r_e - r_i)\frac{z_e - z}{z_e - z_i} \quad (4\text{-}16)$$

or:

$${r_0}^2 = [r_i + (r_e - r_i)\frac{h}{H}]^2, h = z - z_i \quad (4\text{-}17)$$

Combining equation (4-17) with equation (4-15), there

$$\int_0^H {r_0}^2 dh = \int_0^H [r_i + (r_e - r_i)\frac{h}{H}]^2 dh = \frac{H}{3}({r_e}^2 + r_e r_i + {r_i}^2) \quad (4\text{-}18)$$

Combining (4-18) with equation (4-15), there

$$Q_0 = -\frac{\pi q v_0 H(1-e^{-3})}{3}({r_e}^2 + r_e r_i + {r_i}^2) \quad (4\text{-}19)$$

It can be drawn from the equation (4-19):

$$qv_0 = -\frac{9Q_0 e^3}{\pi(e^3-1)} \cdot \frac{1}{H({r_e}^2 + r_e r_i + {r_i}^2)} \quad (4\text{-}20)$$

Combining equation (4-20) and equation (4-15), there

$$qv(r,z) = -\frac{9Q_0 e^3}{\pi(e^3-1)} \cdot \frac{1}{z_e - z_i({r_e}^2 + r_e r_i + {r_i}^2)} \cdot \exp(-\frac{3r^2}{{r_0}^2}) \quad (4\text{-}21)$$

where，

$$Q_0 = \eta P + P_r,\ r_0 = r_0(z) = r_i + (r_e - r_i)\frac{z - z_i}{z_e - z_i}$$

Where, Q_0（W/m^3） is the total heat input in the welding process, P is laser energy input, η is the laser energy absorptivity of material, and P_r is the resistance heat of hot wire.

According to the previous experimental result, the macrograph of welding molten pool is used as the standard model to verify the simulated heat source model. Although the CC case laser welding belongs to the multi-pass welding, the first layer of root welding has the maximum impact to the back temperature and potential damage of superconducting coil. The finite element models for plate of heat source simulation and coil sample welding were built in the Visual Mesh software (developed by ESI).The mesh size is refined in and near the welding centre, and it gradually become rougher farther from the weld centre. The mesh models are shown in Figures 4.23-4.24.

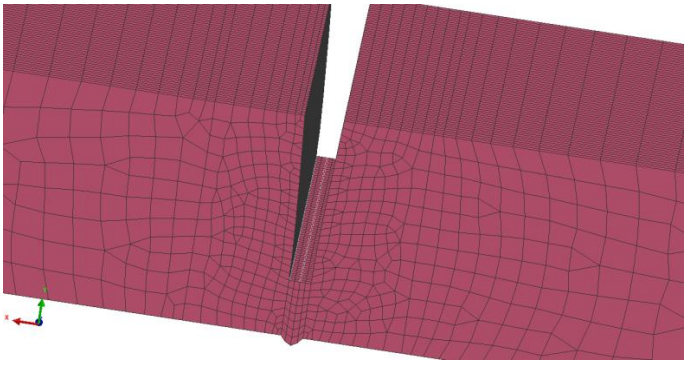

Figure 4.23 Mesh model for plate of heat source simulation

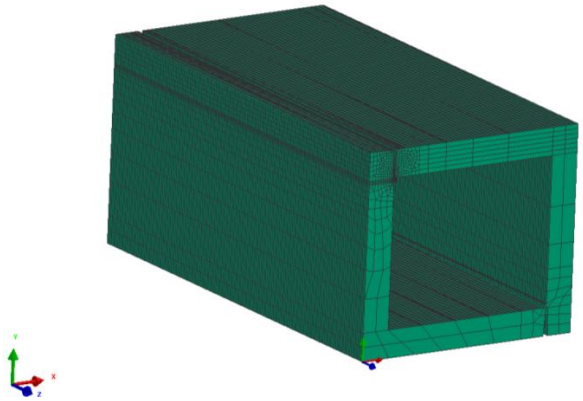

Figure 4.24 Mesh model for case sample

The Heat Input Fitting (HIF) is a tool for adjusting the heat source in SYSWELD and allows the user to define heat source they expect. In the HIF tool, a small amount of computation based on the building of the smaller model is used to optimize the definition of the heat source in an iterative method. The heat source was adjusted by the variables of equation (4-22), re and ri are the Gaussian parameters which are used to adjust the width of the pool; ze and zi are the Gaussian parameters representing the upper and lower plane of the model which are used to adjust the depth and vertical position of the pool.

The heat source model is calibrated repeatedly by adjusting the Gaussian parameters until the fusion zone matches the macrograph of welded joint. The heat source and macrograph of welded joint in this study are displayed in Fig 4.25. From the figure, the morphology of simulated heat source is found to be very close to the real welded joint sample. Due to the welding parameters of positive defocusing distance and a small amount of hot wire, the molten pool has a reversed conical morphology. The result was obtained in the form of an adjusted heat source model and was saved to the heat function database for further use in the simulation of the coil sample.

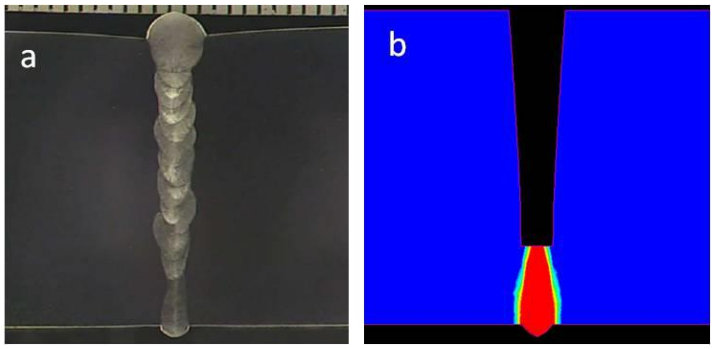

Figure 4.25 Comparison of molten pool morphology: (a) macrograph example; (b) predicted fusion zone (region of the weld above 1400℃) using heat input fitting tool

The heat source model simulated from plate was then used to simulate the case sample, SYSWELD computes the thermal results of the coil sample. The simulation runs for a time period of 100s. In order to achieve the temperature changes of weld centre, a node located in the weld centre is chosen. The heat cycle curve of that node is shown in Figure 4.26. The figure shows the node temperature rapidly rose to 1550℃ when the heat source reached the location of the node. The node temperature plunged to 400℃ when the heat source was moved away. These data are associated with the characteristically high heating and cooling rates of the laser welding. Obviously, the cooling speed was lower than the rising speed, especially the second half of cooling speed. This is because after the heat source leaves the node, the molten pool of the node starts to cool but it is also affected by the molten pool behind it. Furthermore, 316LN steel has the characteristics of low thermal conductivity lead to relatively slow cooling and lower cooling speed.

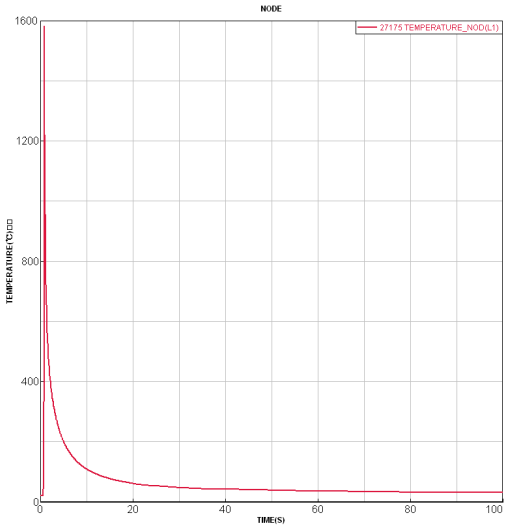

Figure 4.26 Heat cycle curve of weld center

Some nodes are extracted from the inner face of the case, at the bottom centre, where the backing strips are located, and 2 mm and 4 mm away from the fusion line. Their heat cycle curves are shown in Figure 4.27(a), (b) and (c) respectively. According to the figures, the nodes highest temperature of bottom centre of back strip, 2mm and 4mm away from fusion line were 255℃, 220℃ and 155℃ respectively. The ground insulation of ITER correction coil is composite made from fiberglass and epoxy glue. The fiberglass is wrapped around the superconducting cable and cured together with epoxy glue using a vacuum pressure impregnation process. After this process, 3mm thick layer of fiberglass will be wrapped around the external surface before the case welding. The epoxy glue is an organic compound that is formed by mixing epoxy resin, plasticizer, and hardner in a certain proportion. The curing properties will be destroyed if the temperature exceeds 250℃. But the tolerable temperature of fiberglass is usually above 600℃. To reduce the temperature of the ground insulation during the welding of case and to protect the ground insulation properties, there is a gap between the inner surface of coil case and superconducting coil. Thus, the temperature of the surface of the superconducting coil is lower than the temperature of the inner face of the coil case. Also, according to the results of the heat cycle curves of the nodes, the highest temperature of the inner face of case is 255℃ which is far less than the tolerable temperature of fiberglass. The simulation results show that the laser welding process can meet the temperature requirement of the coil.

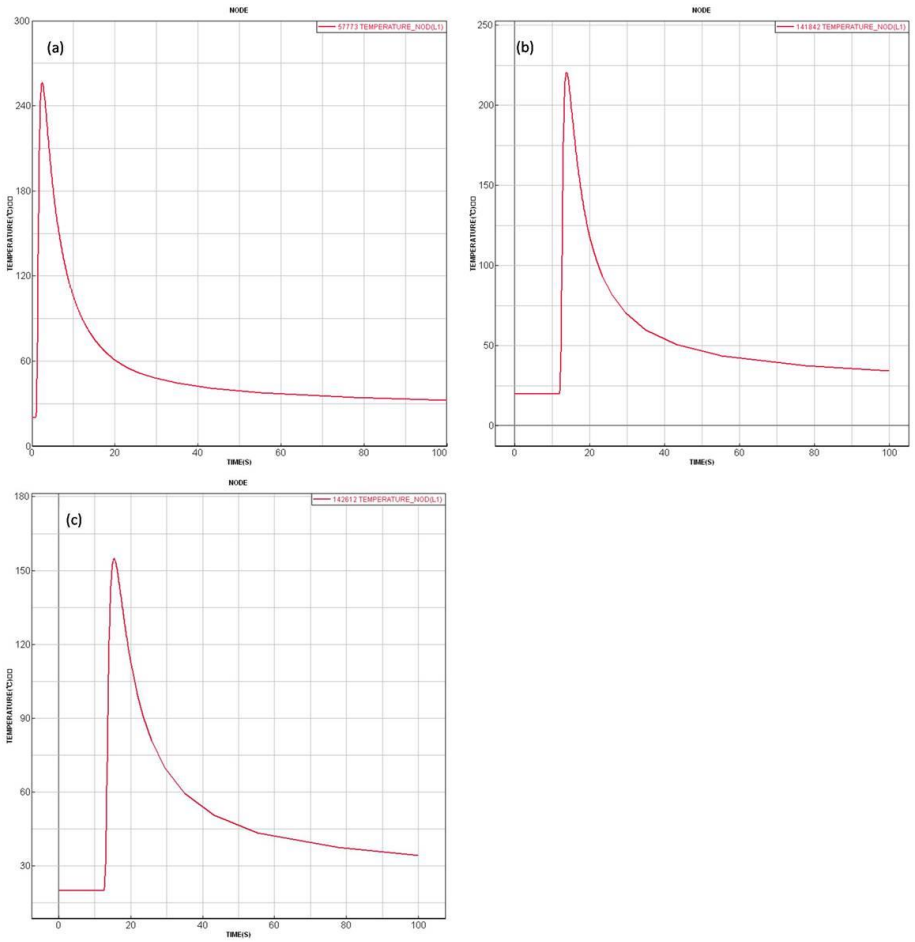

Figure 4.27 Heat cycle curves (a) heat cycle curve of backing strip, (b) heat cycle curve of 2 mm away from fusion line, (c) heat cycle curve of 4 mm away from fusion line.

The main purpose of this experimental work was to record the temperatures curve of the inner face of the case and surface of the superconducting coil, and to compare them to the temperature distribution results predicted by SYSWELD. Thermocouples were used to record the temperature values. They were inserted into and fixed on the surface of the superconducting coil and inner surface of case in this experiment. All welding parameters matched the parameters used for the plate sample welding (laser power, heating current, voltage, and welding speed). Also the positions of the thermocouples were consistent with the simulated nodes extracted from the model in the SYSWELD. Figure 4.28 shows a general view of the experimental setup employed to record the temperature curves during the welding process.

Fig 4.29 shows the heat cycle curves of centre of backing strip, 2 mm and 4 mm away

from fusion line measured from the experiment. Their maximum recorded temperatures were approximately 250℃, 222℃ and 160℃ respectively. The maximum temperatures in these position predicted by the FEA model were approximately 255℃, 220℃ and 155℃ which agree well with the measured values. The highest temperature recorded of the surface of superconducting coil was 59℃ far less than the 600℃. The experimental result verified that the thermal simulation is accurate and the case laser welding process will not destroy the property of superconducting coil.

Figure 4.28 Experimental setup to record the heat cycle

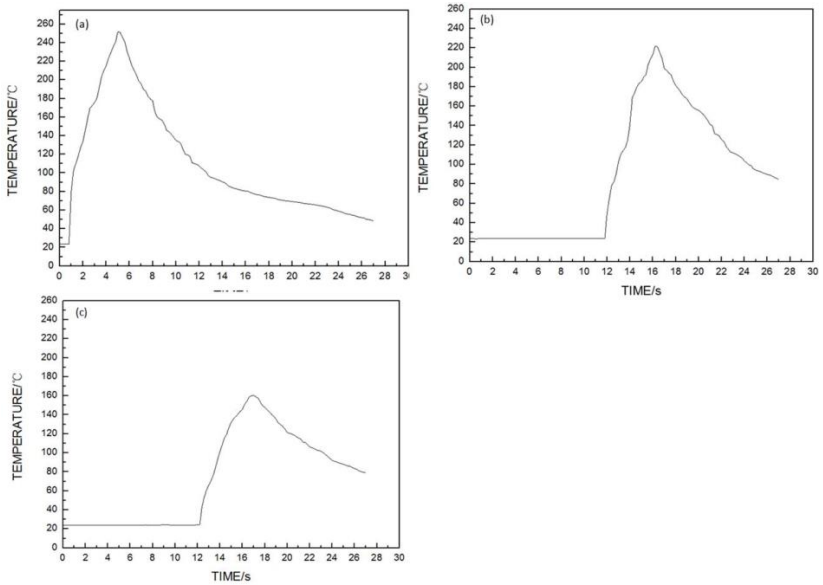

Figure 4.29 Experimental recorded temperature curves (a) temperature curve of backing strip, (b) temperature curve of 2 mm away from fusion line, (c) temperature curve of 4 mm away from fusion line.

5 Laser welding on the model case

In order to study the welding quality and welding deformation of case, a SCC model case was designed. The welding procedure of model case was developed and the welding quality and the welding deformation were studied.

5.1 Structural characteristic and material property

SCC model case retains the sectional dimension and typical structural characteristic of actual SCC case. The drawing of model case is shown in Figure 5.1. Because of special structure of the large arc segments and small arc segments of SCC case, the model case was designed to decrease proportion of the linear segment of SCC case. The model case was composed of two large arc segments with radius of 11287 mm and central angle of 15°, four small arc segments with radius of 300mm, and two linear segments with length of 120mm. The material of model case is also 316LN, the material properties of room temperature and low temperature were shown in table 2.1.

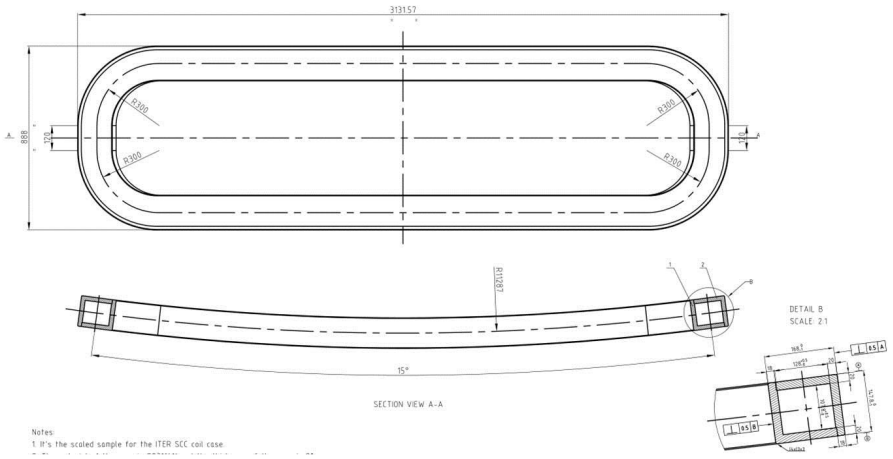

Figure 5.1 Drawing of model case

5.2 Model case closure welding

5.2.1 Deforamtion analysis and control

1. Welding deformation analysis

Model case was a large-size and complex structural weldment, its welding deformation was analysed and mainly includes shrinkage deformation, bending deformation, angle deformation and twist deformation (Fang, 2008; Fu, 2006).

Shrinkage deformation includes transverse shrinkage deformation and longitudinal shrinkage deformation. Because of the long weld seam of model case, the longitudinal shrinkage deformation will be occurred and presents the size to shorten in the direction of weld seam length. And the same time, the transverse shrinkage deformation will be occurred and presents the groove contraction and size to shorten in the direction of weld seam width.

During the welding process, the longitudinal shrinkage of weld seam will cause the bending deformation of weldment if the weld seam is misalignment with the neutral axis of cross-section of weldment. The weld seam of model case were located at the two sides and present skew symmetry, the bending deformation may be occurred.

Due to the V-shaped groove with root of model case, the transverse shrinkage of weld seam will cause the angel deformation. Because of the entirety and self-restrained weldment, the angel deformation will not large based on the reasonable welding fixture.

Due to the small cross-section and large size of characteristic structure of model case, the case can be thought of long and thin weldment. The nonuniformity of transverse shrinkage and longitudinal will cause the twist deformation.

2. Welding deformation control

Due to the different deformation and their reasons of different weldment, the solution to restrain the welding deformation is different. Generally, in order to control welding deformation of large size weldment, the welding structure design will follow the principles of less weld quantity, small weld cross-section and symmetrical weld location. During the welding process, three methods of reasonable fixture constraint, reasonable welding procedure and reverse deformation were used to restrain the welding deformation (Zuo and Wang, 2008; Zhang, 2007; Zhao, 2015).

In the welding structure design of model case, the weld seam presents skew symmetry which is same to actual SCC case. In addition, the 20mm depth of weld was designed to the small cross-section of narrow gap groove.

In the design of welding fixture, model case is only the reduction of overall dimension and keeps the same structural characteristic and cross-section. The welding fixture for the SCC case can be used on the model case directly.

In the welding process, the narrow gap multi-pass laser welding with characteristic of

low heat input was applied on the model case welding. In the welding sequence, each layer will using segmental and skip welding, positioned welding and continuous welding after, and the reasonable welding sequence will be designed to keep the heat evenly of each layer. Also, the laser welding of model case exists rotated process to keep the heat evenly of two sides.

5.2.2 The welding procedure

The welding procedure for model case closure welding main includes welding parameters and welding sequence. The welding parameters will using the parameters which are obtained from butt plate and the welding sequence will using the principle of segmental, skip, symmetrical welding and appropriate rotation.

Before the continuous welding, the position welding with short length will be done to decrease the deformation and assembly stress of welding fixture. The position welding length will be controlled inside 50mm and using the root welding parameter. The positioned welding sequence is shown in Figure 5.2. According the welding sequence, the welding passes of 1-14 of front side (the case present arch is defined to front side, otherwise back side) will be positioned welded, the case will be rotated and the other back side will be positioned welded.

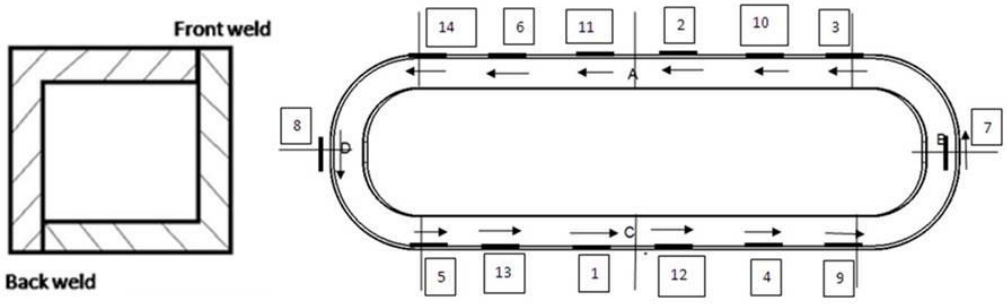

Figure 5.2 The positioned welding sequence of model case closure welding

After the positioned welding, the continuous welding of root will be executed while the locations of positioned welding will not be welded again. In order to ensure the heat evenly of two sides, the special welding sequence was developed. According to the symmetrical welding principle and working space of robot arm, the welding sequence was shown in figure 5.3. Based on the overall dimension of model case, root layer was segmented to 12 passes. Figure 5.3 (a) show the welding sequence of front side and Figure 5.3(b) shows the welding sequence of back side.

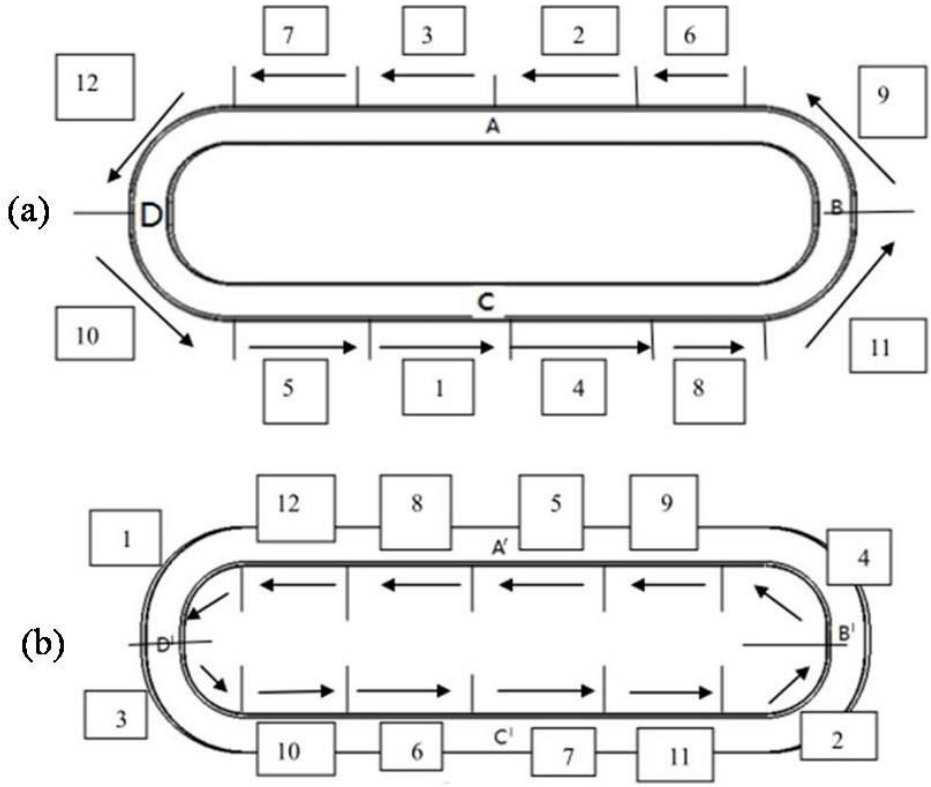

Figure 5.3 Segmental welding sequence of each layer

After the root continuous welding, the filling and cosmetic welding will be executed. The welding parameters are corresponding with the parameters of butt plate. The welding sequence of filling and cosmetic welding was same with root continuous welding. According to the welding experience of butt plate, there remain 8-10 layer to finishing the following weld after root welding(due to the same welding parameter but the a little difference of groove size, the layer quantity will has a little difference). In order to reasonable controlling the heat input of two sides and controlling the welding deformation, the reasonable rotating sequence should be developed during the multi-pass welding. Defining 10 layers weld of each side of case (including root layer), the case will be rotated each 1-2 layers, and so forth to completing the case welding. The detailed separated layer sequence was shown in Figure 5.4.

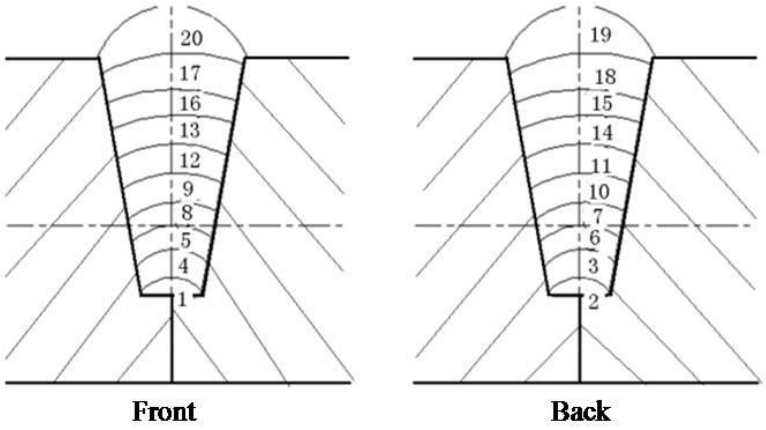

Figure 5.4 Separated layer welding sequence

Due to the overall dimension of mode case, each layer will be segmental welded. The positioning transfer type and cooperation with grinding was developed for processing of overlapping position of neighbouring weld. Figure 5.5 shows the processing of overlapping position. The welding transfer points will be setup by teaching robot before welding and the raised welded seam will be grinding to keep flat.

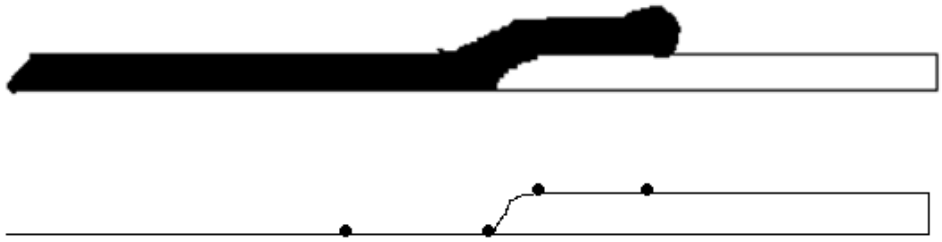

Figure 5.5 Processing of overlapping position

5.2.3 The welding procedure

According to the above welding procedure, the model case closure welding is completed. Before and after laser welding of model case are shown in Figure 5.6. Flat and smooth weld seam of inside groove and surface forming are shown in Figure 5.7(a) and Figure 5.7(b) respectively.

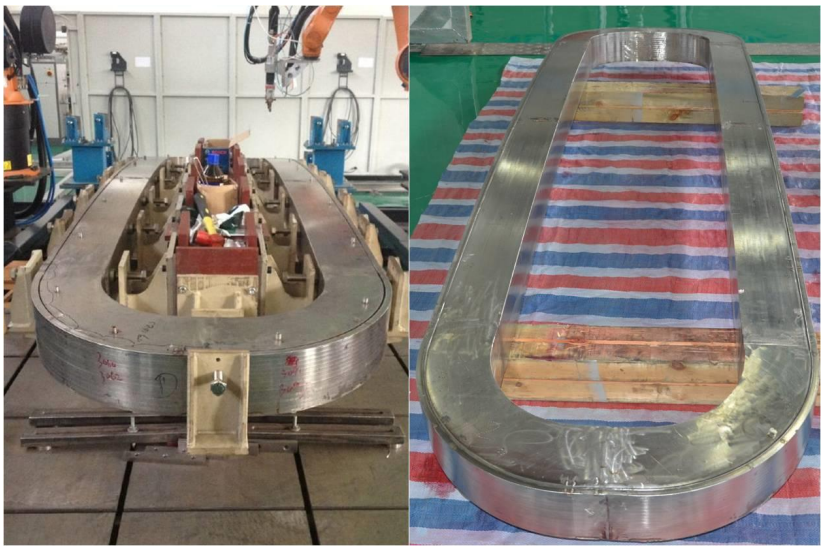

Figure 5.6 Before and after laser welding of model case

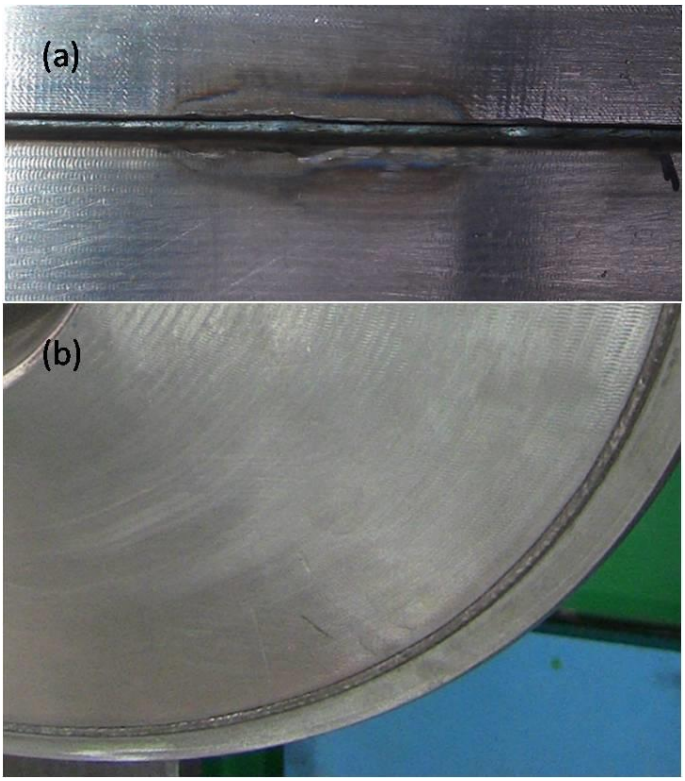

Figure 5.7 Flat and smooth weld of model case

The surface forming and internal of weld seam was observed during and after the welding process. The formation reason and control measures of some defects which appeared in the weld seam are analysed.

Several typical surface defects are shown in Figure 5.8, (a) shows the surface local incomplete fusion and (b) shows the surface local pit. The groove machining of model case is more complex than butt plate which means the groove size is difficult to control in standard size. The incomplete fusion is the problem on the width direction of weld seam, while the surface pit is the problem on the depth direction of weld seam. The diameter of wire is smaller than size of groove, the weld seam will presents the characteristic of convex in the middle and concave in two sides during the welding process. In the wider groove, this type of weld seam easy to occurring the incomplete fusion of one side or two sides. Thus, in order to control the incomplete fusion, the groove size should be ensured in the machining and two passes of cosmetic welding can be used on the wider size of groove. Based on the same welding parameter, the different groove size will cause the different welding depth. Before the cosmetic welding, the residual welding depth was inconformity in different position. The surface pit easy generated in the position of residual welding depth is oversize when the cosmetic welding is executed directly. In order to control the surface pit, the feasible opportunity of cosmetic welding should be considered. The residual welding depth before cosmetic welding should be controlled based on the measurement and local repair welding. According to the welding experience, the cosmetic welding cannot be executed until the residual welding depth is less than 1.5 mm.

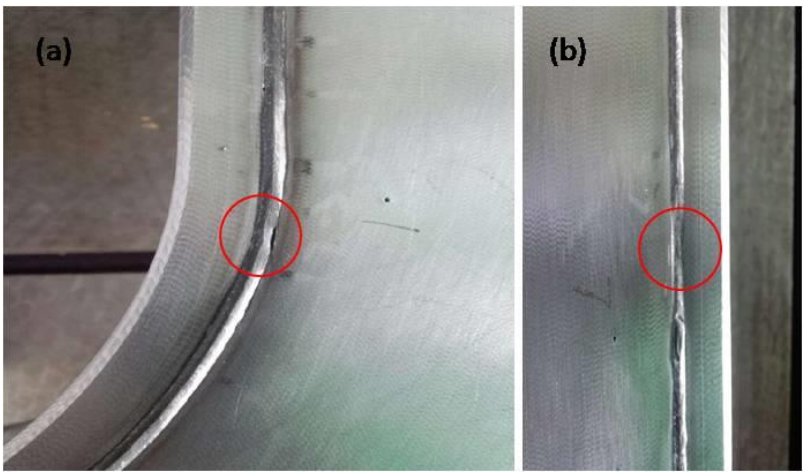

Figure 5.8 Weld surface defects of model case

Figure 5.9 show the porosity defect in the weld seam. In the multi-pass laser welding, the porosity defect main includes pore of fusion line as shown in Figure 5.9 (a) and pore

of interlayer as shown in Figure 5.9 (b) and (c). From the Figure, it was found that the pore present regular circular which is typical metallurgy hydrogen pore. From the Figure 5.9(b), it was found there was irregular oxide film in the local of pore. The generation of pore includes the processes of nucleation and stable growing, its condition of stable existence is (Chen, 2003):

$$P_G = P_a + \frac{2\sigma}{r_c} \tag{5-1}$$

Where, P_G is the pressure inside bubble, P_a is atmosphere, σ is interfacial tension between molten metal and bubble, r_c is critical radius of pore, $\frac{2\sigma}{r_c}$ is the additional pressure of bending molten metal affects on the bubble. Once the bubble nucleated and stable existence, the diffusible gas around of bubble will enter the bubble and cause the bubble growing and spill. If the bubble is not enough spill before the metal solidification, the bubble remained in the weld will form the pore defect.

The generation of porosity defect is depended on the spill velocity of bubble and the solidification velocity of weld metal. Thus, the generating condition of pore is:

$$V_p \leq V_s \tag{5-2}$$

Where, V_p is the spill velocity of bubble, V_s is the solidification velocity of weld metal. The spill velocity of bubble can be presented by stocks equation (Wenyue Chen, 2003):

$$V_p = \frac{2}{9} \cdot \frac{(\rho_l - \rho_G) g r^2}{\eta} \tag{5-3}$$

Where, ρ_l is desity of liquid metal, ρ_G is the density of bubble, g is acceleration of gravity, r is radius of bubble, η is viscosity of liquid metal.

It is easy to found that the solidification velocity of weld metal has the great effect on the generation of pore. Under constant other conditions, the higher solidification speed make more unfavourable the spill of bubble and generating pore defect.

In the mode case closure welding, the bubble which generated in the bottom will continuous absorb hydrogen separated from the around metal solution during the rising

process. The size of bubble will growing with the rising process and the spill difficult will increased when the bubble reach the position close to the upper fusion line and affected by high viscosity of metal solution. Furthermore, laser welding has the characteristic of high solidification velocity, the bubble will not fully spill before the solidification of metal solution, remain in the weld and generating the porosity defect.

In addition, the instable laser filling welding process is the main reason of pore of fusion line and interlayer. Due to the interaction effect of each layer, the problem of any layer will impact the instability of whole welding process. In order to ensure the stable welding process of each layer, the weld should be cleaned fully before the welding. If the laser beam is irradiating on the uneven weld bead with existent inclusion, the wave of molten pool will be intensified. All kinds of convection (free convection, forced convection cause by surface tension), confusion of different morphology and shear flow around the bubble will affect the bubble, and rapid flow of molten pool easy to absorbing the gas and generating the porosity defect finally (Yang, 2014). In order to overcome above factors to affects the welding process, the remained inclusion and oxide should be cleaned and ensure the weld seam is flat and clean before welding of each layer.

Figure 5.9 Porosity defects of weld seam in model case

5.2.4 Welding deformation analysis

The welding deformation control is the most important quality requirement of CC case closure welding, also is the direct reason to selecting the laser welding of concentrated heat input and low deformation. Before the detection of welding deformation of the full-scale CC case, the welding deformation of model case has the important referential meaning.

In order to detailed detect the welding deformation of model case closure welding, 18 feature points both of front and back sides were defined. These feature points will be detected and recorded by laser tracker during the whole welding process. The basic layout of 18 feature points were shown in Figure 5.10, the layout of feature points of back side is same to front side.

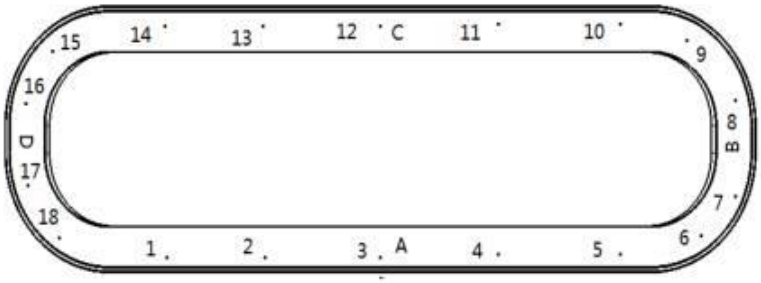

Figure 5.10 Feature points of deformation detection for model case

The distance of two feature points was measured by laser tracker during the welding process (before welding, each layer and after welding). Aim at the overall deformation of length direction and width of model case, recorded data of front side and back side were processed and analyzed.

5.2.4.1 Front of model case

1. Analysis of width direction

The 4 groups of data were used to analyse the welding deformation of width direction.

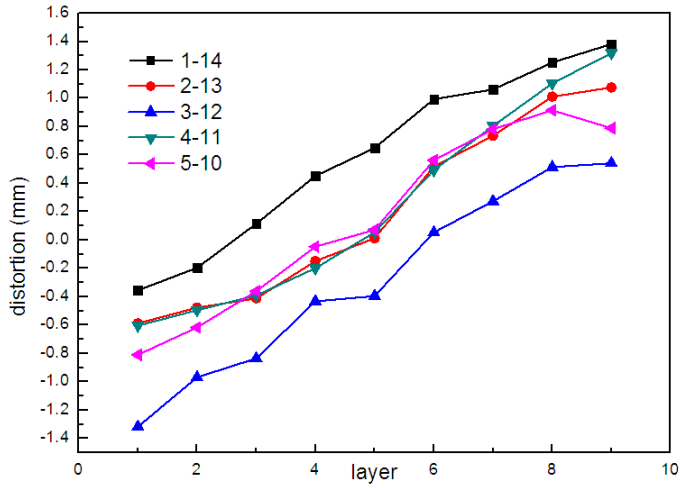

Figure 5.11 Processing plot of welding deformation on width direction of front

The horizontal axis represent the welding layer of 1-9, vertical axis represent the deformation of measuring point. The measuring data before welding was defined as initial value. The measuring value of each layer subtract the initial value was represented as the deformation value. Positive value indicates the size is extended, while negative value indicates the size is shorten. According to this processing method, the welding deformation of each layer is expressed clearly.

According to the processing plot, the following results were obtained. (1) During the welding process, the size on width direction of case is gradual extended. The extension length of each group is inconformity which indicates that twist deformation of the case has occurred. Because of the long longitudinal direction of weld and asynchronism and opposite direction of welding of two sides, the transverse shrinkage of longitudinal weld was uneven and the twist deformation was occurred. (2) Due to the measuring points of each group are all located the inner side of longitudinal weld, the groove will continuous shrinkage with the welding process lead to the size on width direction is gradual extended. (3) Because of the shrinkage of longitudinal weld of four small arc segment, the width size of case is shorten in the earlier layers. The width size of case starts gradual extended with the welding process based on the interaction of longitudinal shrinkage of small arc segment and transverse shrinkage of groove. From the figure, it

is found that the deformation value is negative first, then gradual increase to 0 and positive.

2. Analysis of length direction

The 2 groups of data were used to analyse the welding deformation of length direction. The 2 groups were 8-16 and 7-17. The processing plot was shown in Figure 5.12.

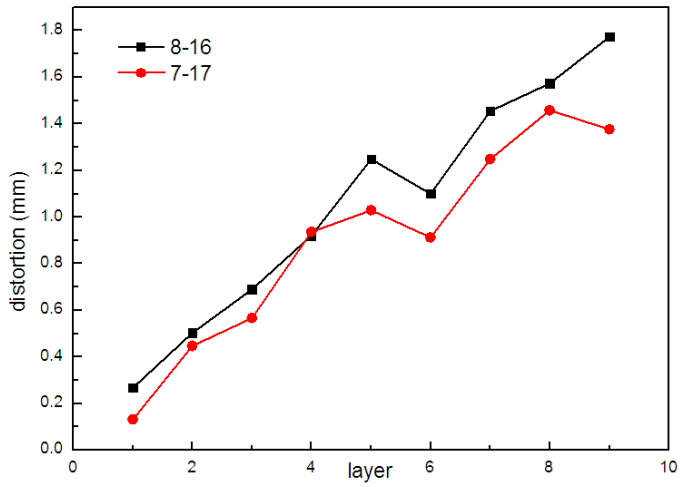

Figure 5.12 Processing plot of welding deformation on length direction of front

According to the processing plot, the following results were obtained. (1) Because of the transverse shrinkage of small arc segment, the size on length direction of case is gradual extended during the welding process. (2) The longitudinal shrinkage of the large arc segment causes the length size was shorten. Due to the large arc segment was welded first and the longitudinal shrinkage is not big based on the free shrinkage. (3) The assemble gap and groove size of small arc segment is higher than large arc segment, the welding parameter with higher heat input was used and cause the transverse shrinkage of groove is higher. (4) The transverse shrinkage of groove is higher than longitudinal shrinkage of large arc segment which lead to the length size is gradual extended during the welding process.

5.2.4.2 Back of model case

1. Analysis of width direction

The 5 groups of data were used to analyse the welding deformation of width direction. The 5 groups were 1-14, 2-13, 3-12, 4-11 and 5-10. The processing plot was shown in Figure 5.13.

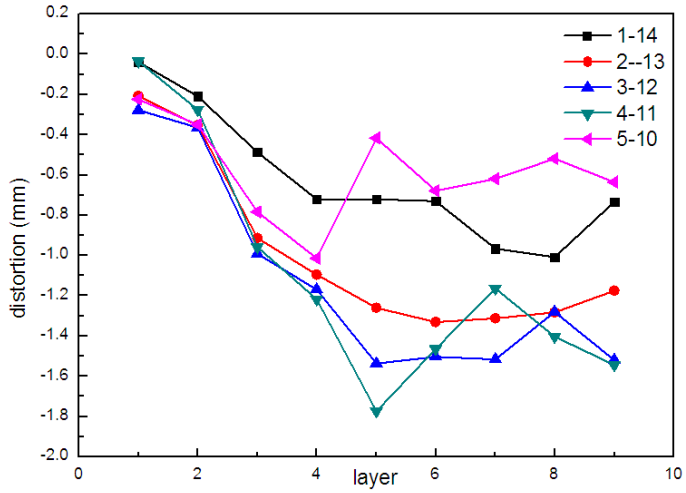

Figure 5.13 Processing plot of welding deformation on width direction of back

According to the processing plot, the following results were obtained. (1) During the welding process, the size on width direction of case is gradual shorten. The shorten length of each group is inconformity which indicates that twist deformation of the case has occurred. (2) The small arc segment was welded first and the width size was shorten based on the longitudinal shrinkage of groove. (3) The stiffness of the case is increased gradually with the welding process. From the figure, it is found that the shortening of size was gradual slow after the 5-6 layers which indicate the welding deformation was main concentrated in earlier several layers.

2. Analysis of length direction

The 2 groups of data were used to analyse the welding deformation of length direction. The 2 groups were 8-16 and 7-17. The processing plot was shown in Figure 5.14.

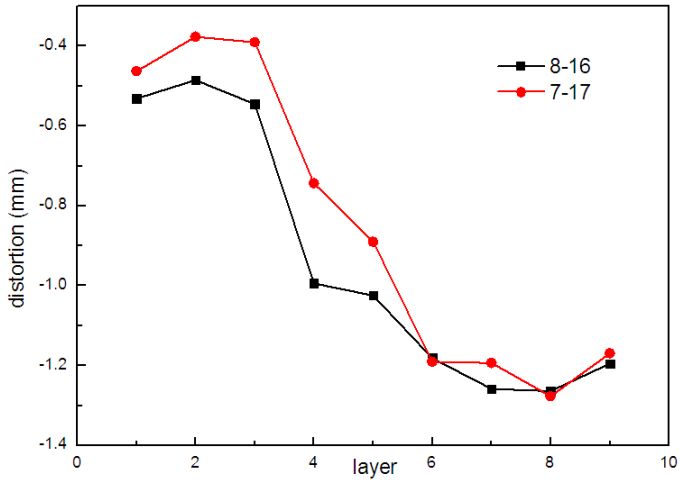

Figure 5.14 Processing plot of welding deformation on length direction of back

According to the processing plot, the following results were obtained. (1) During the welding process, the size on length direction of case is gradual shorten. (2) The length size of case starts gradual shorten with the welding process based on the interaction of transverse shrinkage of small arc segment and longitudinal shrinkage of large arc segment.

5.2.4.3 Comparison of front and back

Due to the interaction of welding deformation of two sides and the different welding sequence, the different deformation condition was obtained. Because of the complexity of welding deformation, the absolute value of final deformation of two sides which includes average value and maximum value was compared.

1. Comparison of welding deformation of front and back in width direction

According to the 5 groups of data of width direction on the two sides, the average value and maximum value of welding deformation was obtained, and the processing plot was shown in Figure 5.15.

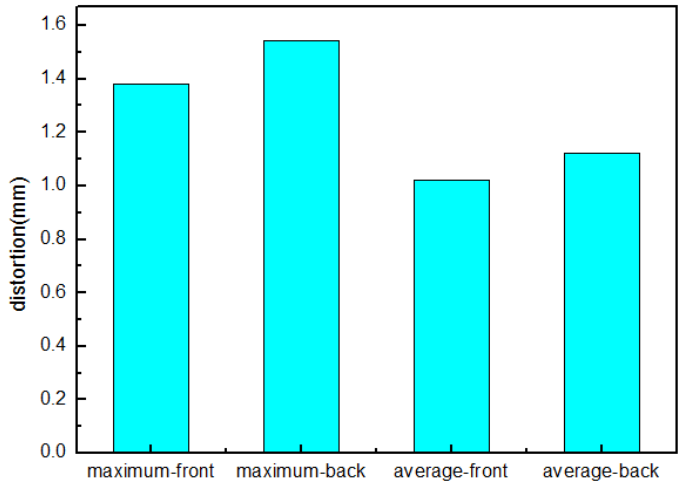

Figure 5.15 Processing plot of welding deformation on the width direction

From the figure, it was found that the average and maximum value of back are all less than that of front. The average and maximum value of back are 1.122 and 1.544, the average and maximum value of front are 1.021 and 1.382.

2. Comparison of welding deformation of front and back in length direction

According to the 2 groups of data of length direction on the two sides, the average value and maximum value of welding deformation was obtained, and the processing plot was shown in Figure 5.16.

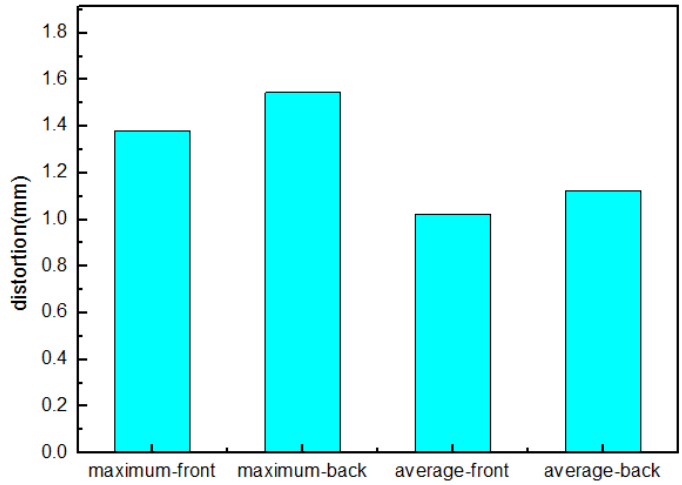

Figure 5.16 Processing plot of welding deformation on the length direction

From the Figure, it was found that the average and maximum value of front are all less than that of back. The average and maximum value of front are 1.774 and 1.576, the average and maximum value of front are 1.182 and 1.195.

According to the analysis and comparison of above data, the case size of front side in the length direction and width direction are all present extended and the case size of back side are all present shorten based on the traverse shrinkage and longitudinal shrinkage of weld. The inconsistency of welding deformation in width direction of two sides indicates the twist deformation of case was occurred. The inconsistency of welding deformation in length direction of two sides indicates the bending deformation of case was occurred.

According to the measuring result of welding deformation, the overall deformation of case are all controlled inside of ±2mm. From the overall dimension of model case, this welding deformation is satisfied. Also, the detection of deformation indicate that the laser welding system can effective control the welding deformation and meet the requirement during the welding process based on the suitable welding procedure.

6 Conclusions and recommendations

6.1 Key results of the work

The contents of this study is to develop a set of suitable welding system for the actual situation and requirements of the ITER CC case closure welding, based on much research, scheme design and analysis. And by specific tests aim at the key engineering technology challenges, the feasibility of the welding system has been verified, which could meet the requirements of the case closure welding and provide strong technical support for the official production of ITER CC.

The following conclusions were obtained from this study:

1. Due to the strict welding deformation requirement for the large dimensional CC cases, the traditional arc welding was not taken and some welding methods include NG-TIG welding, LBW and EBW were serious considered. Three preliminary schemes were designed depends on different welding method and it shows each of three welding processes has the feasibility for the ITER CC closure welding and can achieve the welding requirements. The laser welding scheme was determined as the best alternative to be applied, because of its hardware cost and no electron radiation compared with EBW, non-contact high-energy welding which is easier to implement than NG-TIG welding.

2. Based on the detailed analysis and study of the welding scheme, the BTCC case is located in the middle of the welding area and the SCC case is located outside of the BTCC case, and the two welding robots with their external lineal rails are designed and locate between the SCC and BTCC case. While, because of the large dimension of CC case, the simulation result of robotic welding motion process shows that there exsits the dead zone where the robot arm can not doing the effective welding and the robot welding workspace should be increased. Limited to the abilities of robot and external axis, a slip plate module for the welding robot can be added to assist travel, after that, the result shows that robot has good covering all weld seams in the case.

3. In order to realize the welding process, the welding fixture should be developed to support the welding platform, adjust the assembly tolerance and provide the rigid constrain to control the welding deformation. A number of the ground supports match with the C-type clamps was designed to special distributed aim at the geometric profile of case, which could easily meet the basic requirements. Because of the three-dimensional structure of SCC case, it needs two types of welding fixture to

meet its two different welding positions with arched and concave shape. Their ground supports was special developed with two parts, which can alternate their workstation by rotating to provide welding platform for two welding position of case, Moreover, a welding tilter was required to realize the turn over function of SCC case to alternate its two different welding position. This welding tilter was designed to consist of a main tilter framework with same shape to SCC case, a single central axis as the rotating axis, and a number of loading-bearing jigs to fix the case, According to the structural FEA results, the highest stress were always occurred at the two side of the rotating axis in the rotating process, which were caused by discontinuous structural characteristic. Based on the stress evaluation result, it is clear to found that the strength of the welding tilter can meet the rotating process easily.

4. The narrow gap multi-pass laser welding was determined as the basic welding process based on the laser power and the welding thickness. The design of optical propagation on the narrow gap was studied and the groove was developed to V-shaped with 2 mm root width and 5 mm root thickness, and 6° groove angle. The hot wire type was applied to increase the stability of wire feed process and obtain better welding quality. The welded joint with defects-free was obtained based on the reasonable welding parameters of root layer, filling layer and cosmetic layer were carried out, The microstructure shows the fully austenitic microstructure with fine cellular and dendrite grain in the weld metal, and these grains perpendicular to the fusion line and growth to the weld centre. These characteristics indicate the primary austenitic solidification was occurred on the welded joint because of the ratio of chromium equivalent and nickel equivalent and rapid solidification of laser welding. Also, the welded joint shows the good mechanical properties of tensile strength and impact toughness. All these welding inspection indicate that this laser welding process with the appropriate welding parameters can achieve the weld quality requirement of CC case.

5. In order to protect the superconducting coil inside of case, the backing strip with pony-size was designed behind of the case in the actual welding structure of CC case. Aim at the welding difficulty, the laser welding of backing strip was developed based on suitable laser beam angel and welding position. A short sample was fabricated and used to study the temperature distribution of the welding process based on the FEA and measured by the thermocouples. The heat source was adjusted depends on the 3D Gaussian heat source model and contrast with the actual molten pool. With the accuracy heat source, the FEA temperature distribution shows good agreement with the experimental measurements. The highest temperature of the inner face of case was 255℃, and the highest temperature record of surface of internal coil was 59℃. The result shows the laser welding process will not harm the superconducting coil,

and the welding process based on the laser welding system can meet the temperature control requirement.

6. A SCC model case was designed, fabricated and welded to study the welding deformation. The principle of positioning welding before continuous welding, as well as segmented , skip, symmetry and repeated turn over, was developed to keep uniform heating of the model case to control the welding deformation. According to the measurement data, the deformation of the model case was occurred and it presents the size was extended on the front side and was shorten on the back side. The inconsistency of welding deformation in width direction and length direction of two sides indicate that the twist and bending deformation was occurred in the case welding. As a whole, the overall welding deformation was controlled below ±2 mm. The satisfactory results of welding deformation of model case certify the welding structure, system and process is feasible to control the welding deformation during the CC case closure welding.

6.2 Suggestion for the future work

At present, the laser welding system for ITER CC case closure welding has already built and the feasibility study has verified by simulation and experiments. The main research works in the future as following suggestion:

- The basic engineering technologies of CC case closure welding have been solved, more theoretical and scientific works should be further considered. Such as, more detailed studies on the laser welding mechanism, the effects of different clamping conditions and welding assembly sequences on the generated force and distortion during welding.

- All the experiments which have done are all based on the plate or the sub-scale model case. Because of the machining and assembly difficulty, the full-scale CC case with the same welding structure and geometry to the plate and model case is more complicate to ensure the welding quality and control the welding deformation. The welding procedure should be further developed to study the impact of assembly tolerance to the welding quality and welding deformation.

- Due to the complex geometry and welding structure of CC case, the manual teaching was used to realize the laser welding process. The welding efficiency was low to such a great quantity of welding work. Thus, the full automatic laser welding process should be developed to decrease the preparation time for welding.

- On the basis of guarantee of the welding quality, the welding procedure with fewer welding layer may be developed to increase the welding efficiency and decrease number of the rotating process of SCC case.

References

Yuquan Ma. (2005). Development and application of nuclear energy. Chemical industry press, Beijing.

Chinese Academy of Sciences. (2002). High technology development report, Science press, Beijing.

Jiangang Li, et al. (2008). Bulletin of Chinese Academy of Sciences.

Wessen J. (1987). Tokamaks, Clarendon Press, Oxford.

Binren Shi. (1999). Principle and practice of magnetic confinement fusion, Rtomic energy press, Beijing.

Qiuliang Wang. (2008). Highfield superconducting magnet science, Science press, Beijing.

Lijian Qiu. (2008). Fusion energy and its application. Science press, Beijing.

D. F. H. Start, et al. (1998). DT fusion with ion cyclotron resonance heating in the JET tokamak, Physical review letters, 80(21): 4681.

A. Gibson, et al. (1998). Deuterium–tritium plasmas in the Joint European Torus (JET): Behavior and implications, Physics of Plasmas, 5(5): 1839-1847.

J. D. Strachan, et al. (1994). Fusion power production from TFTR plasmas fueled with deuterium and tritium. Physical review letters, 72(22): 3526.

IAEA.(2001).ITER Feat Outline Design Report—ITER EDA Documentation series NO.18,Vienna.

Yuanxi Wan. (2011). The development of magnetic confinement fusion and international thermonuclear experimental reactor (ITER). In proceedings the 16th Chinese conference on atomic and molecular physics.

Junyu Zhao. (2004). The international thermonuclear experimental reactor program. Physics, 33(04): 257-260.

Yiming Zhang. (2013), ITER project and fusion energy development strategy, Nuclear fusion and plasma physics, 33(4):360-365.

M. Onozuka et al., (2000). Design and Thermal/ Hydraulic characteristics of ITER-FEAT Vacuum Vessel, 21st Symposium on Fusion Technology, Madrid.

Andres Dans, et al., (2014). Challenging issues in the design and manufacturing of the European sectors of the ITER vacuum vessel, Fusion Engineering and Design, 89:1769-1774.

Lawrence Jones, et al., (2012). Manufacturing preparations for the European Vacuum Vessel Sector for ITER, Fusion Engineering and Design, 87: 700-705.

K.R. Nightingale, et al., (2002). Economic demonstration of an ITER-like EB gun column on an ITER-like weldment, The Welding Institute Report, UK,13371/1/2/02.

A,Martin, et al., , (2009). Simulation and measurements of electron beam welding distortions for the ITER vacuum Vessel, in: Asme Pressure Vessels & Piping Conference, Czech Republic.

F. Coste, et al., (2002). VV intersector joining-development of adaptive hybrid hot wire multipass Nd:YAG laser welding (TE1-TVV/LWELD), CLFA Intermediate Report 01-P024.

Tommi Jokinen, et al., (2003). Hgih power Nd:YAG laser welding in manufacturing of vacuum vessel of fusion reactor, Fusion Engineering and Design, 69: 349-353.

Huapeng Wu, et al., (2011), IWR-solution for the ITER vacuum vessel assembly, Fusion Engineering and Design, 86: 1834-1837.

Foussat. A, et al. (2010). Overview of the ITER Correction coils design, Applied superconductivity, 20(3):402-406.

N. Mitchell, et al.(2008). The ITER Magnet System, IEEE Trans. Appl. Super, 18 (2): 435-440.

M. Huguet, et al.(2001). Key engineering features of the ITER-FEAT magnet system and implications for the R&D programme. Nuclear fusion, 41(10): 1503.

N. Mitchell, et al.(2009). Status of the ITER magnets. Fusion Engineering and Design, 84: 13-121.

Wei Wen. (2013) Research of winding process and technology for ITER correction coils. Ph D thesis, Chinese Acadyme of Science.

C. Fang, et al. (2014). Study on the laser welding of case closure weld for ITER Correction coil, IEEE Trans.Appl.Supercond, 24(3): 4201103.

Z. Zhou, et al. (2012).Research on Manufacture and Enclosure Welding of ITER Correction Coils Cases, IEEE Trans.Appl.Supercond, 22(3): 4202603.

ITER_D_22HV5L v2.2, ITER Description Document DDD1, Magnet Section 1.Engineering Descripion.

ITER_D_2FMHHS v2.0, ITER magnet structural design criteria part 1: Main structure components and welds.

Wanyuan Liu. (2010). Structure design and finite element analysis of side correction coils for ITER, Master thesis, Chinese Academy of Science.

Arnaud Foussat.(2010). Correction Coil Case fabrication, NDT requirements, ITER-CERN Meeting, 14-15 January.

ITER_D_2N6NUK v1.13, ITER Design Description Document 11-5: Correction Coils and strcuture.

J. Wei et al., (2010). R&D of the ITER correction coil magnet system in China, presented at the 23rd IAEA FEC, Daejeon, Korea, Oct. 2010. Proceedings of the 23rd IAEA Fusion energy conference, Daejeon, October 11-16, Korea.

J. Wei et al. (2014). Progress of the ITER Correction coils in China, IEEE Trans.Appl.Supercond, 24(3): 4202005.

Wen Fang, et al. (2011). Analysis for the vacuum electron beam welding of ITER correction coil case, Welding technology,40(5)：16-19.

C. Fang, et al. (2014). The laser welding with hot wire of 316LN thick plate applied on ITER correction coil case, Journal of fusion energy, 33(6): 752-758.

Xiangfu Zhang. (2011). TIG auto-welding technology on heavy wall thickness large diameter and narrow gap welded pipe. Welded pipe and tube. 34(10)：30-32.

Xuebing Yang, Wei Tang. (2010). Research on TIG/MAG/SAW in narrow gap welding. Electric welding machine. 40 (7): 14-19.

K. Koizumi, et al. 2001. ITER R&D: Vacuum Vessel and In-Vessel Components: Vacuum Vessel[J], Fusion Engineering and Design ,55:193-203.

Jiajin Wang. (1992). Laser processing technology, Chinese metrology press, Beijing.

Huanming Chen. (2004). Basis of welding uniform design. Aviation industry press. Beijing.

AUGEY R. (2008). Finite element modeling of ITER Correction Coils， DWO-11-177-AFT.

Songhao Liu. (2003). The new progress of optical fiber lasers, Optoelectronic Technology & Information, 16(1)：1-8.

Qing Yang. et al. (2002). The survey of optic fiber lasers, Optoelectronic technology & information. 15(5)：13-18.

Richardson D J, Minelly J D. (1997). Fiber laser systems shine brightly. Laser Focus world, 23(9): 87~96.

Tiechuan Zuo. (2002). Laser processing of high strength aluminum alloy, National defense industry press. Beijing.

Kunli Peng. (2009). Research and development of control system for high power diode laser based on PLC, Master thesis, Beijing University of Technology.

Ning Guo. (2009). Research on molten pool behaviour and control technology of rotating arc narrow gap horizontal welding. Master thesis. Beijing University of Technology.

Ruijun Xie. et al, (2008). Twin-wire welding technology and corrosion resistance of weld seam for 7A52 aluminum alloy. Transactions of the China welding institution. 29 (12):57-63.

S. Beretta and B. Previtali. (2009). Estimate of maximum pore size in keyhole laser welding of carbon steel, Science and Technology of Welding and Joining.14(2): 106-116.

Fanrong Kong, Wei Liu, Junjie Ma, et al. (2013). Feasibility study of laser welding assisted by filler wire for narrow-gap butt-jointed plates of high-strength steel. Weld World,57:693-699.

M. Dahmen, F. Coste, G. Kapper et al. (2000). Application of a Modern High-Power Laser to Heavy Section Welding. Proceedings of SPIE, USA：404-410.

M. Dahmen, F. Coste, G. Kapper, et al. (2000). Multiple Pass Laser Beam Welding of Heavy Sections. Laser institute of America-proceedings, USA:147-156.

T. Tsukamoto, H. Kawanaka and Y. Maeda. (2011). Laser Narrow Gap Welding of Thick Carbon Steels Using High Brightness Laser with Beam Oscillation. ICALEO,United states：141-146.

Rittichai Phaoniam, Kenji Shinozaki, Motomichi Yamamoto, et al. (2013). Development of a highly efficient hot-wire laser hybrid process for narrow-gap welding-welding phenomena and their adequate conditions. Weld World, 57:607-613.

Shirong Xiao, et al, (2006). Innovative laser beam welding process of high strength aluminum alloy with thick plate. New technology & new process.5:63-65.

Chunyang Yu. (2010). Study on the technology and filler wire melting dynamics during the laser welding with filler wire. Ph D thesis, Huazhong University of Science &Technology.

Yangchun Yu, et al. (2010). Microstructures and property of butt laser joints of aluminium alloy 5A06 sheets with filler. Laser technology, 31(1):34-52.

Yoshiaki ARATA, Hiroshi MARUO,Isamu MIYAMOTO, et al. (1986). High power CO2 laser welding of thick plate--Multipass welding with filler wire.Ttansactions of JWRI (Japanese Welding Research Institute), 15(2):27-34.

Coste F,Janin F,Hamadou M,et al. (2003). Deep penetration laser welding with Nd:Yag lasers combination up to 11 kW laser power. Proceedings of SPIE, 4831:422-427.

Shunhong Liu, (2011). Laser materials processing, Huazhong university of science and technology press, Wuhan.

Guowei Zhang, (2014). Theoretical and experiment investigation on ultra-narrow gap fiber laser beam welding for heavy sections, Ph. D thesis, Beijing University of Technology.

Kitahara Y, et al., (2011). Hot wire laser welding for automative. Industrial laser solution for manufacturing.

Dzelnitzki Dirk, (2004). Wire feed systems for laser welding. Industrial laser solutions for manufacturing, 9-14;

Jones M, et al., (2004). Laser hot-wire welding for minimizing defects. In: Proceeding of the 23th international congress on application of laser and electro-optics, San-franscico, CA, USA.

Phillips R, et al., (1992). Laser beam welding of HY80 and HY100 steels using hot welding wire addition. Welding research supplement, 71(6):201-208.

Dilthey U, Schneegans J. (1994). Studies into laser beam welding with filler wire addition of unalloyed and low-alloyed steel, Weld and Cut,46(3):40-42.

Shiqing Zheng, et al. (2014). Research on wire transfer and its stability in laser hot wire welding process. Chinese journal of lasers, 41(4):0403008.

Peng Wen, et al. (2011). Experimental research on laser narrow gap welding with filling hot wire, Chinese journal of lasers, 38(11): 1103004.

H.C. Kim, K. Kim, Y.S. Lee, S.Y. Cho, H. Nakajima. (2009). Study on the weld characteristics of 316LN by magnetization measurement. Journal of Nuclear Materials,386–388:650–653.

J.A. Brooks, M.I. Bakes, L.A. Boatner. (1991). Metall. Trans. 22A, 915.

J.C Lippold, D.J Kotecki. (2005). Welding Metallurgy and Weldability of Stainless Steels ,Wiley, Hoboken.

V. Shankar, T.P.S. Gill, S.L. Mannan, S. Sundarlsan. (2003). Solidification cracking in austenitics stainless steel welds. Sadhana, 28(2–4):359–382 .

S.C. Tjong, S.M. Zhu, N.J. Ho, H.S. Ku. (1995). Microstructural characteristics and creep rupture behavior of electron beam and laser welded AISI 316L stainless steel. Journal of Nuclear Materials, 227:24–31.

ITER Design Description Document, Magnets DDD 11 ITER_D_2N6NUK v1.13, 5. CC Coils and Structures. Sept 2009.

Chinese industrial Standards NB/T 47014-2011, Welding procedure qualification for pressure equipment.

A. Chakravati.(1986). Prediction of distortion and residual stress in panel welds, in: Computer Modeling of Fabrication Process and Constitutive Behavior of Metals, Canadian Government Publishing Centre, Ottawa, 547-561.

S. Fujii. (2000). Development of 2D simulation model for laser welding, in: Proceedings of SPIE, vol.3888.

C.T. Karlesson. (1989). Finite element analysis of temperatures and stresses in a single pass butt-welded pipe-influence of mesh density and material modeling, Eng. Com. 6: 133-141.

S. Brown.(1992).Finite element simulation of welding of large structure, J. Eng. Ind. 114:441-451.

B.L. Josefson. (1993). Prediction of residual stresses and distortions in welded structures, J Offshore Mech. Arctic Eng. 115: 52-57.

J. Canas. (1996). A simplified numerical analysis of residual stresses in aluminum welded plates, Comput. Strct. 58(1):59-69.

P. Michaleris. (1997). Prediction of welding distortion, Weld. J. 76(4): 172-184.

S.Sarkani. (2000). An efficient approach for computing residual stresses in welded joints, Finite Elem. Anal. Des. 35:247-268.

C.K. Leung. (1990). Finite element modeling of a single pass weld, Weld. Res. Council Bull. 356:1-10.

T.L. Teng. (2001). Analysis of residual stressed and distortion in T-joint fillet welds, Int. J. Vessels Piping, 78:523-538.

M.R. Frewin. (1999). Finite elemen model of pulsed laser welding, Weld. J., 15-22.

G. Reinhart. (1999). Finite element simulation for planning of laser welding applications, in proceedings of the 18th International Congress on Applications of Lasers and Electro-Optics(ICALEO'99), San Diego, CA.

C. Carmignani.(1999).Transient finite element analysis of deep penetration laser welding process in a single pass butt-welded thick steel plate, Comput. Meth. Appl.Mech.Eng. 179:197-214.

D.H. Kang.(2001).Analysis of laser weldment distortion in the EDFA LD pump packing, Finit Elem, Anal, Des. 37:749-760.

Giuseppe Casalino, Elhem Ghorbel. (2008). Numerical model of CO2 laser welding of thermoplastic polymers, Journal of materials processing technology, 207:63-71.

K.N. Lankalapalli, et al. (1999). A model for estimating penetration depth of laser welding process, journal of physics d-applied physics, 29:1813-1841.

C. Lampa, et al. (1997). An analytical thermodynamic model of laser welding, journal of physics d-applied physics, 30:1293-1297.

K. Williams, et al. (1999). Development of laser welding theory with correlation to experimental welding data, lasers in engineering, 8:197-214.

ChuanSong Wu. (2008). Welding thermal process and weld pool, China machine press. Beijing.

Hongyuan Fang. (2008). Welding structure. China machine press. Beijing.

Rongbo Fu. (2006). Control and correction of welding distortion. China machine press. Beijing.

Yanhong Zu, et al. (2008). Welding deformation control methods of large-scale structural components. Welding technology. 37(6):54-57.

Zhiwei Zhang. (2007). Discussing on the structure and technics analysis of welding distortion. Mechanical research & application. 20(3): 18-19.

Zhonggang Zhao. (2015). Discussion on welding deformation control of large-scale structural components, Mechanical research & application. 28(135):126-127.

Wen yue Chen. (2003). The basic principle of welding metallurgy, China Machine Press, Beijing.

Wuxiong Yang. (2014). Investigation of dual beam high brightness laser welding of aluminum alloy with T joint. Ph D thesis, Beijing University of Technology.

ACTA UNIVERSITATIS LAPPEENRANTAENSIS

676. OMAJENE, JOSHUA. Underwater remote welding technology for offshore structures. 2015. Diss.

677. NUUTINEN, PASI. Power electronic converters in low-voltage direct current distribution – analysis and implementation. 2015. Diss.

678. RUSATSI, DENIS. Bayesian analysis of SEIR epidemic models. 2015. Diss.

679. STRAND, ELSI. Enhancement of ultrafiltration process by pretreatment in recovery of hemicelluloses from wood extracts. 2016. Diss.

680. TANNINEN, PANU. Press forming of paperboard – advancement of converting tools and process control. 2015. Diss.

681. VALTONEN, PETRI. Distributed energy resources in an electricity retailer's short-term profit optimization. 2015. Diss.

682. FORSSTRÖM-TUOMINEN, HEIDI. Collectiveness within start up-teams – leading the way to initiating and managing collective pursuit of opportunities in organizational contexts. 2015. Diss.

683. MAGUYA, ALMASI. Use of airborne laser scanner data in demanding forest conditions. 2015. Diss.

684. PEIPPO, JUHA. A modified nominal stress method for fatigue assessment of steel plates with thermally cut edges. 2015. Diss.

685. MURASHKO, KIRILL. Thermal modelling of commercial lithium-ion batteries. 2016. Diss.

686. KÄRKKÄINEN, TOMMI. Observations of acoustic emission in power semiconductors. 2016. Diss.

687. KURVINEN, EMIL. Design and simulation of high-speed rotating electrical machinery. 2016. Diss.

688. RANTAMÄKI, JUKKA. Utilization of statistical methods for management in the forest industry. 2016. Diss.

689. PANOVA, YULIA. Public-private partnership investments in dry ports – Russian logistics markets and risks. 2016. Diss.

690. BAHARUDIN, EZRAL. Real-time simulation of multibody systems with applications for working mobile vehicles. 2016. Diss.

691. MARTIKAINEN, SOILI. Development and effect analysis of the Asteri consultative auditing process – safety and security management in educational institutions. 2016. Diss.

692. TORVINEN, PEKKA. Catching up with competitiveness in emerging markets – An analysis of the role of the firm's technology management strategies. 2016. Diss.

693. NORONTAUS, ANNUKKA. Oppisopimuskoulutus yritysten tuottamana koulutuspalveluna: tavoitteista vaikutuksiin.2016. Diss.

694. HALMINEN, OSKARI. Multibody models for examination of touchdown bearing systems. 2016. Diss.

695. TALONPOIKA, ANNA-MARIA. Financial working capital – management and measurement. 2016. Diss.

696. INKINEN, HENRI. Intellectual capital, knowledge management practices and firm performance. 2016. Diss.

697. YANG, XIAOCHEN. Development of a welding production quality control and management system model for China. 2016. Diss.

698. LEMINEN, VILLE. Leak-proof heat sealing of press-formed paperboard trays. 2016. Diss.

699. LAAKSONEN, LAURI. Spectral retinal image processing and analysis for ophthalmology. 2016. Diss.

700. OINONEN, MINNA. Management of customer co-development in business-to-business markets. 2016. Diss.

701. ALATALO, SARA-MAARIA. Hydrothermal carbonization in the synthesis of sustainable porous carbon materials. 2016. Diss.

702. UZHEGOV, NIKITA. Design and material selection of high-speed rotating electrical machines. 2016. Diss.

703. RICHTER, CHRIS. Digital collaborations and entrepreneurship – the role of shareconomy and crowdsourcing in the era of smart city. 2016. Diss.

704. JAFARI, SHILA. Investigation of adsorption of dyes onto modified titanium dioxide. 2016. Diss.

705. PATEL, YOGINI. Computational modelling of non-equilibrium condensing steam flows in low-pressure steam turbines. 2016. Diss.

706. LEVCHUK, IRINA. Titanium dioxide based nanomaterials for photocatalytic water treatment. 2016. Diss.

707. AMOUR, IDRISSA. Variational ensemble kalman filtering applied to data assimilation problems in computational fluid dynamics. 2016. Diss.

708. SHESTAKOVA, MARINA. Ultrasound-assisted electrochemical treatment of wastewaters containing organic pollutants by using novel Ti/Ta2O5-SnO2 electrodes. 2016. Diss.

709. OLEKSIIENKO, OLGA. Physico-chemical properties of sol-gel synthesized titanosilicates for the uptake of radionuclides from aqueous solutions. 2016. Diss.

710. PATALA, SAMULI. Advancing sustainability-oriented innovations in industrial markets. 2016. Diss.

711. KUORIKOSKI, TERO. Kohti resonoivaa urheilujohtamista – Tavoitteen muodostuminen urheilun kentässä.2016. Diss.

712. LAHTELA, VILLE. Improving the properties of solid Scots pine (Pinussylvestris) wood by using modification technology and agents. 2016. Diss.

713. NEVARANTA, NIKO. Online time and frequency domain identification of a resonating mechanical system in electric drives. 2016. Diss.